

Supplement of Earth Syst. Dynam., 11, 755–774, 2020
<https://doi.org/10.5194/esd-11-755-2020-supplement>
© Author(s) 2020. This work is distributed under
the Creative Commons Attribution 4.0 License.



Earth System
Dynamics
Open Access
EGU

Supplement of

Groundwater storage dynamics in the world's large aquifer systems from GRACE: uncertainty and role of extreme precipitation

Mohammad Shamsuddoha and Richard G. Taylor

Correspondence to: Mohammad Shamsuddoha (m.shamsuddoha@sussex.ac.uk)

The copyright of individual parts of the supplement might differ from the CC BY 4.0 License.

Supplementary Table S1. Characteristics of the world's 37 large aquifer systems according to the WHYMAP database including aquifer area, total number of population, proportion of groundwater (GW)-fed irrigation, mean aridity index, mean annual rainfall, variability in rainfall and total terrestrial water mass (Δ TWS), and correlation coefficients between monthly Δ TWS and precipitation with reported lags.

WHYMAP aquifer number	Aquifer name	Continent	Population (million)	Aquifer area (km ²)	GW irrigation (%)	Climate zones based on Aridity indices	Mean (2002-16) annual precipitation (mm)	Rainfall variability (%)	TWS variance (cm ²)	Correlation between TWS and precipitation (lag in month)
1	Nubian Sandstone Aquifer System	Africa	86.01	2,176,068	1.6	Hyper-arid	30	12.1	1.5	0.16 (13)
2	Northwestern Sahara Aquifer System	Africa	5.93	1,007,536	4.4	Arid	69	17.3	1.9	0.19 (8)
3	Murzuk-Djado Basin	Africa	0.35	483,817	2.3	Hyper-arid	8	36.6	1.3	0.20 (-8)
4	Taoudeni-Tanezrouft Basin	Africa	0.35	720,991	0.0	Hyper-arid	66	14.6	1.2	0.46 (1)
5	Senegal-Mauritanian Basin	Africa	17.77	294,613	1.0	Semi-arid	540	14.6	31.9	0.73 (2)
6	Iullemmeden-Irhazer Aquifer System	Africa	21.57	580,870	0.4	Arid	302	11.7	6.9	0.66 (2)
7	Lake Chad Basin	Africa	32.25	1,516,233	0.4	Arid	415	9.5	16.8	0.82 (2)
8	Umm Ruwaba Aquifer (Sudd Basin)	Africa	10.52	509,174	0.0	Semi-arid	789	10.7	44.4	0.86 (2)
9	Ogaden-Juba Basin	Africa	20.27	1,080,953	0.3	Arid	393	14.2	2.7	0.48 (1)
10	Congo Basin	Africa	34.74	1,487,858	0.0	Humid	1,566	5.6	33.0	0.66 (2)
11	Upper Kalahari-Cuvelai-Zambezi Basin	Africa	6.02	1,000,812	0.1	Semi-arid	819	10.0	145.1	0.66 (2)
12	Lower Kalahari-Stampriet Basin	Africa	0.76	426,487	0.6	Arid	297	24.1	5.3	0.47 (2)
13	Karoo Basin	Africa	14.53	568,213	2.1	Semi-arid	479	17.6	6.5	0.30 (2)
14	Northern Great Plains Aquifer	North America	6.62	1,507,325	14.5	Sub-humid	461	9.7	24.5	0.45 (10)
15	Cambro-Ordovician Aquifer System	North America	13.86	129,588	91.7	Humid	880	11.6	35.1	0.39 (10)
16	California Central Valley Aquifer System	North America	8.10	71,430	57.8	Semi-arid	515	32.0	176.5	0.53 (2)
17	Ogallala Aquifer (High Plains)	North America	2.44	501,374	86.8	Semi-arid	507	16.1	19.7	0.39 (9)

18	Atlantic and Gulf Coastal Plains Aquifer	North America	65.38	1,125,968	55.8	Humid	1,230	11.4	43.1	0.43 (8)
19	Amazon Basin	South America	8.93	2,279,522	1.0	Humid	2,505	8.3	347.2	0.84 (2)
20	Maranhao Basin	South America	10.81	592,680	32.6	Humid	1,502	15.7	217.2	0.82 (2)
21	Guarani Aquifer System (Parana Basin)	South America	47.84	1,834,681	20.5	Humid	1,450	10.6	40.5	0.61 (3)
22	Arabian Aquifer System	Asia	27.43	1,782,954	7.2	Arid	65	15.0	6.1	0.12 (0)
23	Indus River Basin	Asia	155.85	308,436	31.0	Semi-arid	375	16.2	13.0	0.56 (1)
24	Ganges-Brahmaputra Basin	Asia	596.44	616,422	55.8	Humid	1,391	12.1	255.6	0.73 (2)
25	West Siberian Artesian Basin	Asia	12.71	2,703,532	3.4	Humid	483	8.1	39.1	0.71 (8)
26	Tunguss Basin	Asia	0.43	1,241,981	0.1	Humid	432	9.8	38.1	0.66 (8)
27	Angara-Lena Basin	Asia	2.50	620,591	1.3	Humid	472	7.9	21.6	0.55 (8)
28	Yakut Basin	Asia	0.63	861,053	0.7	Humid	386	8.2	19.5	0.58 (-4)
29	North China Plains Aquifer System	Asia	336.70	438,954	37.1	Humid	826	10.0	32.8	0.32 (2)
30	Song-Liao Plain	Asia	54.49	279,044	53.5	Humid	514	17.0	19.5	0.20 (1)
31	Tarim Basin	Asia	7.69	454,288	2.8	Arid	90	23.6	1.9	0.50 (0)
32	Paris Basin	Europe	28.58	178,513	82.3	Humid	727	10.8	32.9	0.24 (6)
33	East European Aquifer System	Europe	100.22	2,859,962	16.6	Humid	606	6.2	35.3	0.54 (7)
34	North Caucasus Basin	Europe	13.30	294,821	4.2	Semi-arid	524	11.6	49.2	0.30 (10)
35	Pechora Basin	Europe	0.19	220,245	0.0	Humid	559	9.5	51.2	0.60 (7)
36	Great Artesian Basin	Australia	0.20	1,765,830	0.9	Semi-arid	444	28.9	20.2	0.55 (2)
37	Canning Basin	Australia	0.01	432,774	0.4	Arid	443	21.2	50.3	0.47 (2)

Supplementary Table S2. Characteristics of the world's 37 large aquifer systems according to the WHYMAP database including mean annual rainfall, mean aridity index, and variability in total terrestrial water mass (Δ TWS), and correlation coefficients between Δ TWS and annual precipitation. The variance (cm^2) in the ensemble GRACE Δ TWS and the proportion of variance explained by surface water and snow water equivalent combined (SWS+SNS), soil moisture storage (SMS) and groundwater storage (GWS) are tabulated.

WHYMAP aquifer number	Aquifer name	Mean (2002–2016) Annual precipitation (mm)	Climate zones based on Aridity indices	TWS variance (cm^2)	Correlation between annual changes in TWS and annual precipitation	TWS variance explained by SWS+SNS combined (%)	TWS variance explained by SMS (%)	TWS variance explained by GWS (%)
1	Nubian Sandstone Aquifer System	30	Hyper-arid	1.5	0.32	0.5	32.4	67.1
2	Northwestern Sahara Aquifer System	69	Arid	1.9	0.62	0.9	14.2	84.9
3	Murzuk-Djado Basin	8	Hyper-arid	1.3	0.08	1.6	1.5	96.9
4	Taoudeni-Tanezrouft Basin	66	Hyper-arid	1.2	0.21	6	14.3	79.6
5	Senegal-Mauritanian Basin	540	Semi-arid	31.9	0.65	14.6	56.6	28.8
6	Iullemmeden-Irhazer Aquifer System	302	Arid	6.9	0.36	12.4	55.7	32
7	Lake Chad Basin	415	Arid	16.8	0.50	14.8	66.6	18.6
8	Umm Ruwaba Aquifer (Sudd Basin)	789	Semi-arid	44.4	0.76	1.7	72.9	25.5
9	Ogaden-Juba Basin	393	Arid	2.7	0.14	1.7	35.9	62.3
10	Congo Basin	1,566	Humid	33.0	0.53	15.6	23.7	60.7
11	Upper Kalahari-Cuvelai-Zambezi Basin	819	Semi-arid	145.1	0.78	0.2	45.6	54.3
12	Lower Kalahari-Stampriet Basin	297	Arid	5.3	0.68	5.7	44.3	50
13	Karoo Basin	479	Semi-arid	6.5	0.72	3.3	1	95.7
14	Northern Great Plains Aquifer	461	Sub-humid	24.5	0.60	4.8	26.5	68.7
15	Cambro-Ordovician Aquifer System	880	Humid	35.1	0.75	1.5	60.1	38.3

16	California Central Valley Aquifer System	515	Semi-arid	176.5	0.46	2.8	56	41.2
17	Ogallala Aquifer (High Plains)	507	Semi-arid	19.7	0.80	2.6	14.6	82.8
18	Atlantic and Gulf Coastal Plains Aquifer	1,230	Humid	43.1	0.61	33.8	51.6	14.6
19	Amazon Basin	2,505	Humid	347.2	0.28	30.6	48.9	20.5
20	Maranhao Basin	1,502	Humid	217.2	0.92	27.5	64.2	8.3
21	Guarani Aquifer System (Parana Basin)	1,450	Humid	40.5	0.38	21	52.3	26.7
22	Arabian Aquifer System	65	Arid	6.1	0.57	5.2	56.7	38.1
23	Indus River Basin	375	Semi-arid	13.0	0.39	4	32.4	63.5
24	Ganges-Brahmaputra River Basin	1,391	Humid	255.6	0.69	17.7	62.7	19.5
25	West Siberian Artesian Basin	483	Humid	39.1	0.71	36.8	11.8	51.4
26	Tunguss Basin	432	Humid	38.1	0.71	57.2	1.9	40.9
27	Angara-Lena Basin	472	Humid	21.6	0.71	23.3	27.1	49.6
28	Yakut Basin	386	Humid	19.5	0.47	26	12	61.9
29	North China Plains Aquifer System	826	Humid	32.8	0.22	0.3	65.4	34.3
30	Song-Liao Plain	514	Humid	19.5	0.62	9.4	59.5	31.1
31	Tarim Basin	90	Arid	1.9	0.32	3	8.3	88.7
32	Paris Basin	727	Humid	32.9	0.86	8.9	57.4	33.7
33	East European Aquifer System	606	Humid	35.3	0.75	39.3	41.2	19.5
34	North Caucasus Basin	524	Semi-arid	49.2	0.86	2.7	59.1	38.2
35	Pechora Basin	559	Humid	51.2	0.56	70	1.8	28.1
36	Great Artesian Basin	444	Semi-arid	20.2	0.89	17.6	55	27.3
37	Canning Basin	443	Arid	50.3	0.85	3	49.1	47.9

Supplementary Table S3. Characteristics of the relationships between CRU precipitation and GRACE ΔGWS in the world's 37 large aquifer systems.

WHYMAP aquifer number	Aquifer name	Mean (1901 to 2016) annual (hydrological year) precipitation (mm)	90 th percentile precipitation (period: 1901–2016)	Rainy season: calendar year (Jan–Dec) or hydrological year (Aug–Jul)	Extreme hydrological years ($\geq 90^{\text{th}}$ percentile) over GRACE period (2002–2016)	Positive change in non-linear trends in GRACE-ΔGWS over the period of 2002–2016 and reported values between two consecutive years (cm)
1	Nubian Sandstone Aquifer System	33	41	Jan–Dec	2014 (51 st)	2014 (0.43) 2015 (0.63)
2	Northwestern Sahara Aquifer System	72	92	Aug–Jul	2003–2004 2005–2006	2005–2006 (0.25) 2015–2016 (0.41)
3	Murzuk-Djado Basin	8	11	Jan–Dec	2015 (78 th)	2015 (0.83) 2016 (0.70)
4	Taoudeni-Tanezrouft Basin	63	75	Jan–Dec	2010	2014 (0.30) 2015 (0.31)
5	Senegal-Mauritanian Basin	548	703	Jan–Dec	2010	2010 (1.96) 2011 (1.53)
6	Iullemmeden-Irhazer Aquifer System	301	377	Jan–Dec	2010 (68 th)	2010 (0.75) 2011 (0.86)
7	Lake Chad Basin	392	460	Jan–Dec	2012	2012 (0.45) 2013 (0.69)
8	Umm Ruwaba Aquifer (Sudd Basin)	788	889	Jan–Dec	2007 (87 th) 2008 (78 th) 2014 (60 th)	2008 (0.83) 2013 (0.98) 2014 (1.27)
9	Ogaden-Juba Basin	376	465	Jan–Dec	2013	2006 (0.92) 2013 (0.69)
10	Congo Basin	1632	1740	Aug–Jul	2015–2016 (56 th)	2013–2014 (5.15) 2015–2016 (2.93)
11	Upper Kalahari-Cuvelai-Zambezi Basin	800	935	Aug–Jul	2008–2009 (74 th) 2010–2011 (70 th)	2008–2009 (3.05) 2010–2011 (5.12)
12	Lower Kalahari-Stampriet Basin	286	386	Aug–Jul	2010–2011	2006–2007 (0.80) 2010–2011 (0.78)
13	Karoo Basin	500	623	Aug–Jul	2010–2011	2010–2011 (1.86) 2011–2012 (1.50)
14	Northern Great Plains Aquifer	429	487	Jan–Dec	2005, 2010, 2013	2005 (1.71) 2010 (2.70) 2011 (2.42)
15	Cambro-Ordovician Aquifer System	819	960	Jan–Dec	2010, 2013, 2015	2010 (2.70) 2011 (2.42)
16	California Central Valley Aquifer System	567	772	Aug–Jul	2005–2006	2004–2005 (3.92) 2005–2006 (4.15) 2010–2011 (2.05)
17	Ogallala Aquifer (High Plains)	489	578	Jan–Dec	2015	2008 (2.26) 2009 (1.83)
18	Atlantic and Gulf Coastal Plains Aquifer	1205	1356	Jan–Dec	2009, 2013, 2015	2009 (1.40) 2013 (0.80) 2015 (0.55)

19	Amazon Basin	2416	2627	Aug–Jul	2005–2006 2007–2008 2008–2009	2007–2008 (2.58) 2011–2012 (3.31)
20	Maranhao Basin	1470	1762	Aug–Jul	2008–2009 2010–2011	2003–2004 (2.45) 2009–2010 (1.83)
21	Guarani Aquifer System (Parana Basin)	1384	1573	Aug–Jul	2009–2010 2015–2016	2010–2011 (1.65) 2015–2016 (5.78)
22	Arabian Aquifer System	74	87	Jan–Dec	2004 (40 th)	2003 (0.15) 2004 (0.12)
23	Indus River Basin	330	452	Jan–Dec	2010, 2015	2014 (0.93) 2015 (0.82)
24	Ganges-Brahmaputra Basin	1483	1663	Jan–Dec	2011 (59 th)	2011 (1.44)
25	West Siberian Artesian Basin	452	505	Jan–Dec	2013, 2014, 2015	2013 (2.57) 2014 (3.08) 2015 (2.17)
26	Tunguss Basin	415	461	Jan–Dec	2007, 2008, 2015	2005 (3.25) 2006 (3.25) 2013 (4.49)
27	Angara-Lena Basin	456	512	Jan–Dec	2006, 2008, 2009	2006 (1.71) 2013 (1.80)
28	Yakut Basin	342	402	Jan–Dec	2005, 2006, 2007, 2008, 2013	2005 (1.89) 2006 (2.15)
29	North China Plains Aquifer System	793	916	Jan–Dec	2003	2003 (3.21) 2004 (3.73)
30	Song-Liao Plain	531	629	Jan–Dec	2012, 2013	2013 (2.14) 2014 (1.57)
31	Tarim Basin	78	105	Jan–Dec	2003, 2005, 2010, 2013	2015 (0.74) 2016 (1.04)
32	Paris Basin	724	862	Aug–Jul	2006–2007 2015–2016	2013–2014 (2.34) 2014–2015 (1.84) 2015–2016 (1.53)
33	East European Aquifer System	585	638	Jan–Dec	2004, 2012	2005 (1.84) 2006 (2.17)
34	North Caucasus Basin	514	602	Jan–Dec	2004	2004 (3.32) 2005 (3.21)
35	Pechora Basin	490	583	Jan–Dec	2003, 2007, 2014	2013 (3.37) 2014 (3.21)
36	Great Artesian Basin	438	584	Aug–Jul	2009–2010 2010–2011	2009–2010 (1.72) 2010–2011 (3.34)
37	Canning Basin	377	547	Aug–Jul	2005–2006 2010–2011 2013–2014	2010–2011 (1.46) 2011–2012 (2.37)

Supplementary Table S4. Characteristics of the relationships between GPCC precipitation and GRACE ΔGWS in the world's 37 large aquifer systems.

WHYMAP aquifer number	Aquifer name	Mean (1901 to 2016) annual (hydrological year) precipitation (mm)	90 th percentile precipitation (period: 1901–2016)	Rainy season: calendar year (Jan–Dec) or hydrological year (Aug–Jul)	Extreme hydrological years ($\geq 90^{\text{th}}$ percentile) over GRACE period (2002–2016)	Positive change in non-linear trends in GRACE-ΔGWS over the period of 2002–2016 and reported values between two consecutive years (cm)
1	Nubian Sandstone Aquifer System	32	44	Jan–Dec	2014 (61 st) 2015 (72 nd)	2014 (0.43) 2015 (0.63)
2	Northwestern Sahara Aquifer System	68	94	Aug–Jul	2003–2004 2005–2006 2008–2009	2005–2006 (0.25) 2015–2016 (0.41)
3	Murzuk-Djado Basin	15	23	Jan–Dec	2013 (74 th) 2015 (34 th)	2015 (0.83) 2016 (0.70)
4	Taoudeni-Tanezrouft Basin	91	125	Jan–Dec	2010	2014 (0.30) 2015 (0.31)
5	Senegal-Mauritanian Basin	511	655	Jan–Dec	2010	2010 (1.96) 2011 (1.53)
6	Iullemmeden-Irhazer Aquifer System	275	350	Jan–Dec	2010 (75 th)	2010 (0.75) 2011 (0.86)
7	Lake Chad Basin	385	452	Jan–Dec	2012	2012 (0.45) 2013 (0.69)
8	Umm Ruwaba Aquifer (Sudd Basin)	778	882	Jan–Dec	2006, 2007 (66 th), 2008 (83 rd), 2009 (87 th), 2011 (84 th) 2014 (81 st)	2008 (0.83) 2013 (0.98) 2014 (1.27)
9	Ogaden-Juba Basin	393	481	Jan–Dec	2006	2006 (0.92) 2013 (0.69)
10	Congo Basin	1657	1750	Aug–Jul	2015–2016 (48 th)	2013–2014 (5.15) 2015–2016 (2.93)
11	Upper Kalahari-Cuvelai-Zambezi Basin	840	952	Aug–Jul	2005–2006 2008–2009 (87 th) 2010–2011 (84 th)	2008–2009 (3.05) 2010–2011 (5.12)
12	Lower Kalahari-Stampriet Basin	303	409	Aug–Jul	2006–2007 2010–2011	2006–2007 (0.80) 2010–2011 (0.78)
13	Karoo Basin	500	620	Aug–Jul	2010–2011	2010–2011 (1.86) 2011–2012 (1.50)
14	Northern Great Plains Aquifer	427	484	Jan–Dec	2005, 2010	2005 (1.71) 2010 (2.70) 2011 (2.42)
15	Cambro-Ordovician Aquifer System	834	969	Jan–Dec	2008, 2010	2010 (2.70) 2011 (2.42)
16	California Central Valley Aquifer System	552	749	Aug–Jul	2005–2006	2004–2005 (3.92) 2005–2006 (4.15) 2010–2011 (2.05)
17	Ogallala Aquifer (High Plains)	501	602	Jan–Dec	2015	2008 (2.26) 2009 (1.83)

18	Atlantic and Gulf Coastal Plains Aquifer	1215	1372	Jan–Dec	2004, 2009, 2015	2009 (1.40) 2013 (0.80) 2015 (0.55)
19	Amazon Basin	2500	2661	Aug–Jul	2005–2006 2007–2008 2008–2009 2013–2014	2007–2008 (2.58) 2011–2012 (3.31)
20	Maranhao Basin	1421	1703	Aug–Jul	2008–2009	2003–2004 (2.45) 2009–2010 (1.83)
21	Guarani Aquifer System (Parana Basin)	1378	1535	Aug–Jul	2003–2004 2009–2010 2014–2015 2015–2016	2010–2011 (1.65) 2015–2016 (5.78)
22	Arabian Aquifer System	81	99	Jan–Dec	2003 (66 th) 2005 (52 nd) 2013 (88 th)	2003 (0.15) 2004 (0.12)
23	Indus River Basin	336	466	Jan–Dec	2011, 2015	2014 (0.93) 2015 (0.82)
24	Ganges-Brahmaputra Basin	1490	1650	Jan–Dec	2007 (89 th) 2008 (78 th) 2011 (39 th)	2011 (1.44)
25	West Siberian Artesian Basin	443	497	Jan–Dec	2002, 2007, 2014, 2015	2013 (2.57) 2014 (3.08) 2015 (2.17)
26	Tunguss Basin	389	434	Jan–Dec	2002, 2007, 2008, 2011, 2014, 2015	2005 (3.25) 2006 (3.25) 2013 (4.49)
27	Angara-Lena Basin	422	471	Jan–Dec	2004, 2005, 2006, 2008, 2009	2006 (1.71) 2013 (1.80)
28	Yakut Basin	316	363	Jan–Dec	2004, 2005, 2006, 2007, 2008, 2012 2013	2005 (1.89) 2006 (2.15)
29	North China Plains Aquifer System	795	933	Jan–Dec	2003	2003 (3.21) 2004 (3.73)
30	Song-Liao Plain	534	636	Jan–Dec	2012, 2013	2013 (2.14) 2014 (1.57)
31	Tarim Basin	48	66	Jan–Dec	2003, 2005, 2010, 2013, 2015	2015 (0.74) 2016 (1.04)
32	Paris Basin	750	914	Aug–Jul	2006–2007 2015–2016	2013–2014 (2.34) 2014–2015 (1.84) 2015–2016 (1.53)
33	East European Aquifer System	561	624	Jan–Dec	2004, 2012	2005 (1.84) 2006 (2.17)
34	North Caucasus Basin	488	584	Jan–Dec	2004	2004 (3.32) 2005 (3.21)
35	Pechora Basin	470	565	Jan–Dec	2002, 2003, 2005, 2006, 2007, 2012	2013 (3.37) 2014 (3.21)
36	Great Artesian Basin	429	568	Aug–Jul	2009–2010 2010–2011 2011–2012	2009–2010 (1.72) 2010–2011 (3.34)
37	Canning Basin	438	587	Aug–Jul	2004–2005 2010–2011	2010–2011 (1.46) 2011–2012 (2.37)

Supplementary Table S5. The breakdown of 20 realisations for GRACE-derived GWS estimates using a range of gridded GRACE products (CSR, JPL-Mascons, GRGS) and an ensemble mean of Δ TWS and individual storage component of Δ SMS and Δ SWS from 4 Land Surface Models (LSMs: CLM, Noah, VIC, Mosaic), and a single Δ SNS from Noah model (GLDAS version 2.1).

The breakdown of 20 realisations is given below with 12 realisations being the primary products, whereas the remaining 8 realisations derive from a combination of GRACE Δ TWS and different LSMs to demonstrate the range of uncertainty in the estimation of Δ GWS using GRACE-derived Δ TWS and GLDAS LSMs:

GRACE product for terrestrial water storage	Surface water and soil moisture storage models	Snow water storage model	No of realisation
3 GRACE TWS	4 LSMs (SWS, SMS)	1 LSM (SNS)	12 realisations
1 CSR GRACE TWS	1 mean LSMs (SWS, SMS)	1 LSM (SNS)	1 realisation
1 JPL GRACE TWS	1 mean LSMs (SWS, SMS)	1 LSM (SNS)	1 realisation
1 GRGS GRACE TWS	1 mean LSMs (SWS, SMS)	1 LSM (SNS)	1 realisation
1 Mean GRACE TWS	4 LSMs (SWS, SMS)	1 LSM (SNS)	4 realisations
1 Mean GRACE TWS	1 mean LSMs (SWS, SMS)	1 LSM (SNS)	1 realisation

Supplementary Figure captions

Fig. S1-S36. Time-series data of terrestrial water storage anomaly (Δ TWS) from GRACE and individual water stores from GLDAS Land Surface Models (LSMs): (a) Ensemble monthly GRACE Δ TWS from three solutions (CSR, Mascons, GRGS), (b-c) ensemble monthly Δ SMS and Δ SWS + Δ SNS from four GLDAS LSMs (CLM, Noah, VIC, Mosaic), (d) computed monthly Δ GWS and (e) monthly precipitation from August 2002 to July 2016 for WHYMAP large aquifer systems from no. 1 to 37, except for the High Plains Aquifer System in the USA (no. 17) which is shown as Fig. 2. Values in the Y-axis of the top four panels show monthly water-storage anomalies (cm) and the bottom panel shows monthly precipitation (cm).

Fig. S37. (a) STL decomposition of ensemble GRACE-TWS signal High Plains Aquifer System (17); (b) various S window smoothing parameters; and (c) various T window parameters and fitted. The p-value in each panel derives from a Shapiro-Wilk normality test of the residuals after fitting the STL smooth line.

Fig. S38. Comparison of Δ GWS time series datasets from GRACE and in situ piezometric observations. Δ GWS time-series records in the unconsolidated, alluvial aquifer within the humid Bengal Basin of Bangladesh (a), and a weathered crystalline rock aquifer in the semi-arid Limpopo Basin in South Africa (b). Shaded bands in light-pink and light-blue around Δ GWS lines denote the standard deviation of the estimated mean value. Monthly precipitation records are shown as stair-step lines in blue on both panels with a dashed blue line indicating the long-term monthly mean value.

Fig. S39. Time-series data of terrestrial water storage anomaly (Δ TWS) from GRACE and individual water stores from GLDAS Land Surface Models (LSMs): (a) Ensemble monthly GRACE Δ TWS from three solutions (CSR, Mascons, GRGS), (b-c) ensemble monthly Δ SMS and Δ SWS + Δ SNS from four GLDAS LSMs (CLM, Noah, VIC, Mosaic), (d) computed monthly Δ GWS and (e) monthly precipitation from August 2002 to July 2016 for the Bengal Basin of Bangladesh.

Fig. S40. Time-series data of terrestrial water storage anomaly (Δ TWS) from GRACE and individual water stores from GLDAS Land Surface Models (LSMs): (a) Ensemble monthly GRACE Δ TWS from three solutions (CSR, Mascons, GRGS), (b-c) ensemble monthly Δ SMS and Δ SWS + Δ SNS from four GLDAS LSMs (CLM, Noah, VIC, Mosaic), (d)

computed monthly Δ GWS and (e) monthly precipitation from August 2002 to July 2016 for the Limpopo Basin of South Africa.

Fig. S41-S77. Decomposition of time-series components of GRACE Δ GWS data for all 37 large aquifer systems using a non-parametric, Seasonal-Trend decomposition procedure based on Loess (STL) technique. The graph on the top shows monthly anomaly data and decomposed time-series components of the series into seasonal, trend and remainder components. The graph also shows monthly precipitation records from CRU data along with annual total precipitation values (cm) written next to each annual cycle. The pie chart at the bottom shows the proportion of variance (%) in GRACE Δ GWS explained by the time-series components (S=seasonal, T=trend, R=residual/remainder).

Fig. S78. Time series of ensemble mean GRACE Δ TWS (red), GLDAS Δ SMS (green), Δ SWS + Δ SNS (blue) and computed GRACE Δ GWS (black) showing the calculation of anomalously negative or positive values of GRACE Δ GWS that deviate substantially from underlying trends. Cases for the Upper Kalahari-Cuvelai-Zambezi Basin (11) under a semi-arid climate, the Congo Basin (10) under a tropical humid climate, and the Angara-Lena Basin (27) in given in Fig. 6.

Fig. S79. Uncertainty in the estimates of GRACE-derived GWS from 20 realisations using 3 GRACE (CSR, JPL-Mascons, GRGS) products and 4 LSMs (CLM, Noah, VIC, Mosaic) and their ensemble means for the WHYMAP large aquifer systems from no. 1 to 37, except for the High Plains Aquifer System in the USA (no. 17) which is shown as Fig. 2.

Fig. S80. (a) Location of four boreholes in northwestern Indo-Gangetic Basin, and (b) Long-term in-situ groundwater-level records ($n=4$) (source: MacDonald et al. (2016)).

Fig. S81. Long-term in-situ groundwater-level records from Makutapora Wellfield in central Tanzania ($n=5$) and Limpopo Basin in South Africa ($n=4$). Groundwater levels of from Makutapora site are referenced to a fixed datum (mean sea level, msl) and thus indicate piezometric heads; records in Limpopo Basin are plotted below groundwater level (bgl), hence the negative sign. The frequency of these multi-decadal groundwater-level records varies from daily to monthly with irregular time intervals. Annual rainfall time-series records are shown below each graph with a dashed, grey line denoting the mean of the time series.

Supplementary Fig. S1–S81:

Fig. S1: Nubian Sandstone Aquifer System (1)

Basin-averaged — Non-linear trend — Linear trend - - -

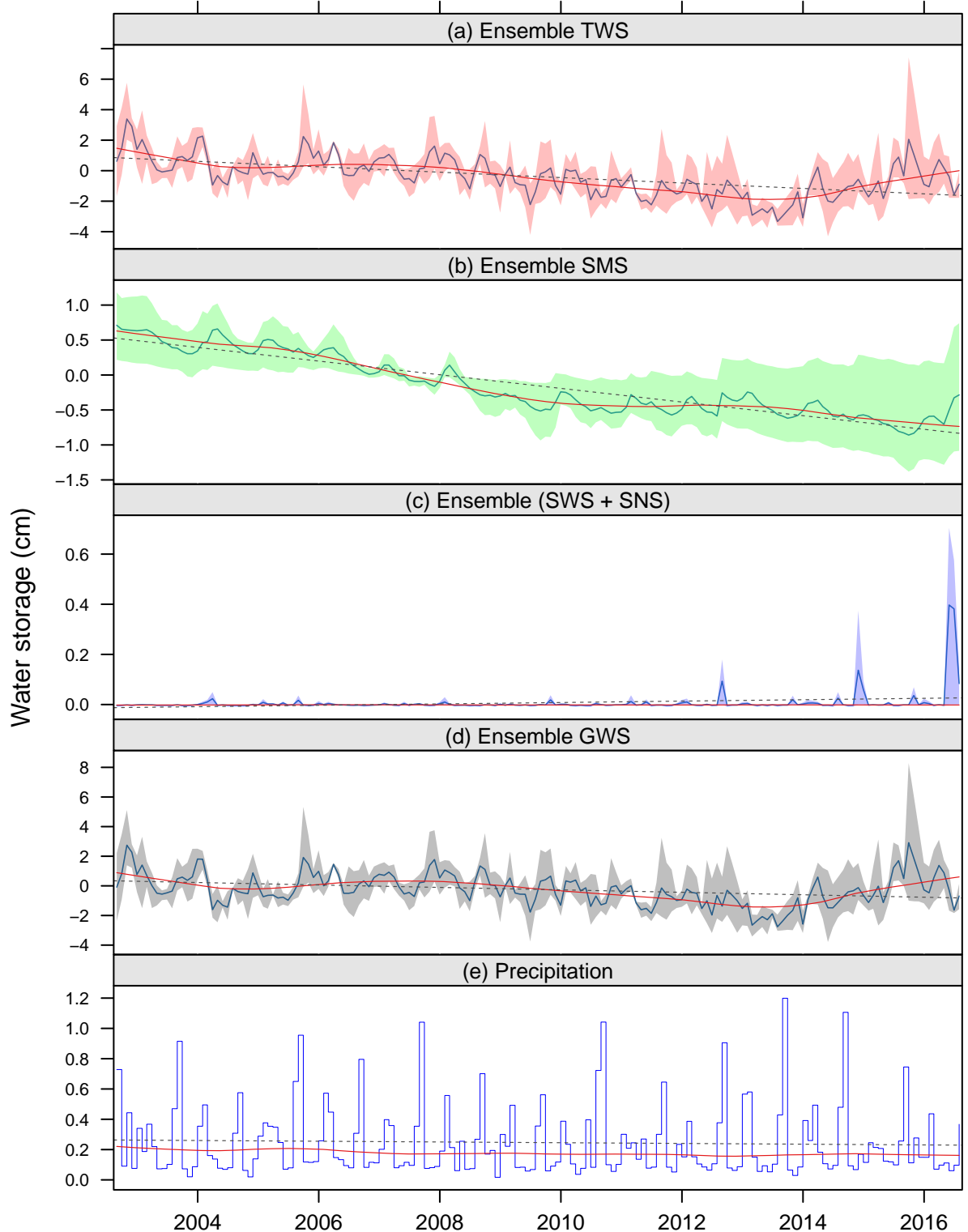


Fig. S2: Northwestern Sahara Aquifer System (2)

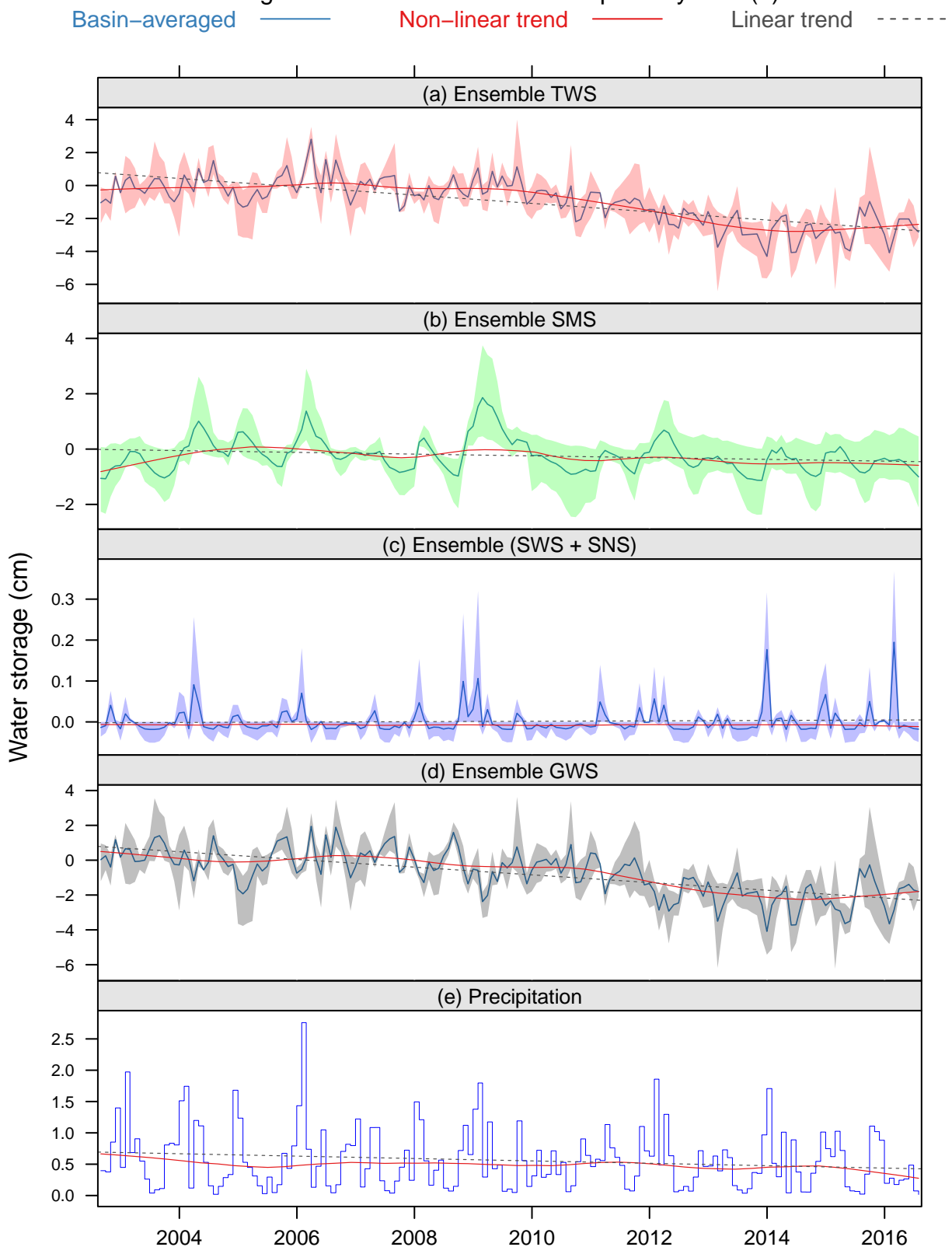


Fig. S3: Murzuk–Djado Basin (3)

Basin-averaged — Non-linear trend — Linear trend - - -

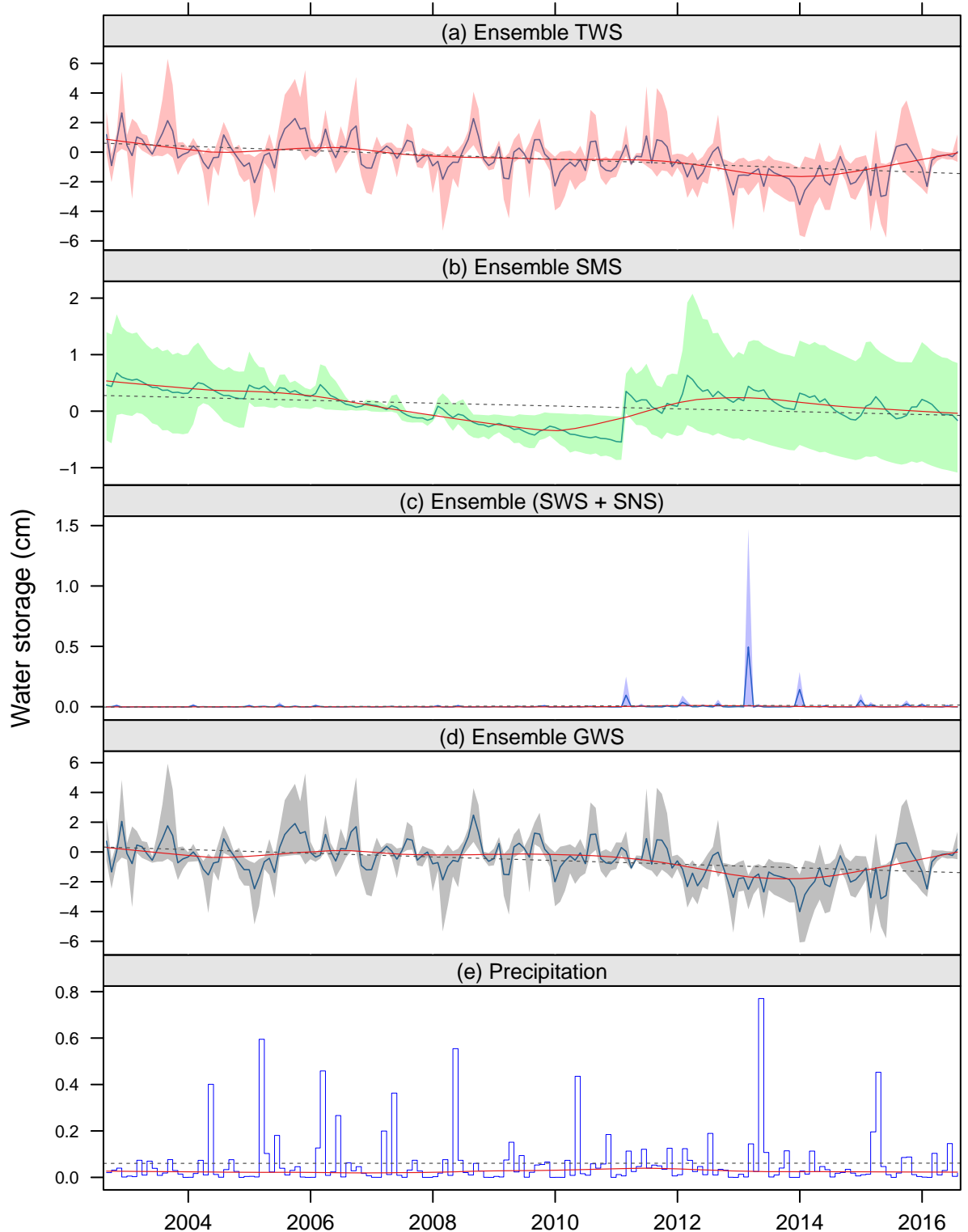


Fig. S4: Taoudeni–Tanezrouft Basin (4)

Basin-averaged — Non-linear trend — Linear trend - - -

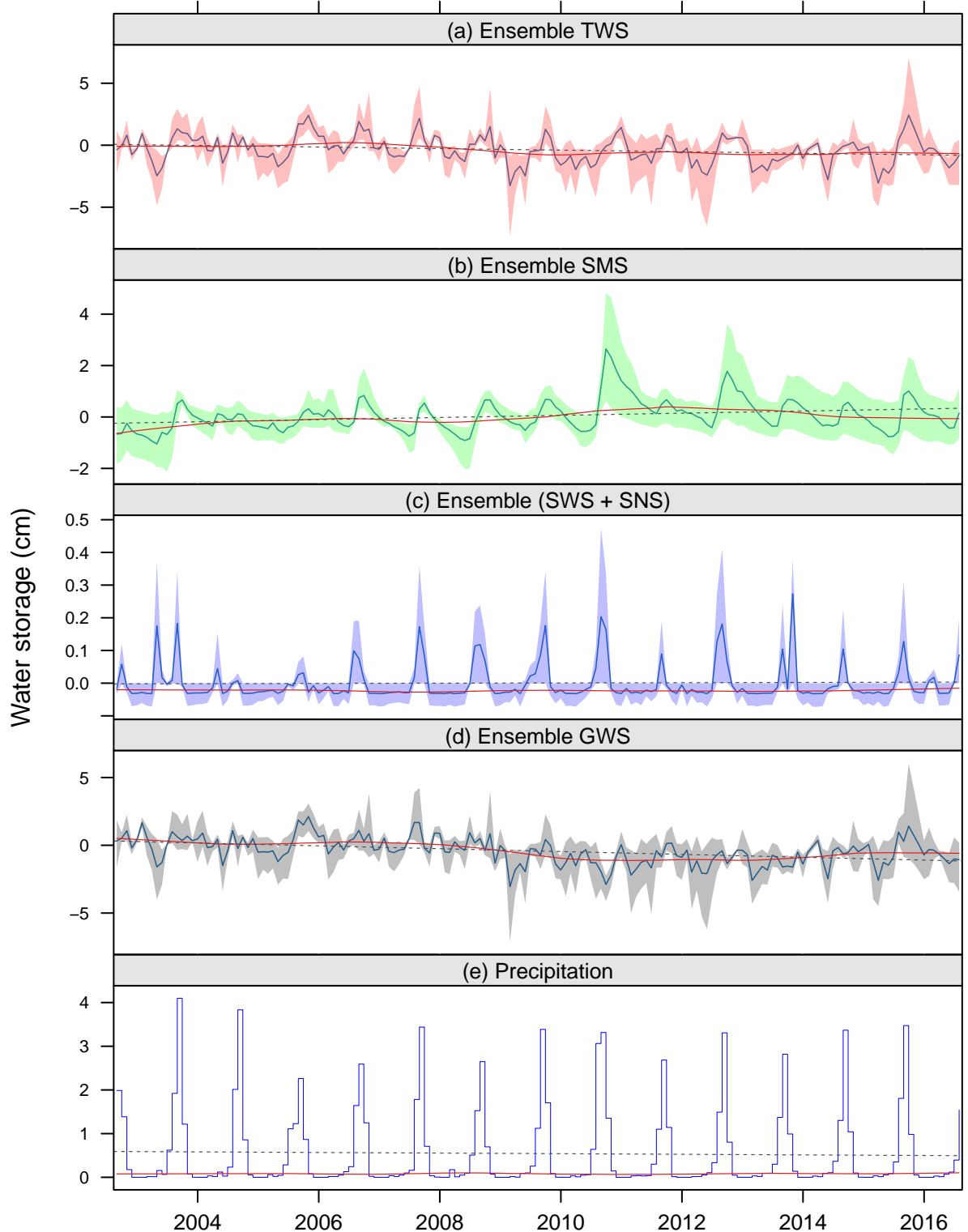


Fig. S5: Senegal–Mauritanian Basin (5)

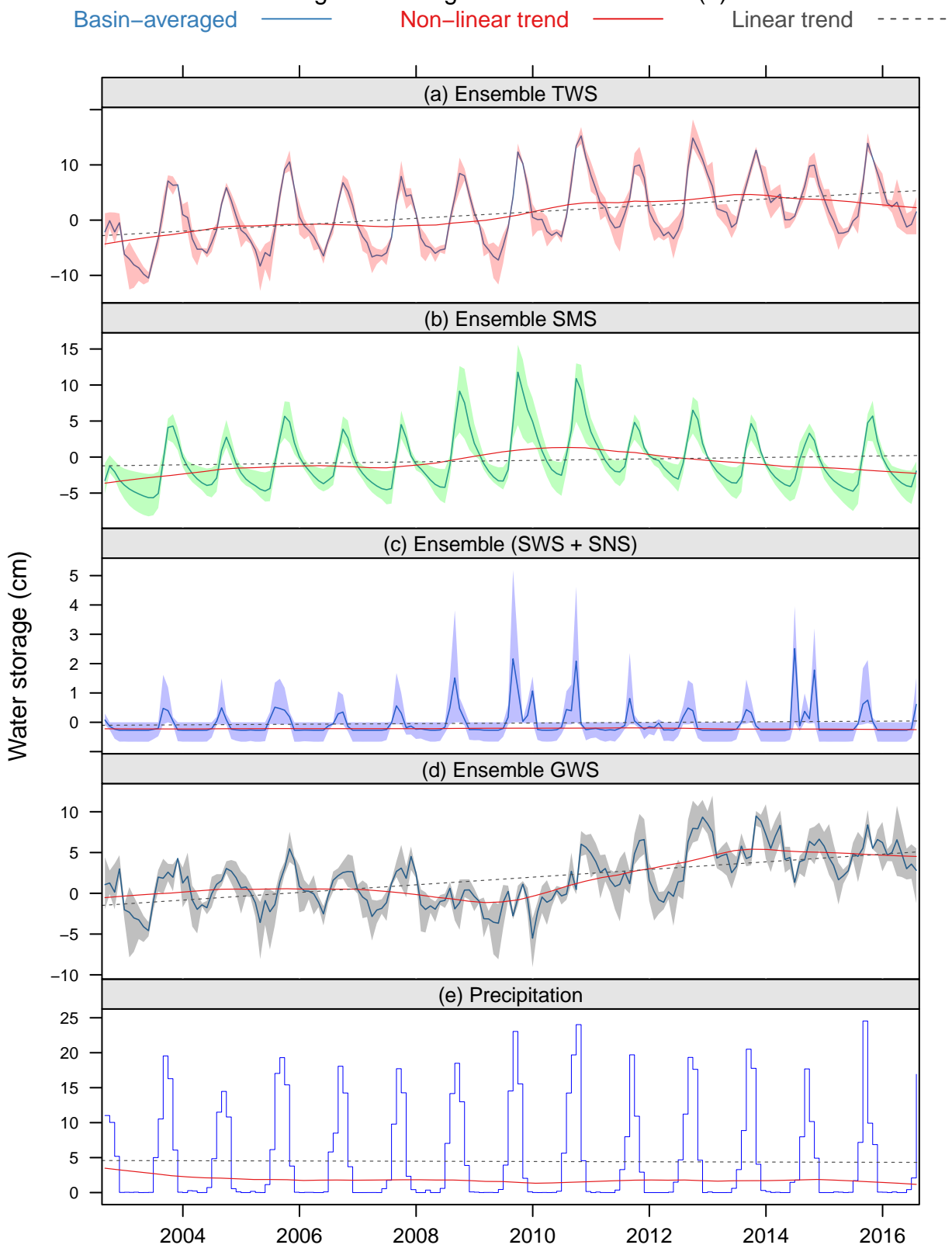


Fig. S6: Iullemmeden–Irhazer Aquifer System (6)

Basin-averaged — Non-linear trend — Linear trend - - -

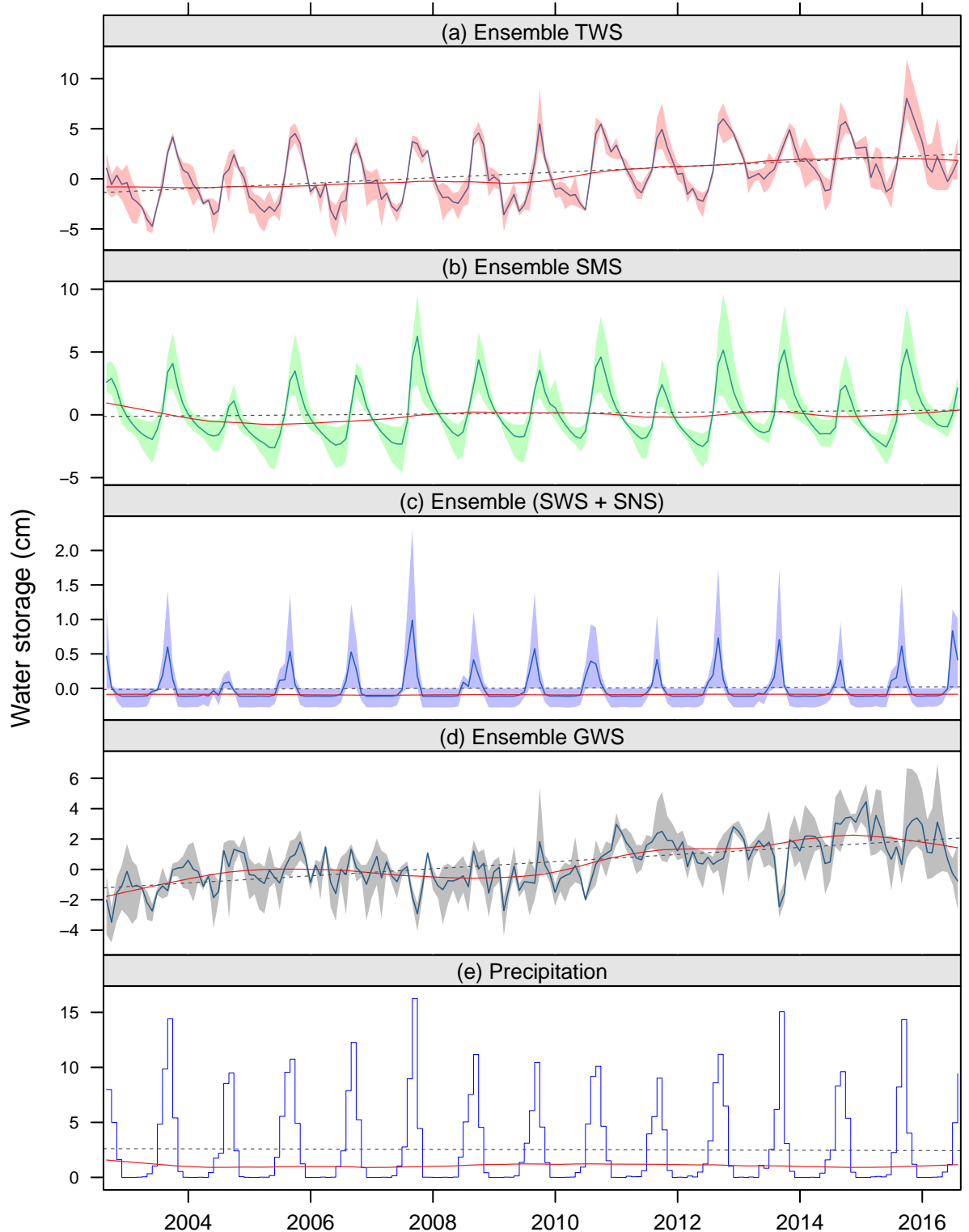


Fig. S7: Lake Chad Basin (7)

Basin-averaged — Non-linear trend — Linear trend - - -

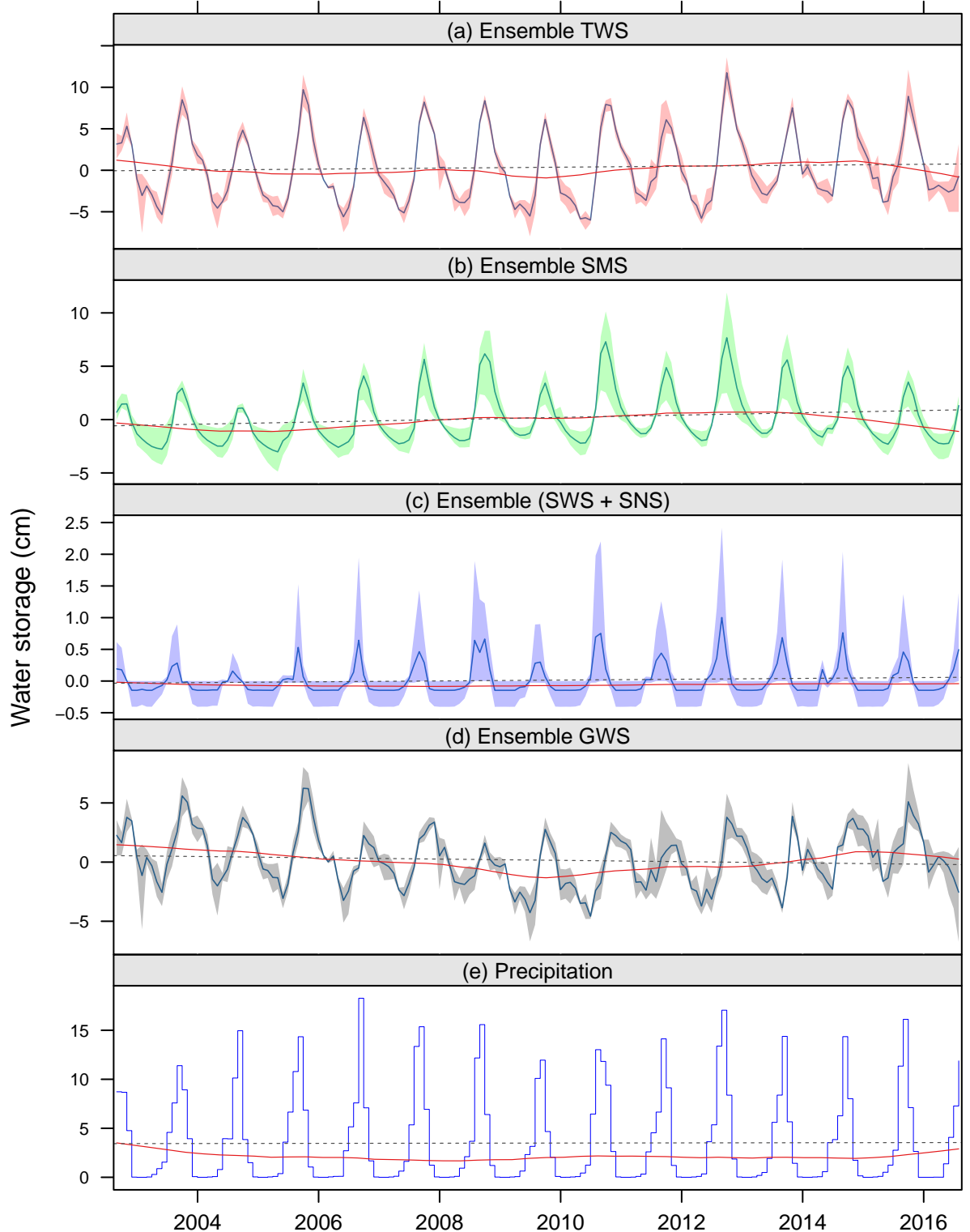


Fig. S8: Umm Ruwaba Aquifer (Sudd Basin) (8)

Basin-averaged — Non-linear trend — Linear trend - - -

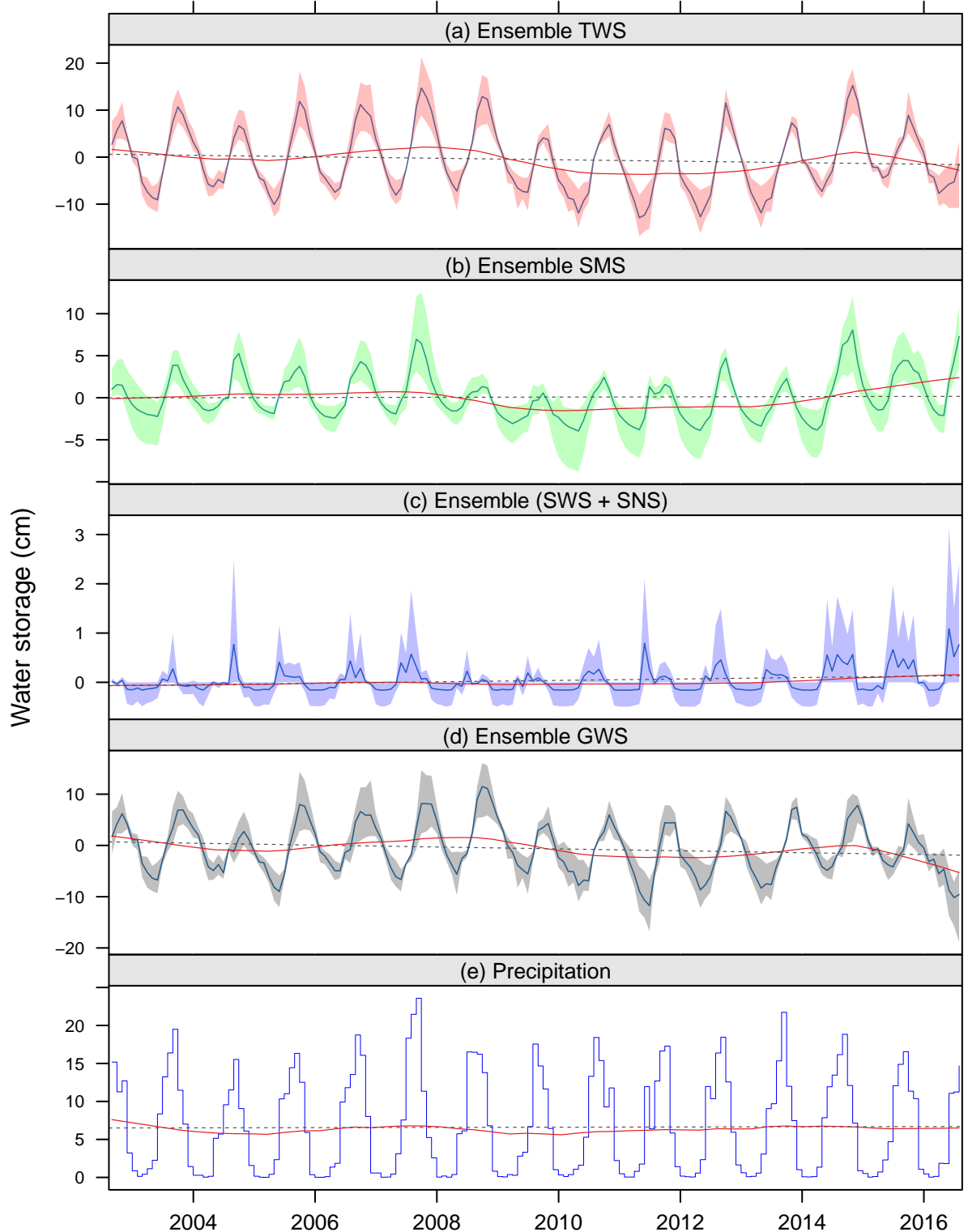


Fig. S9: Ogaden–Juba Basin (9)

Basin-averaged — Non-linear trend — Linear trend - - -

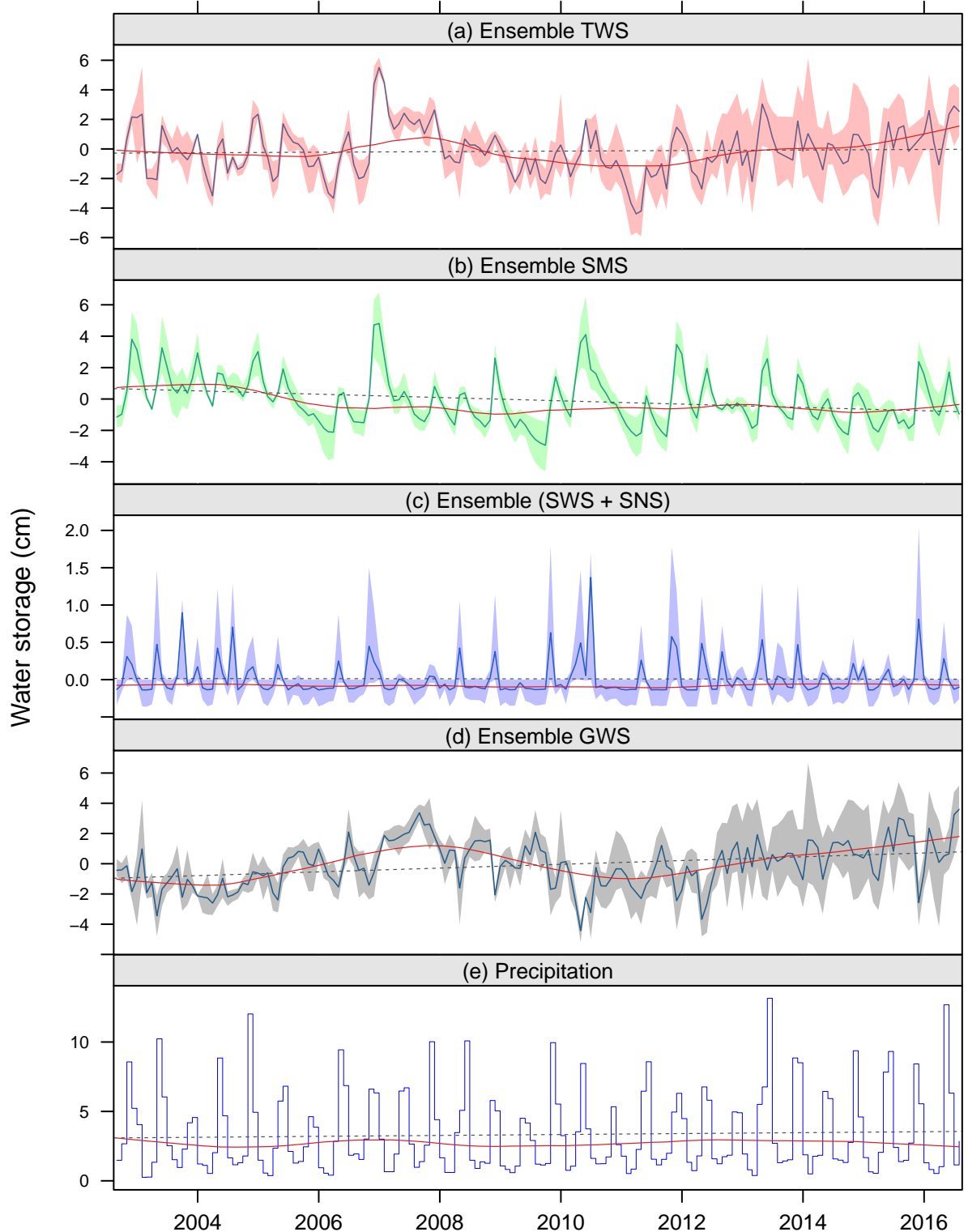
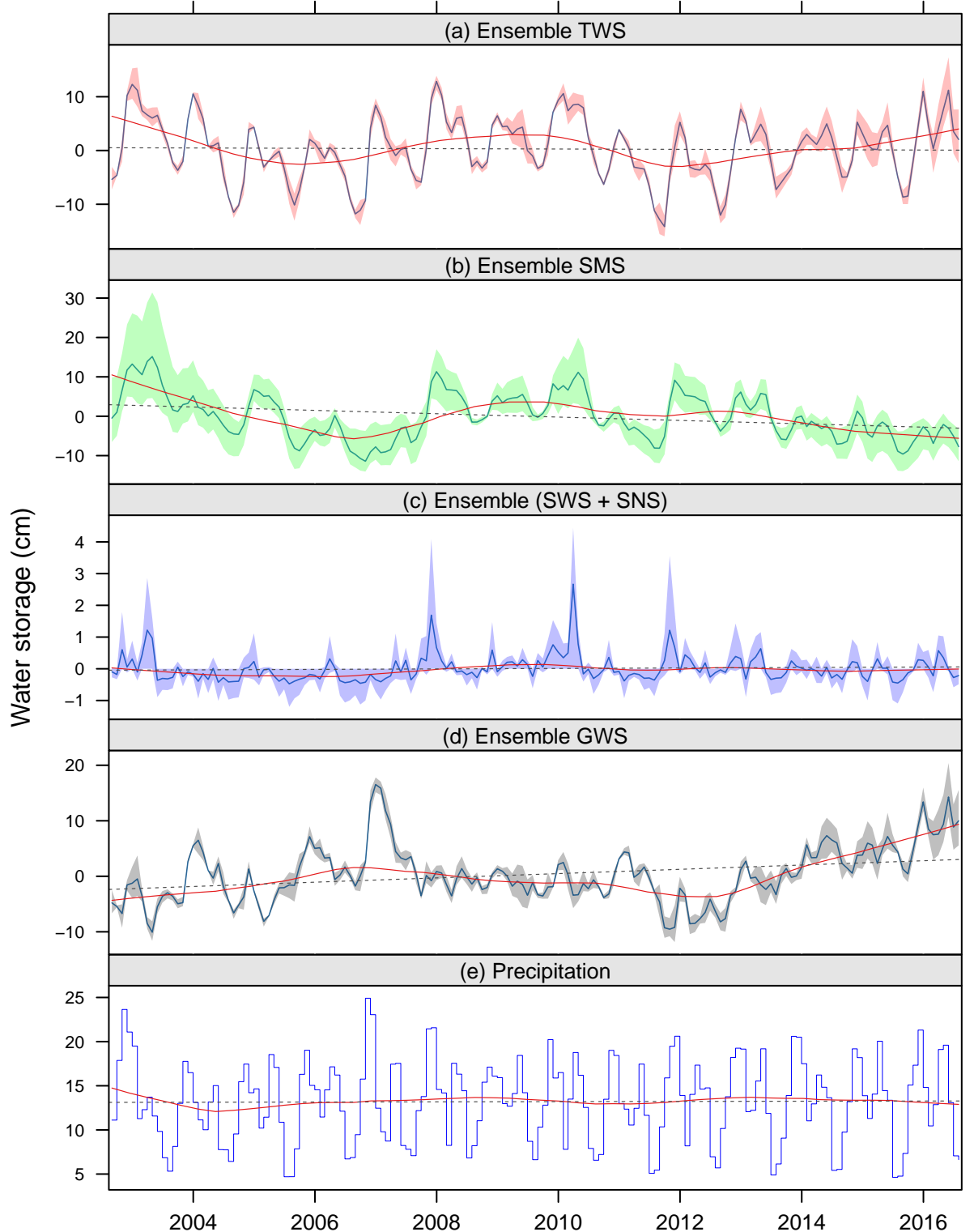
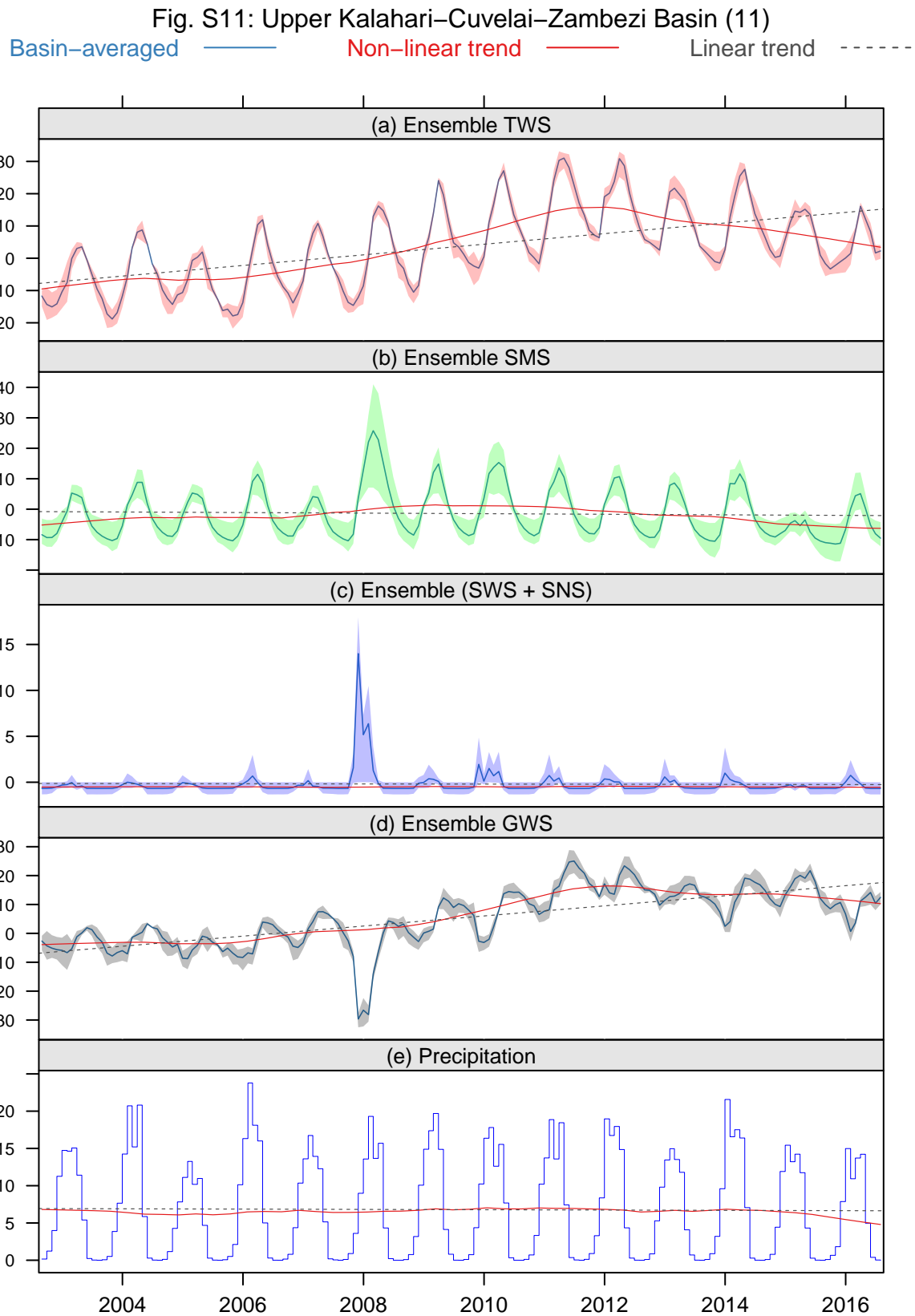


Fig. S10: Congo Basin (10)

Basin-averaged — Non-linear trend — Linear trend - - -





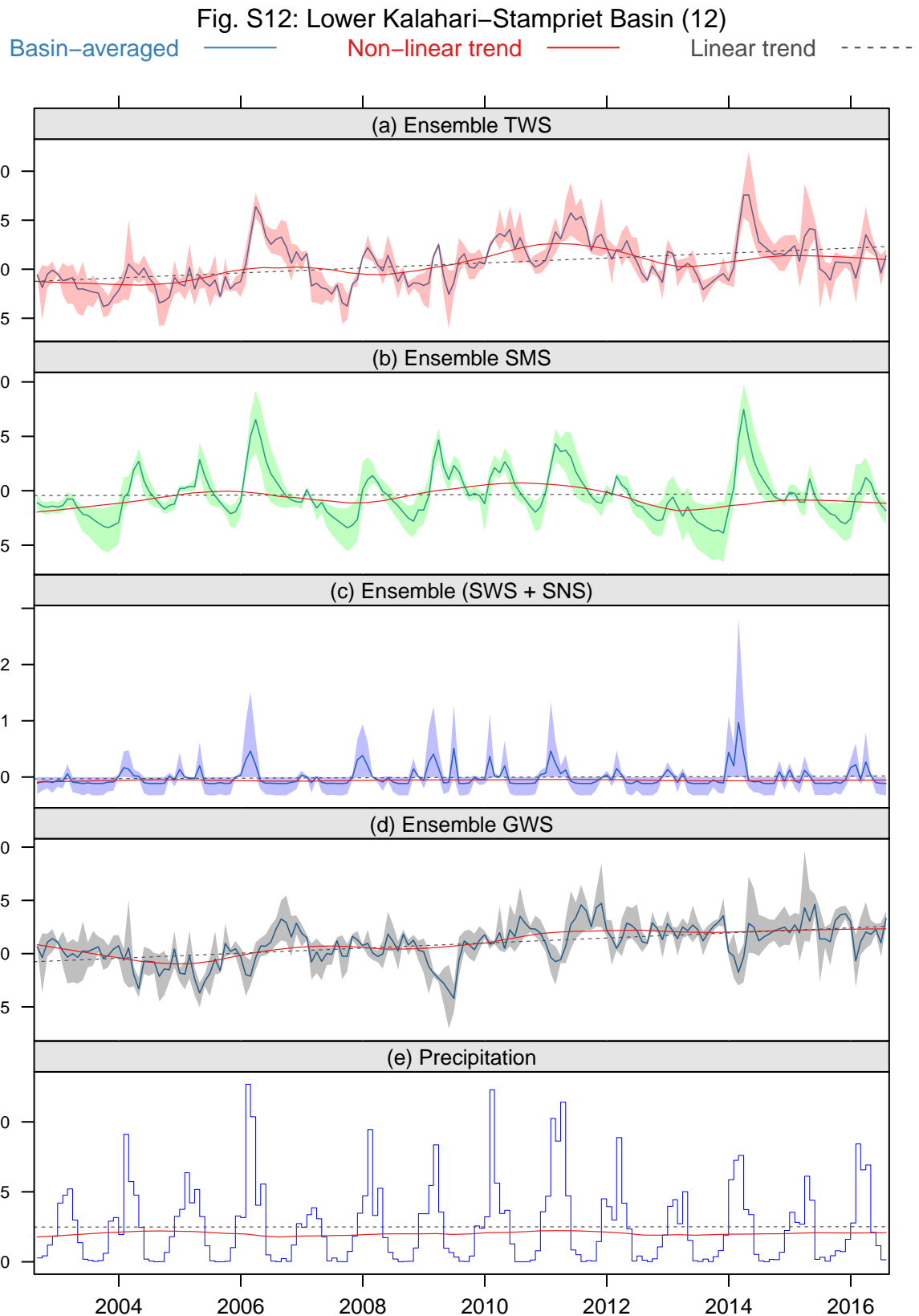
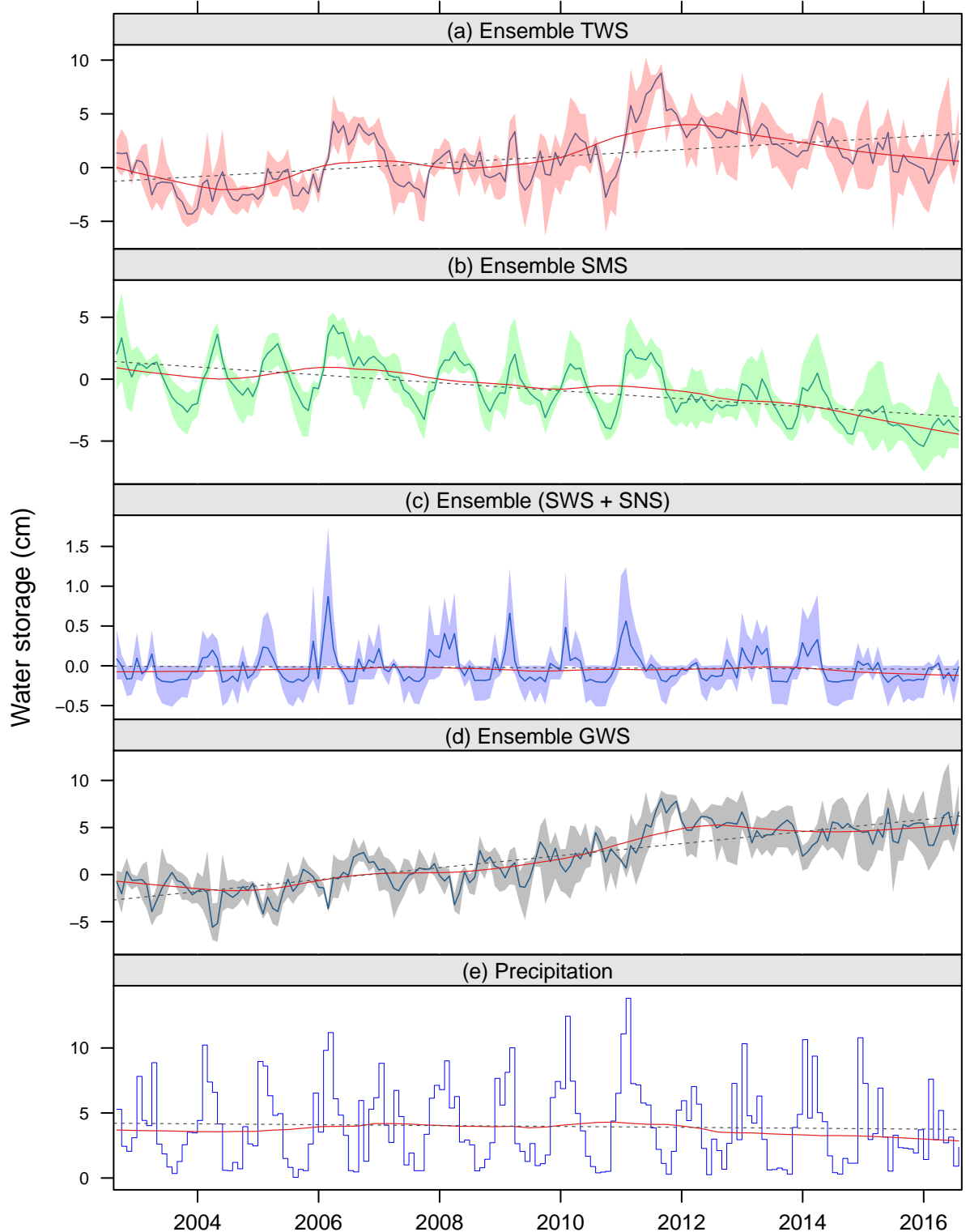


Fig. S13: Karoo Basin (13)

Basin-averaged — Non-linear trend — Linear trend - - -



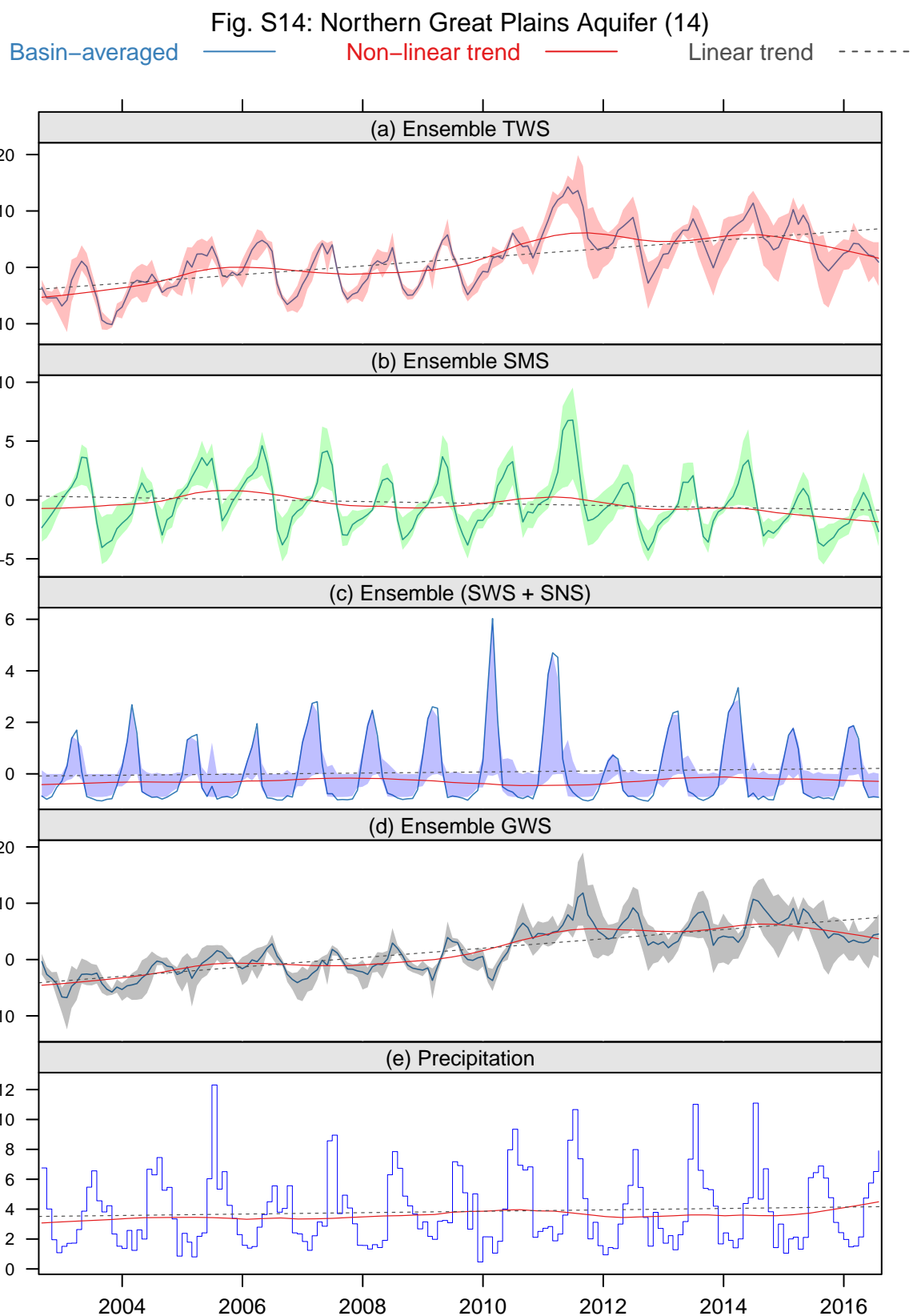


Fig. S15: Cambro–Ordovician Aquifer System (15)

Basin-averaged — Non-linear trend — Linear trend - - -

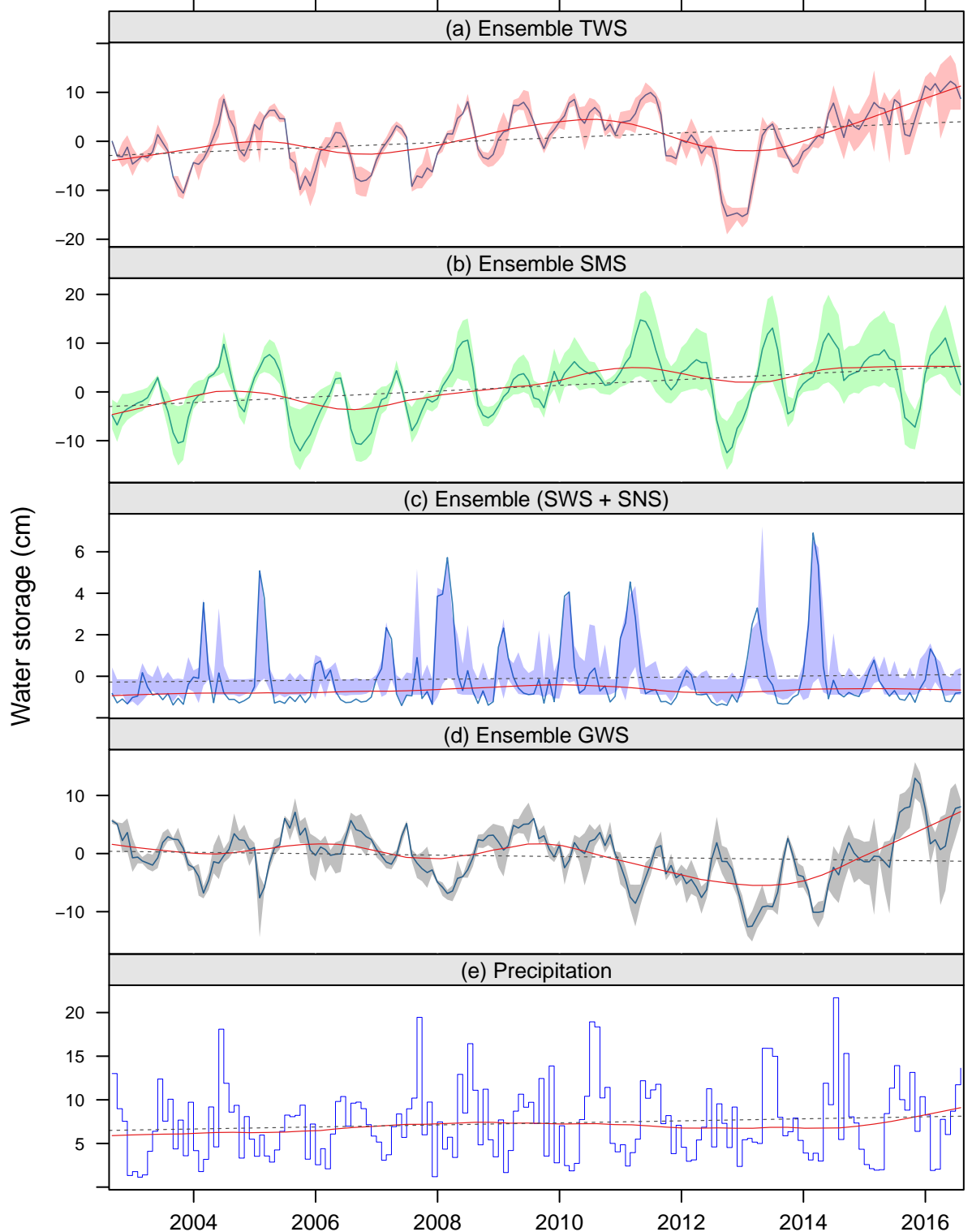
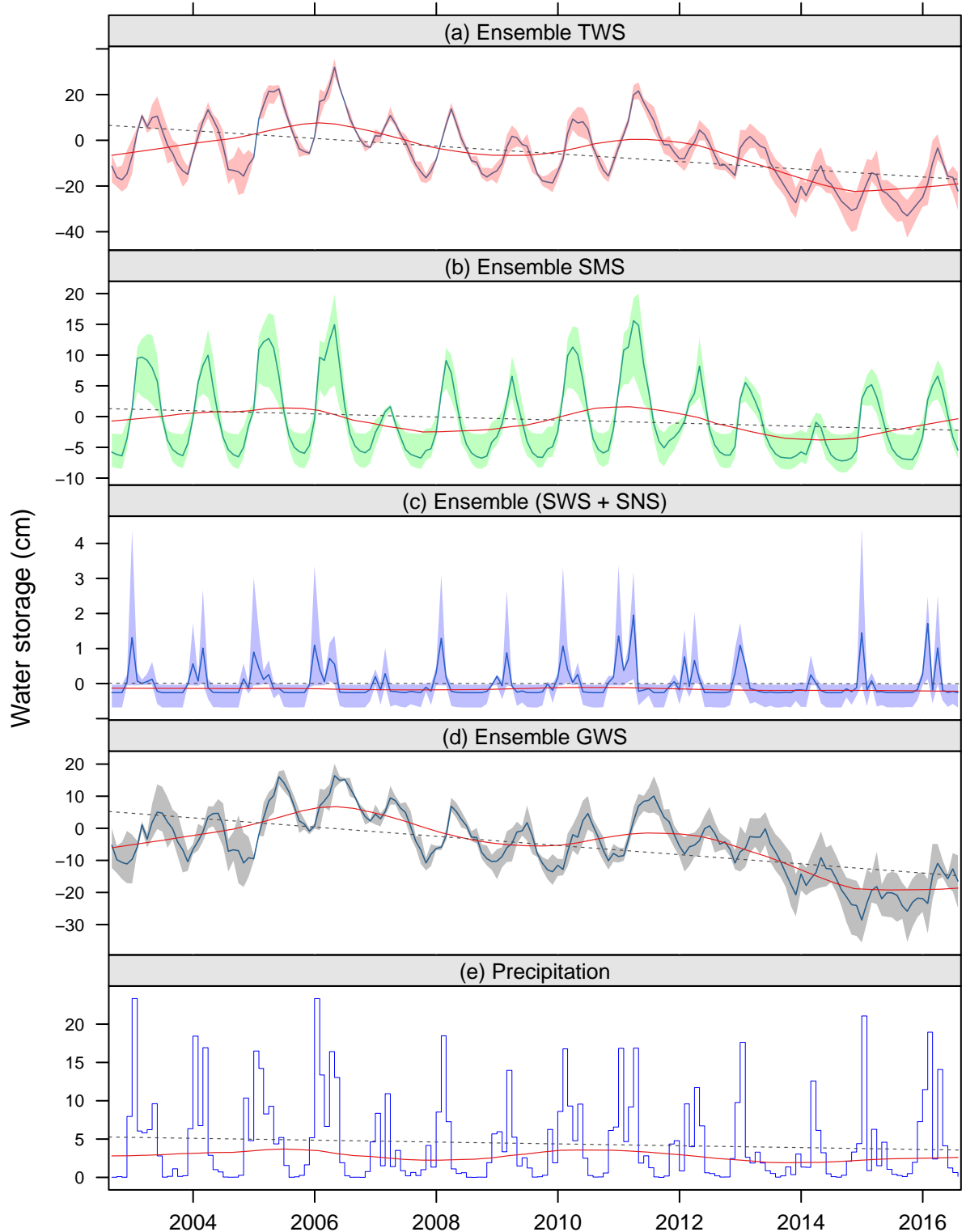


Fig. S16: California Central Valley Aquifer System (16)

Basin-averaged — Non-linear trend — Linear trend - - -



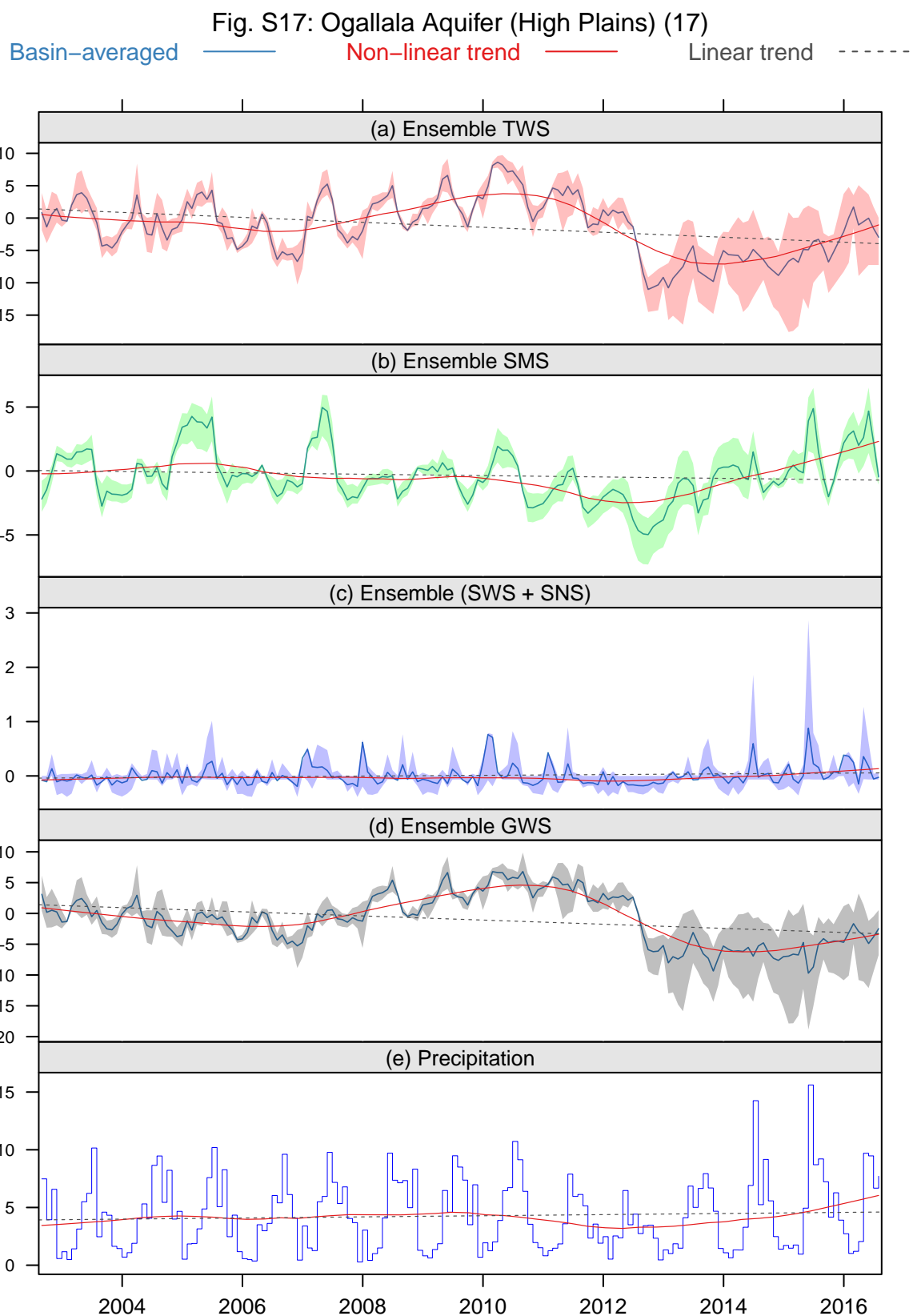
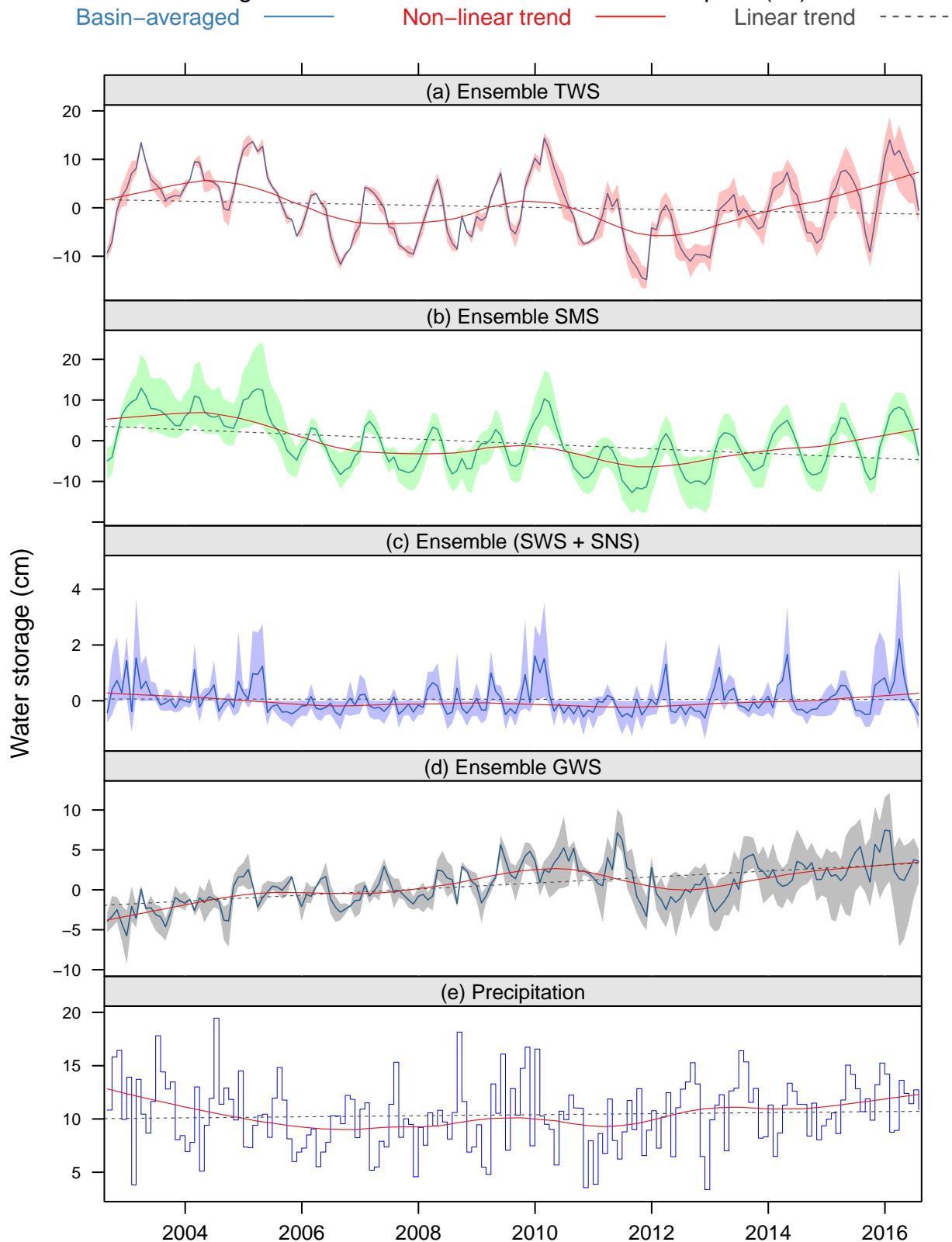


Fig. S17: Atlantic and Gulf Coastal Plains Aquifer (18)



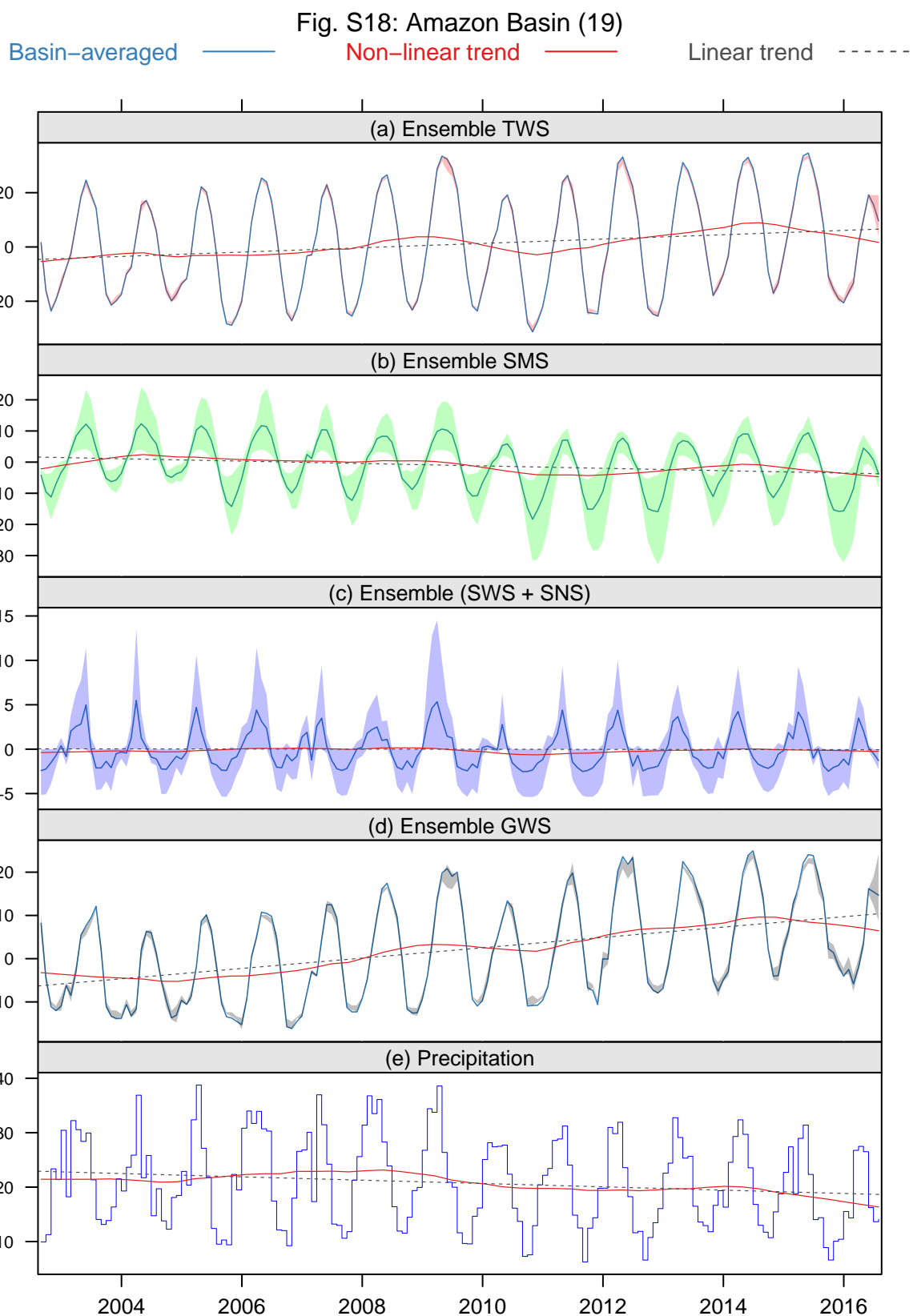


Fig. S19: Maranhao Basin (20)

Basin-averaged — Non-linear trend — Linear trend - - -

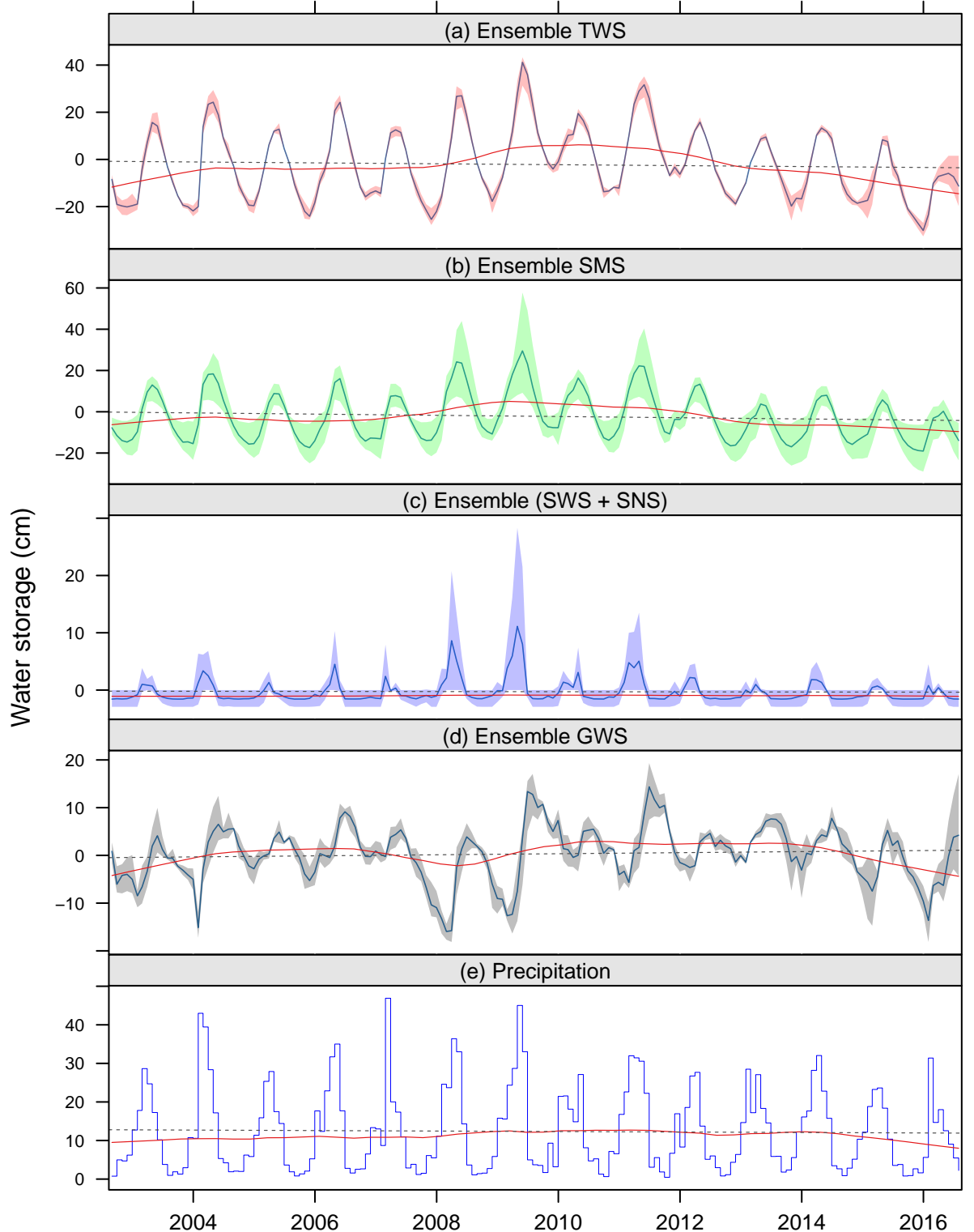


Fig. S20: Guarani Aquifer System (Parana Basin) (21)

Basin-averaged — Non-linear trend — Linear trend - - -

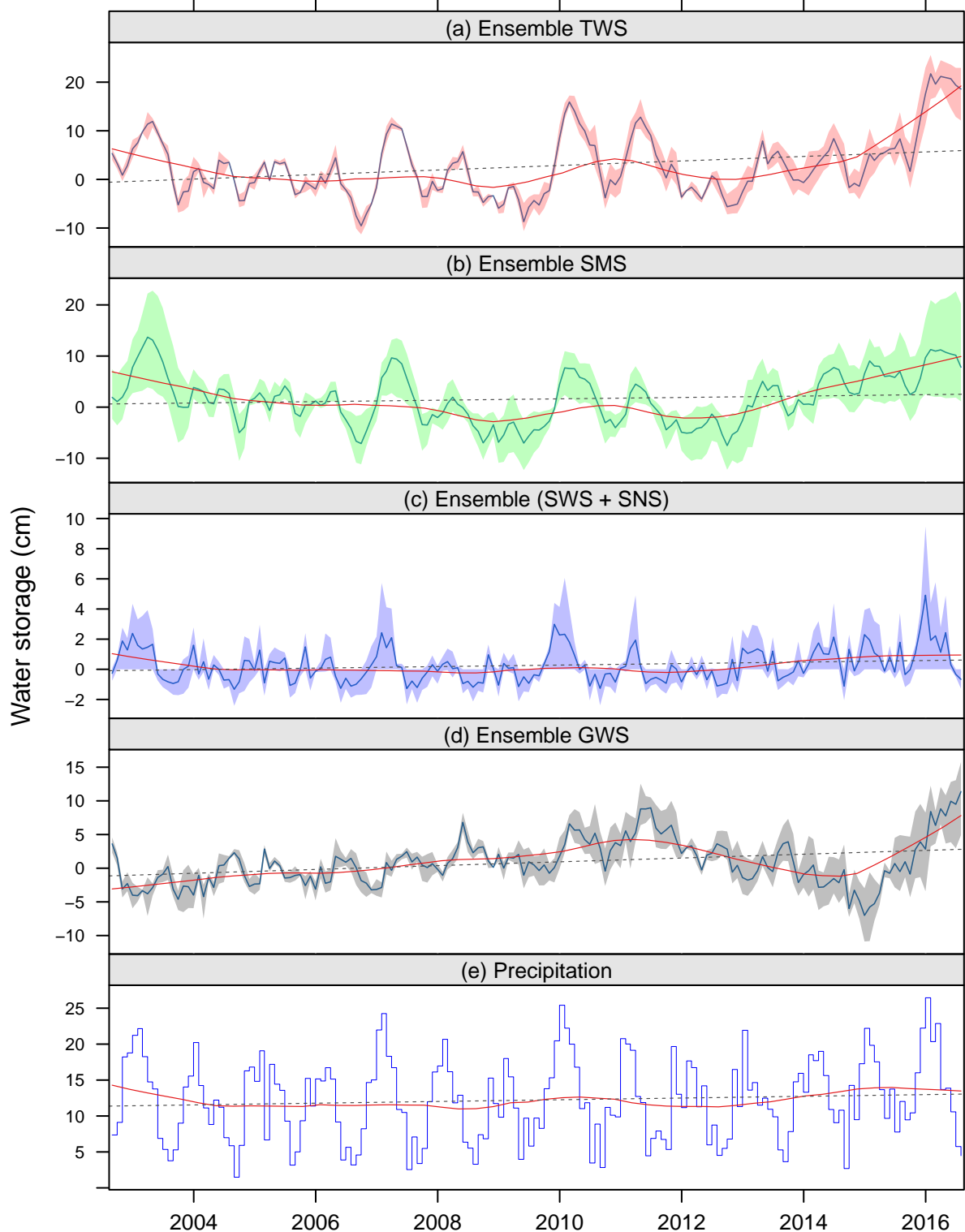


Fig. S21: Arabian Aquifer System (22)

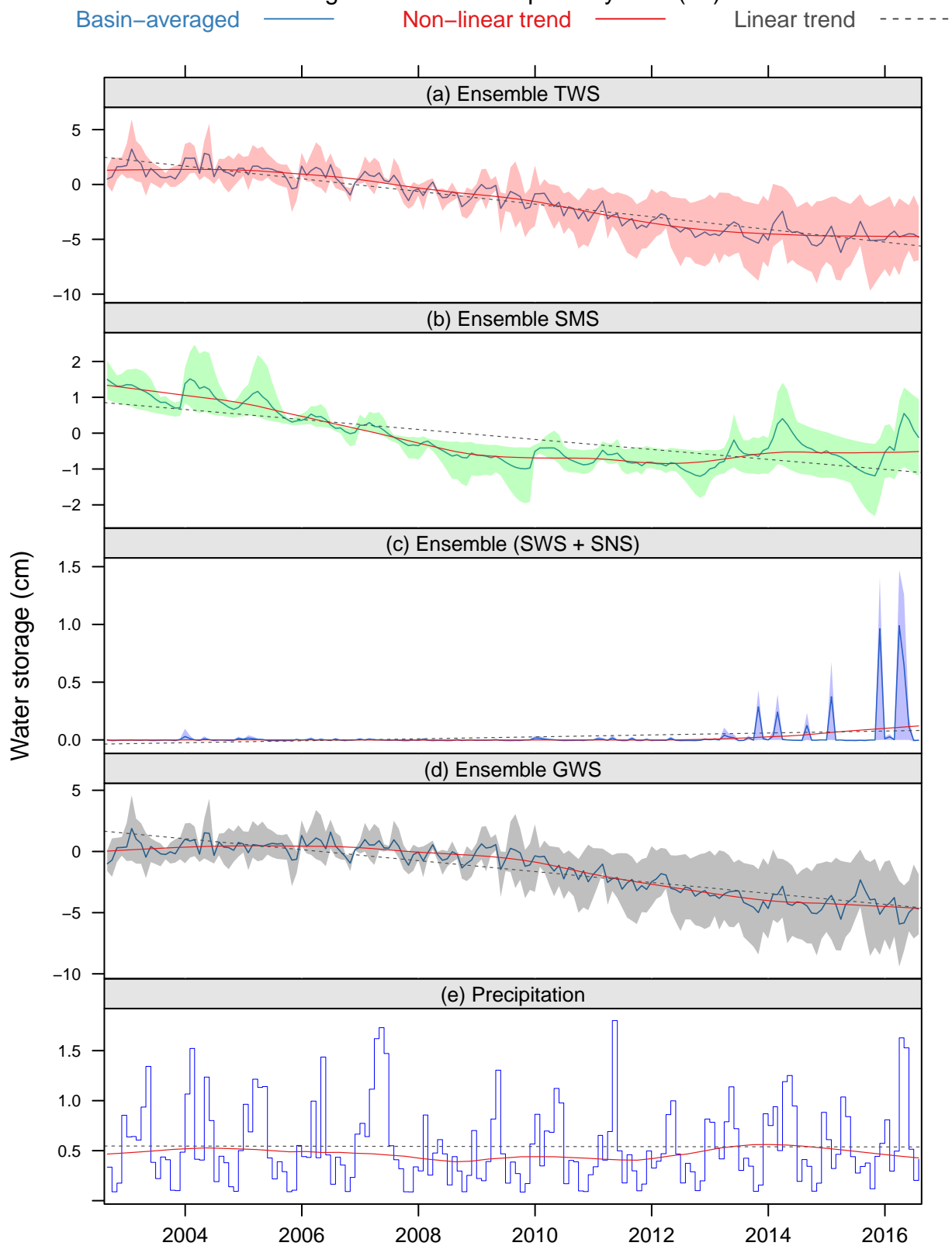


Fig. S22: Indus River Basin (23)

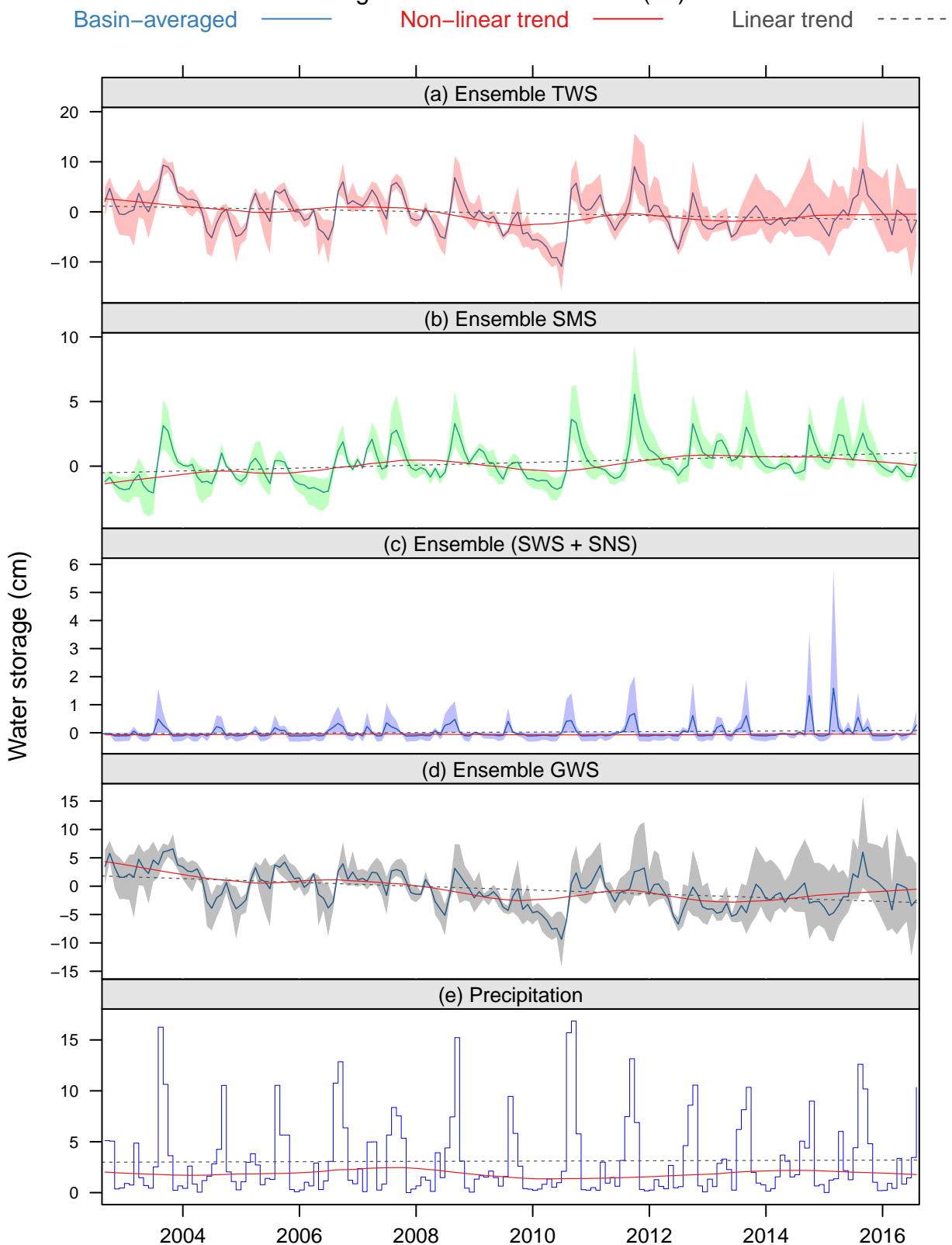


Fig. S23: Ganges–Brahmaputra River Basin (24)

Basin-averaged — Non-linear trend — Linear trend - - -

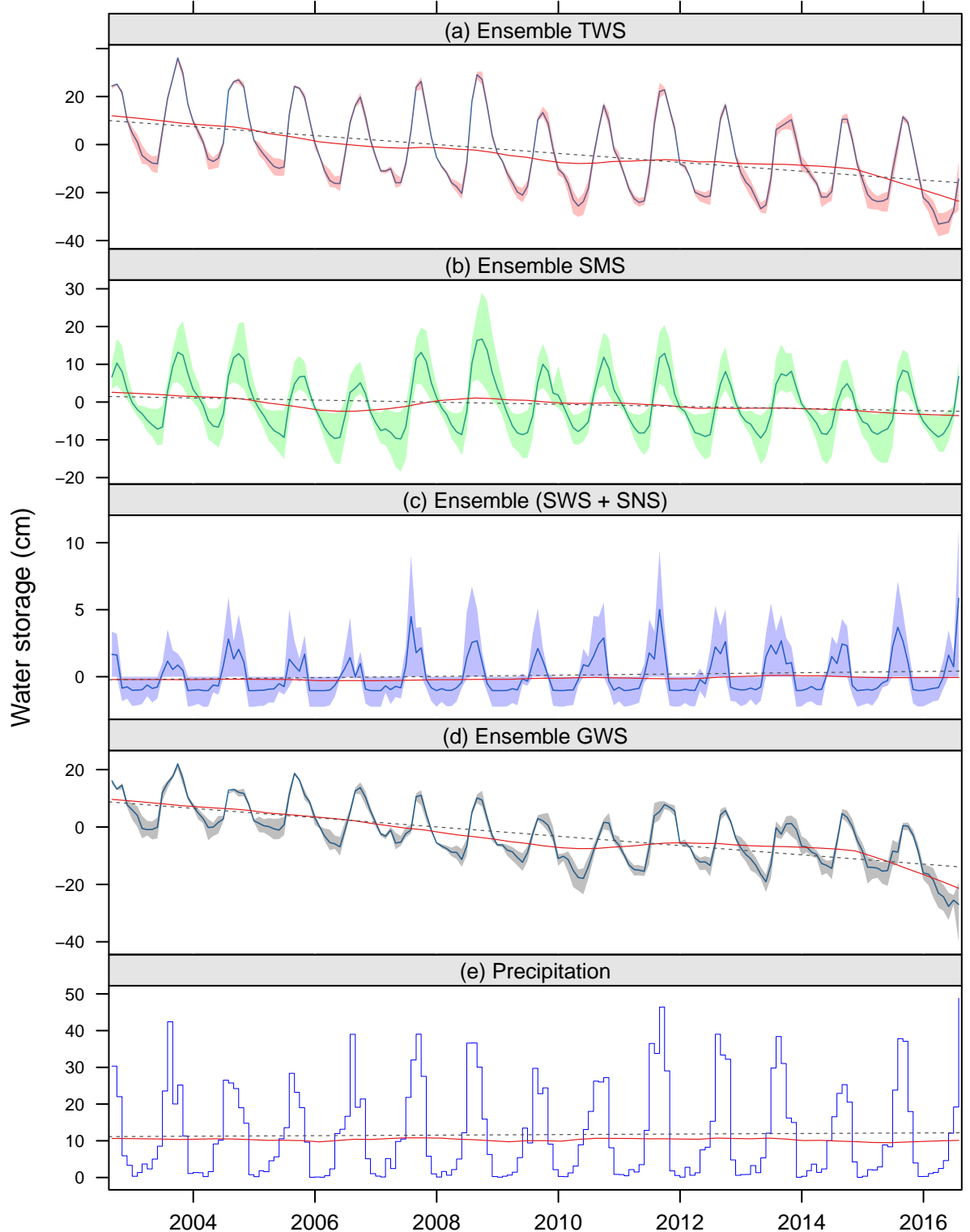
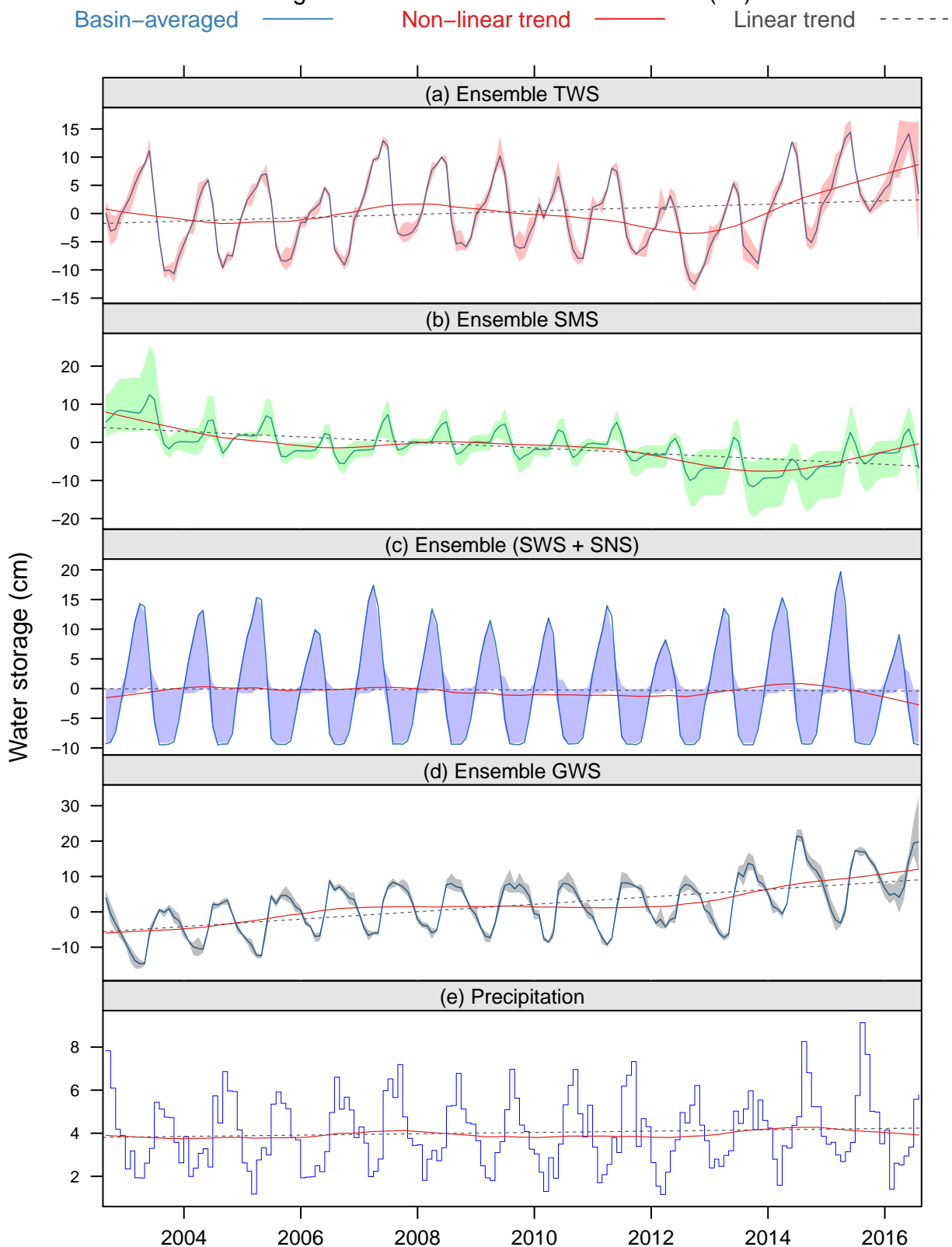


Fig. S24: West Siberian Artesian Basin (25)



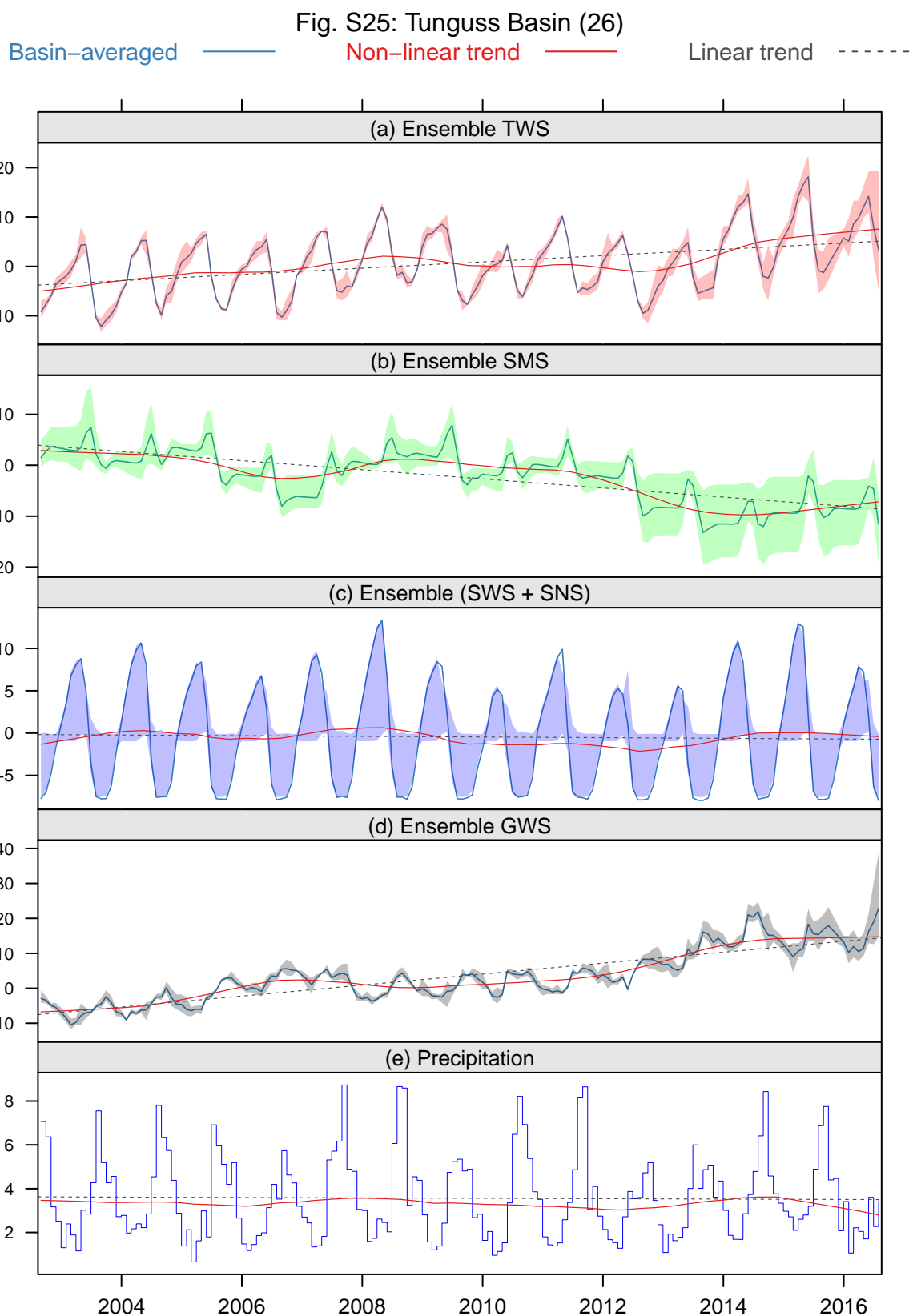


Fig. S26: Angara–Lena Basin (27)

Basin-averaged — Non-linear trend — Linear trend - - -

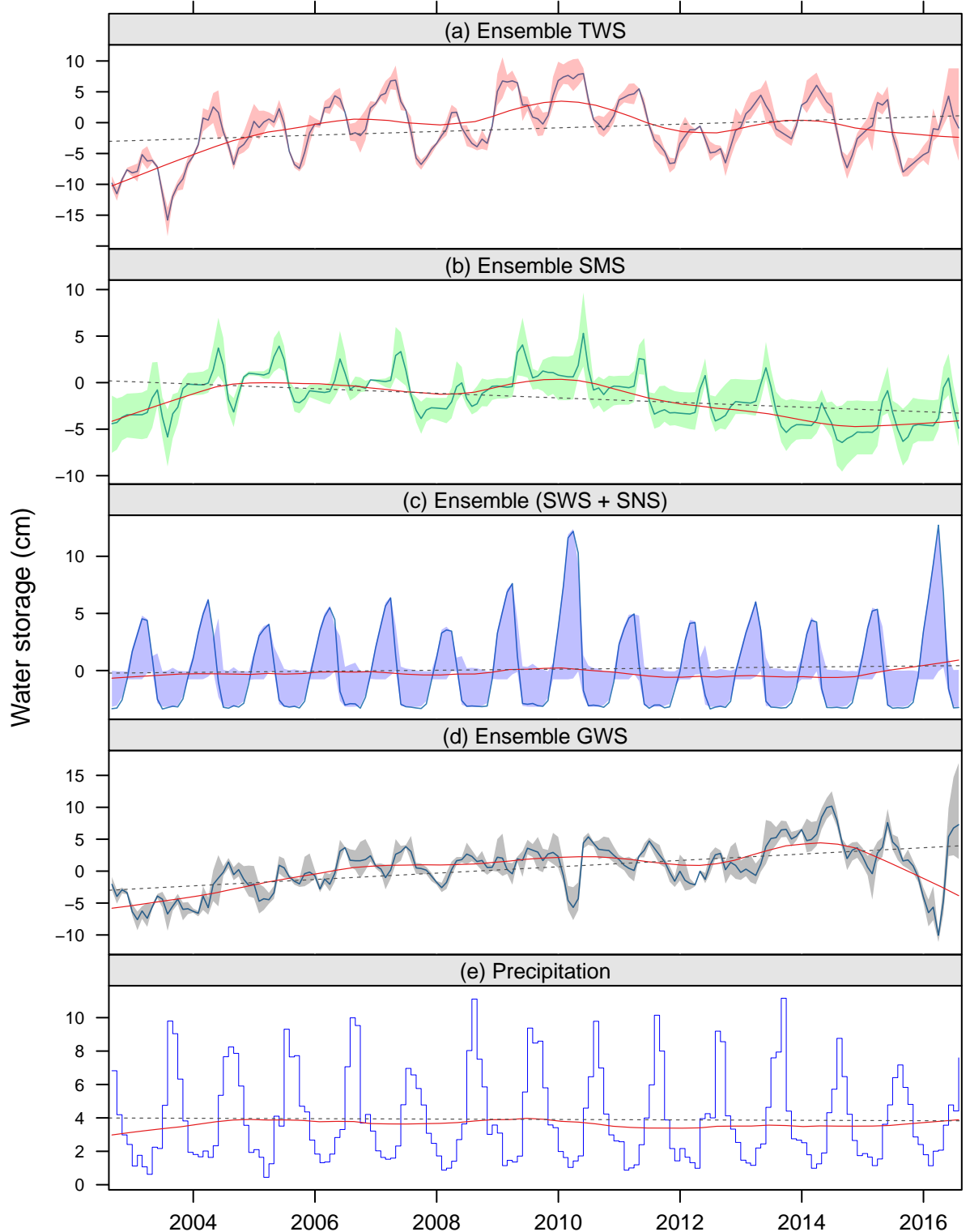


Fig. S27: Yakut Basin (28)

Basin-averaged — Non-linear trend — Linear trend - - -

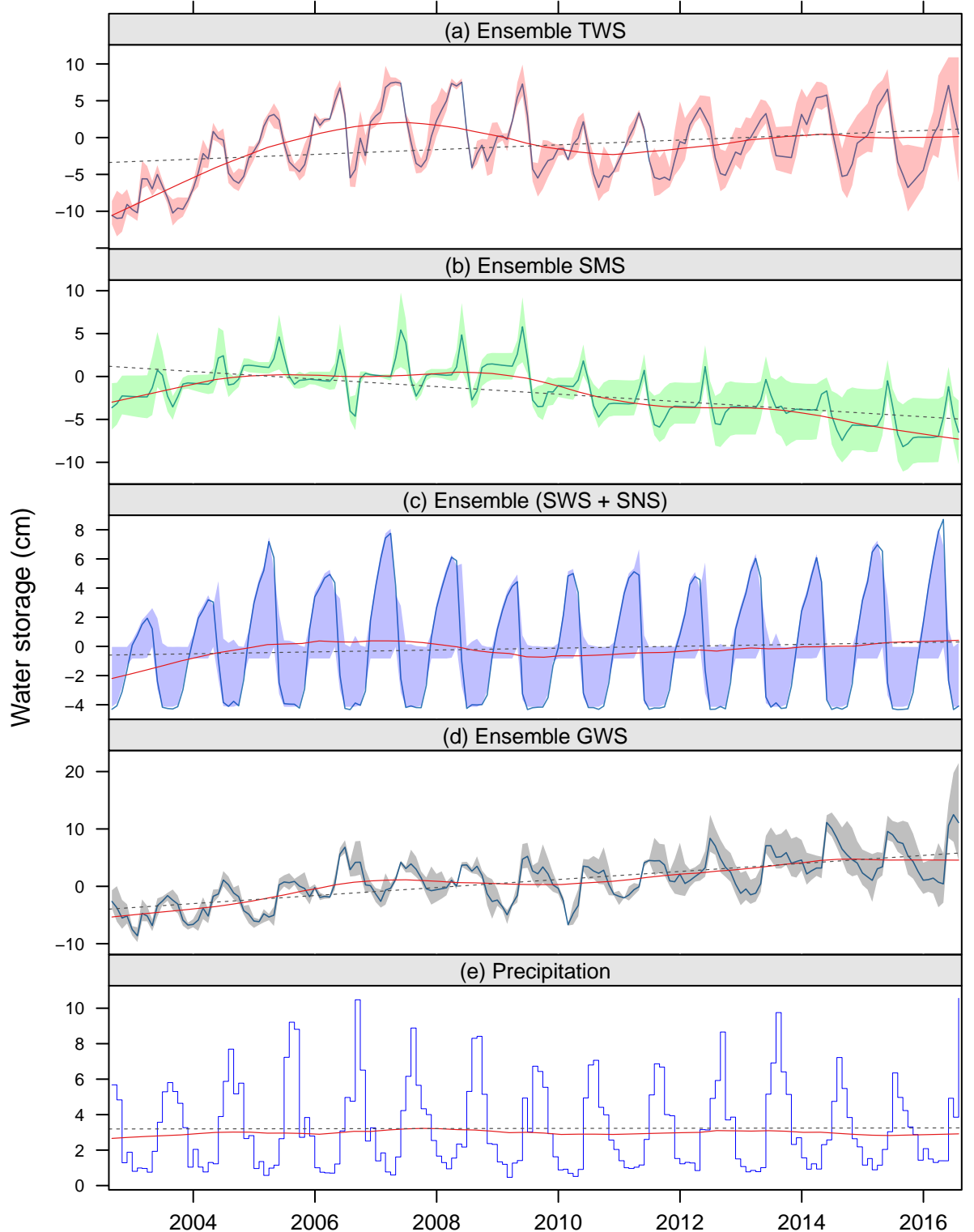


Fig. S28: North China Plains Aquifer System (29)

Basin-averaged — Non-linear trend — Linear trend - - -

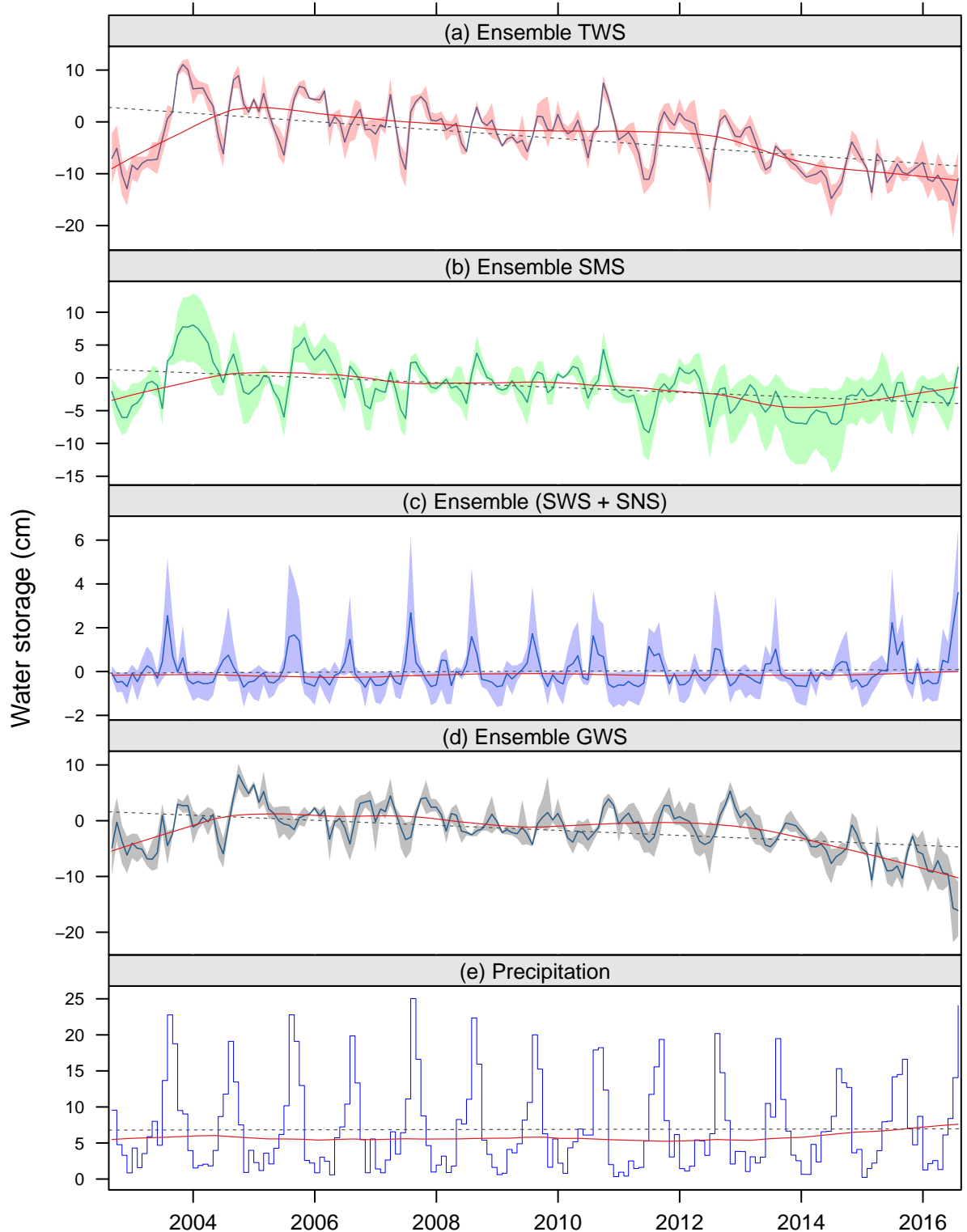


Fig. S29: Song-Liao Plain (30)

Basin-averaged — Non-linear trend — Linear trend - - -

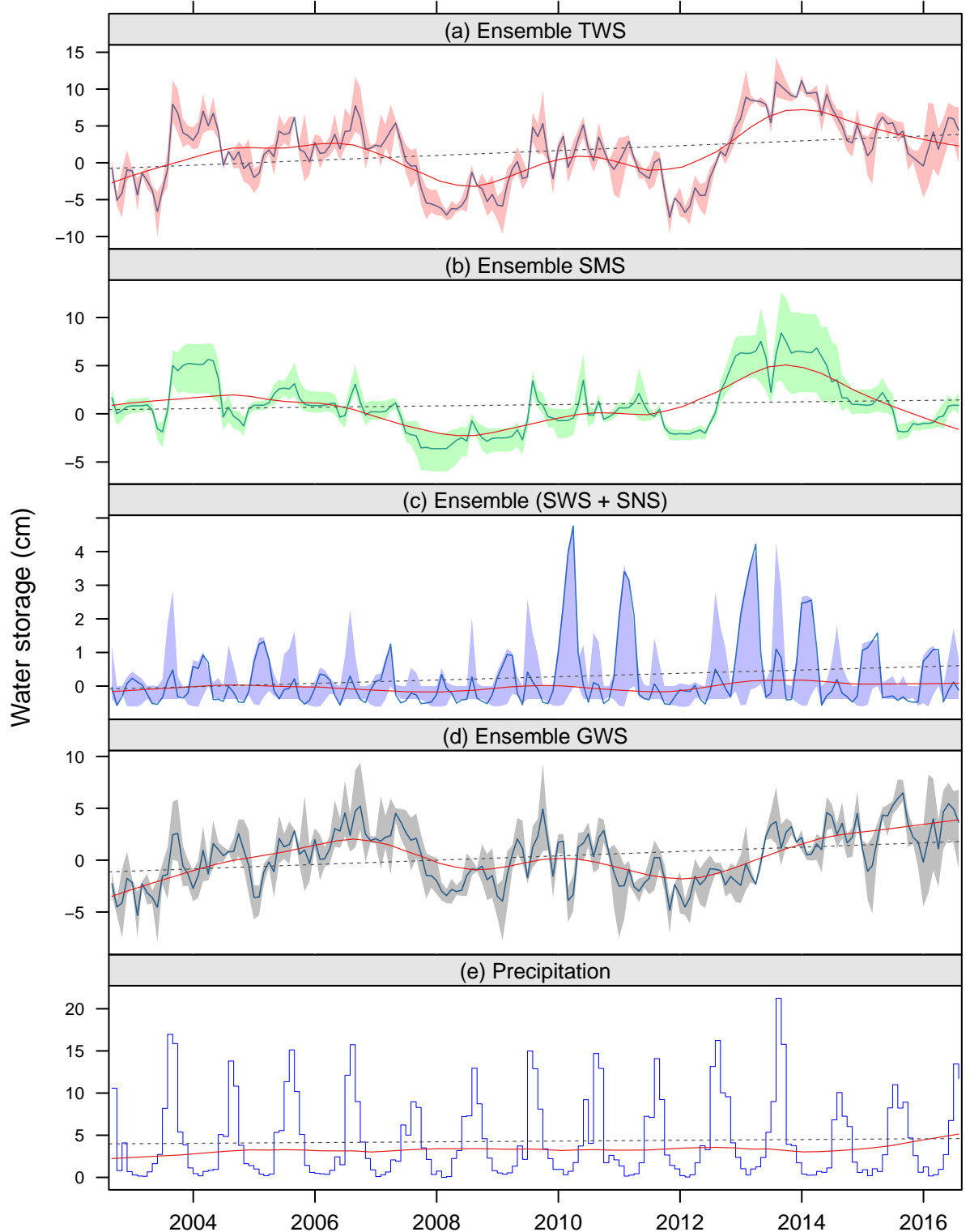


Fig. S30: Tarim Basin (31)

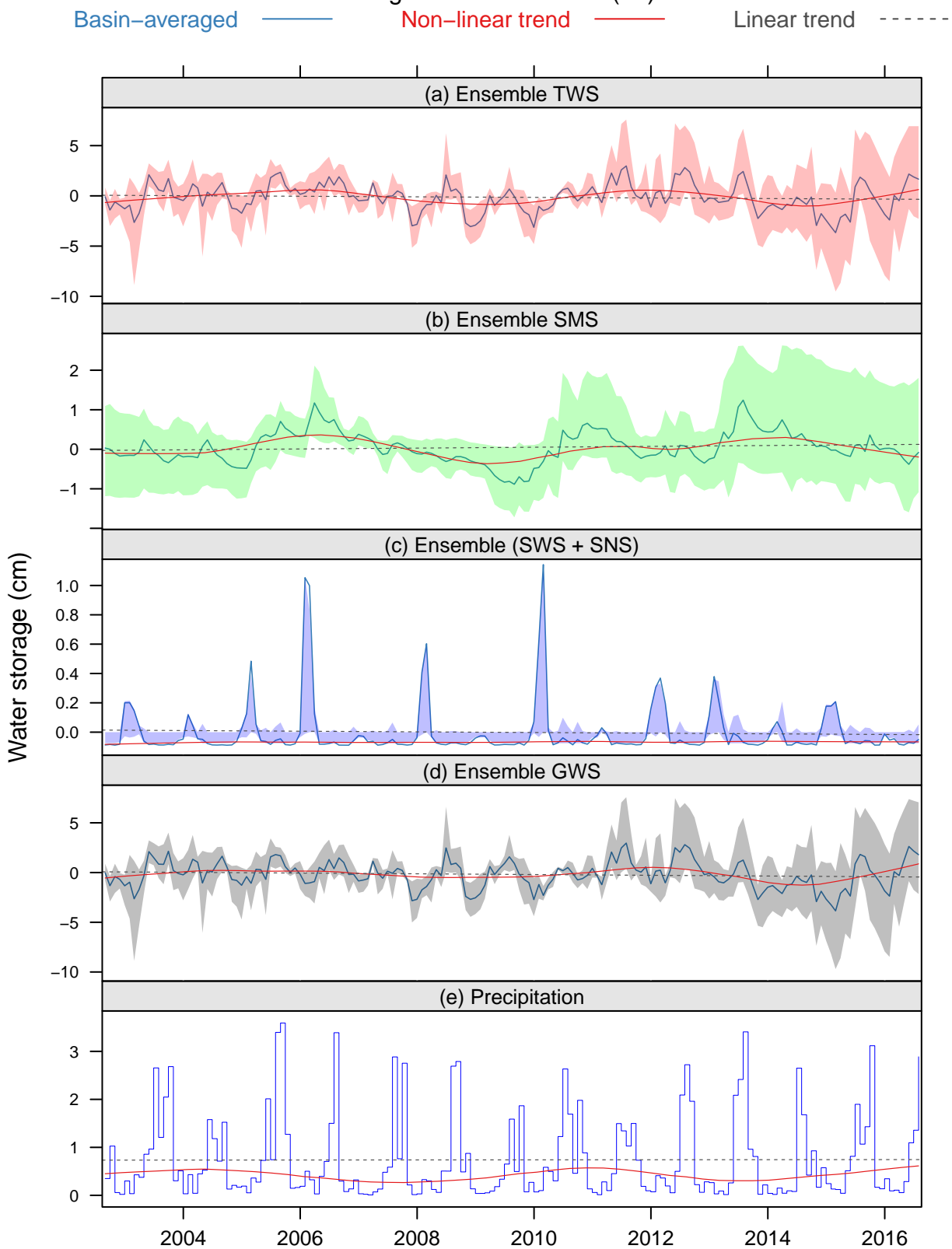


Fig. S31: Paris Basin (32)

Basin-averaged — Non-linear trend — Linear trend - - -

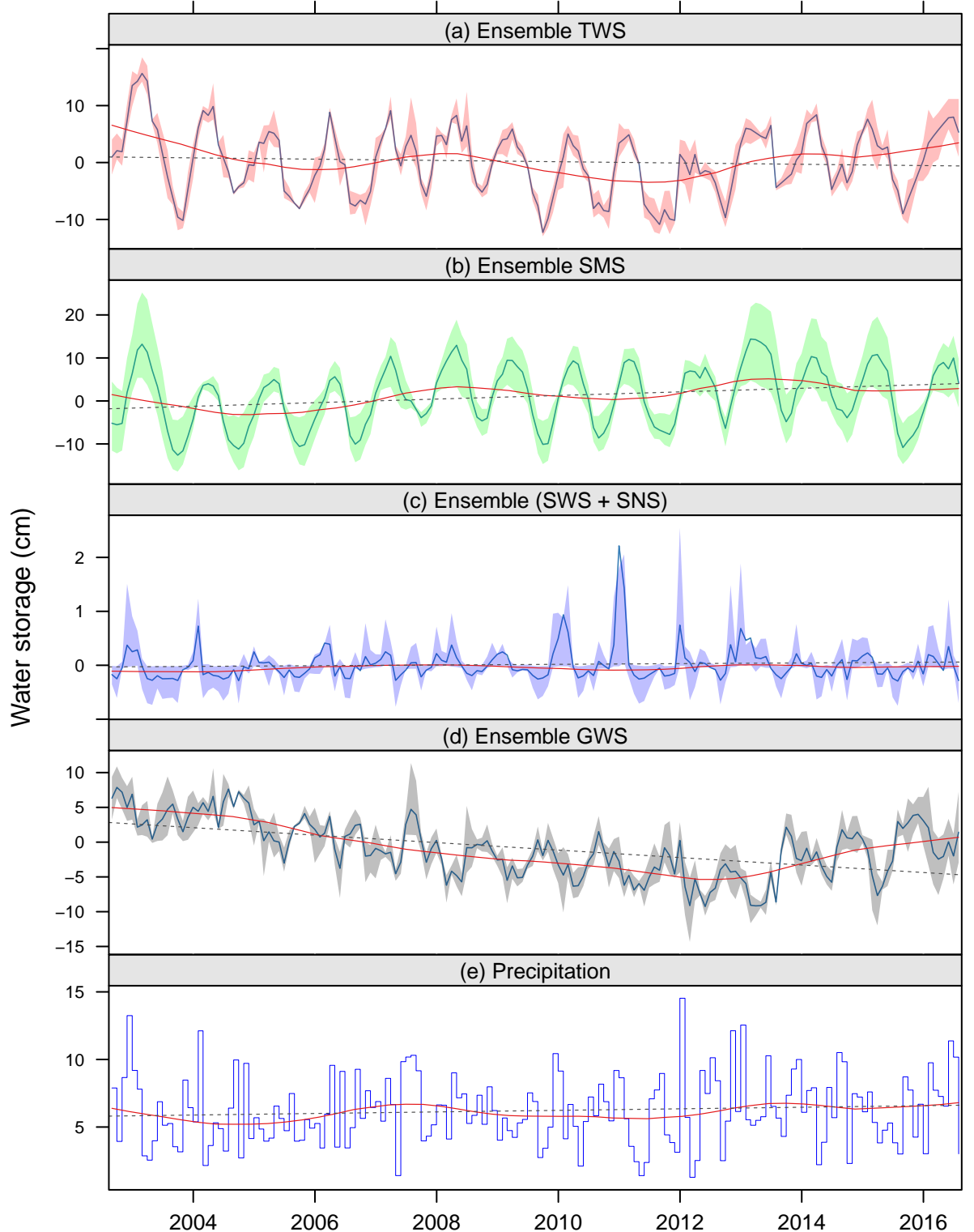


Fig. S32: East European Aquifer System (33)

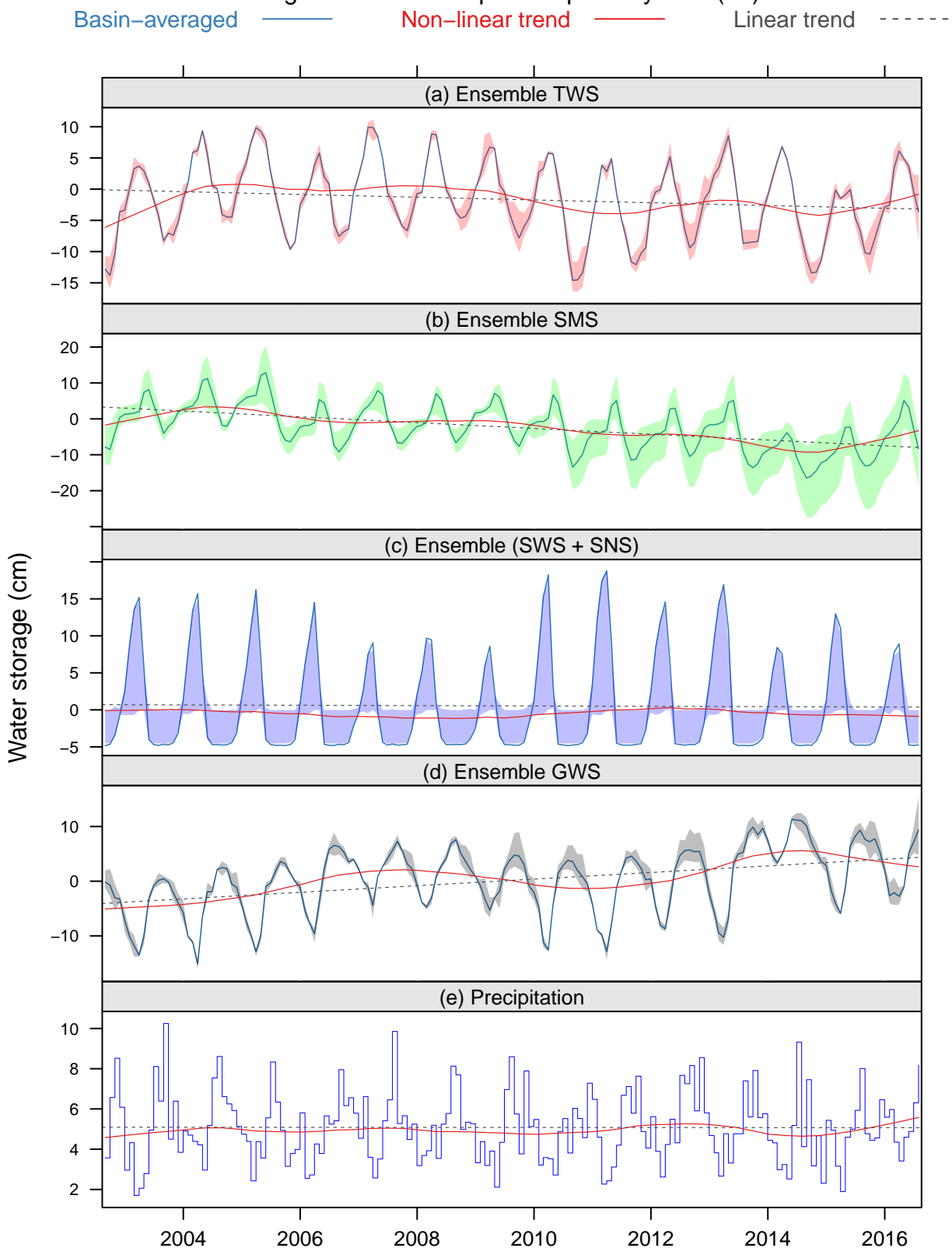


Fig. S33: North Caucasus Basin (34)

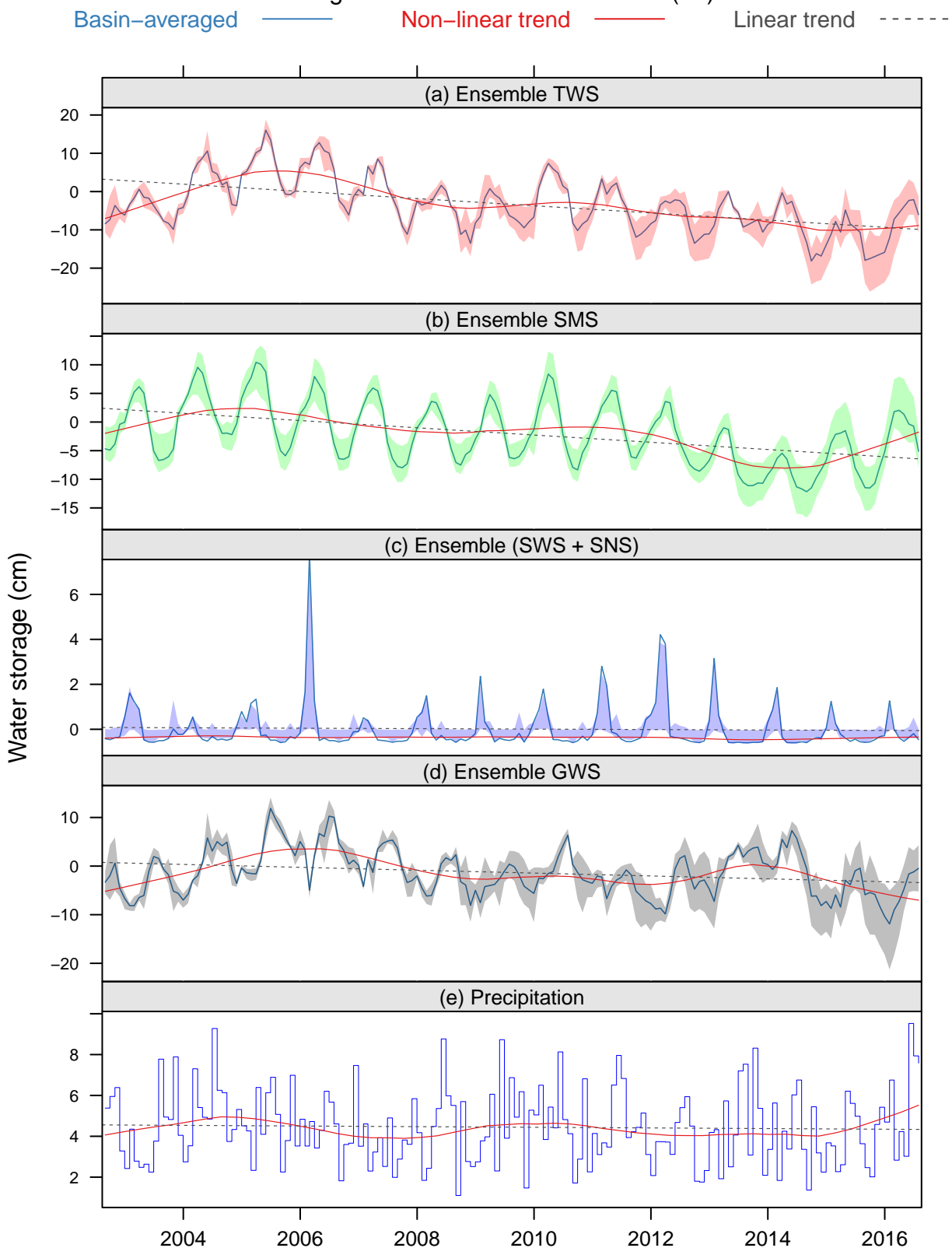


Fig. S34: Pechora Basin (35)

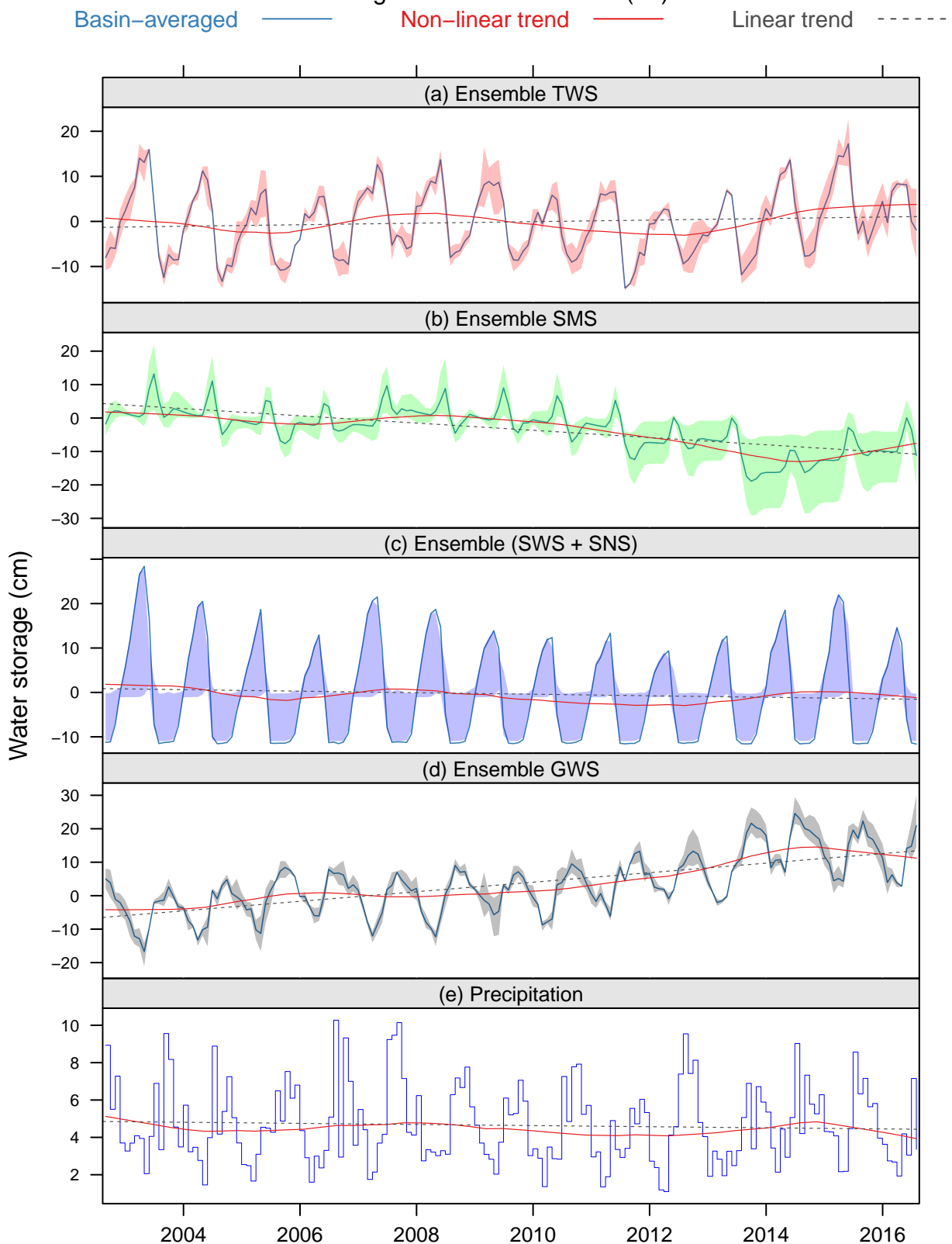


Fig. S35: Great Artesian Basin (36)

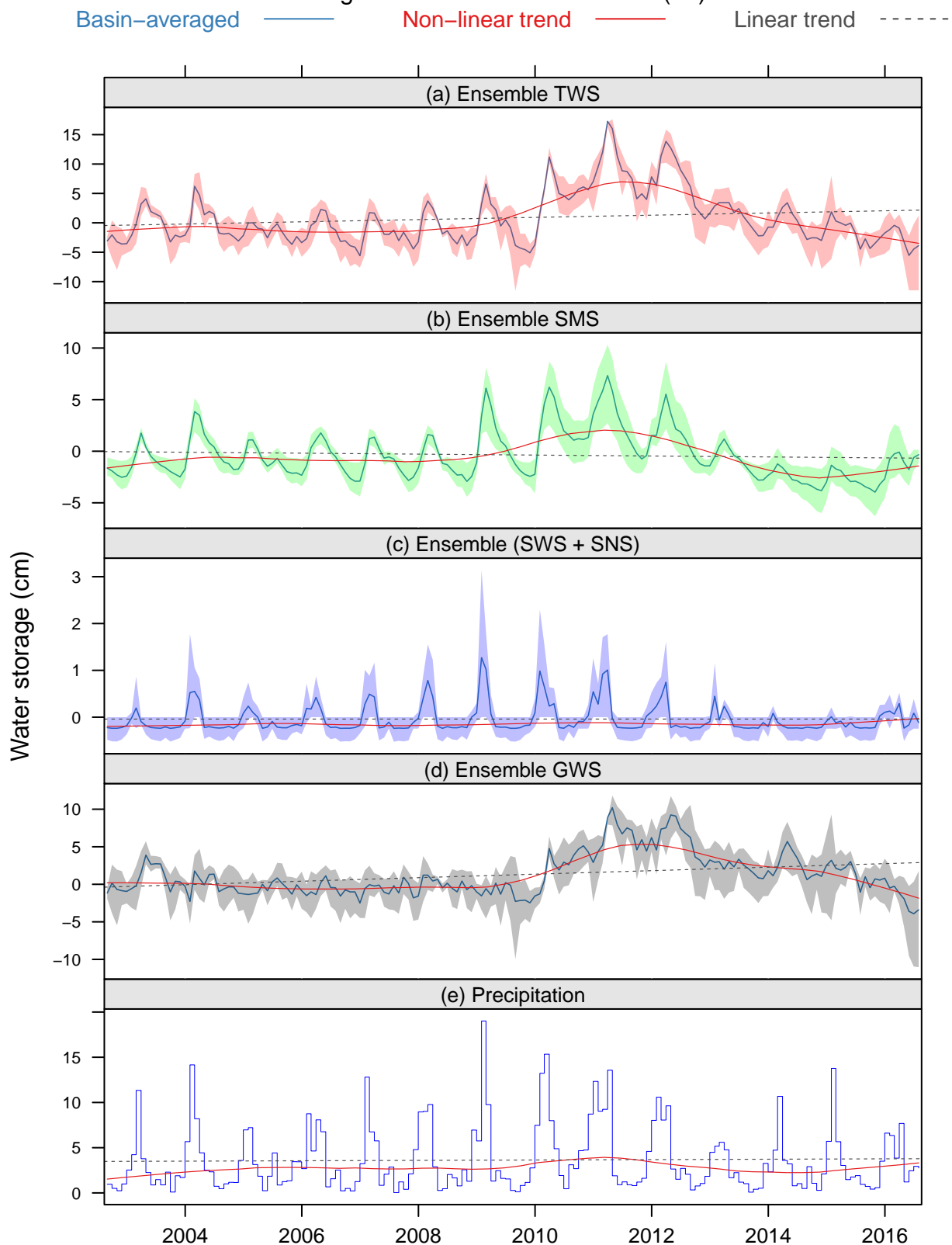


Fig. S36: Canning Basin (37)

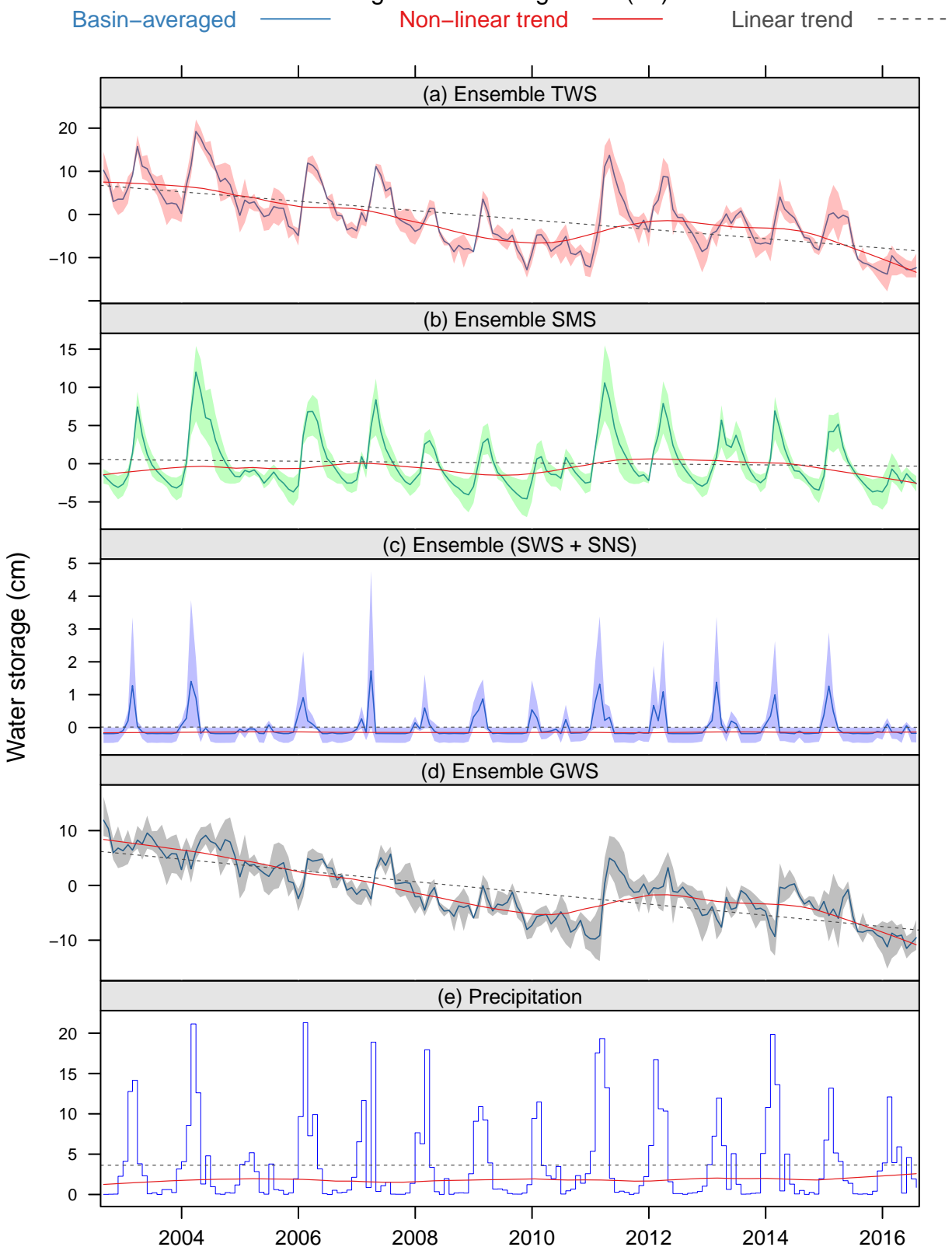
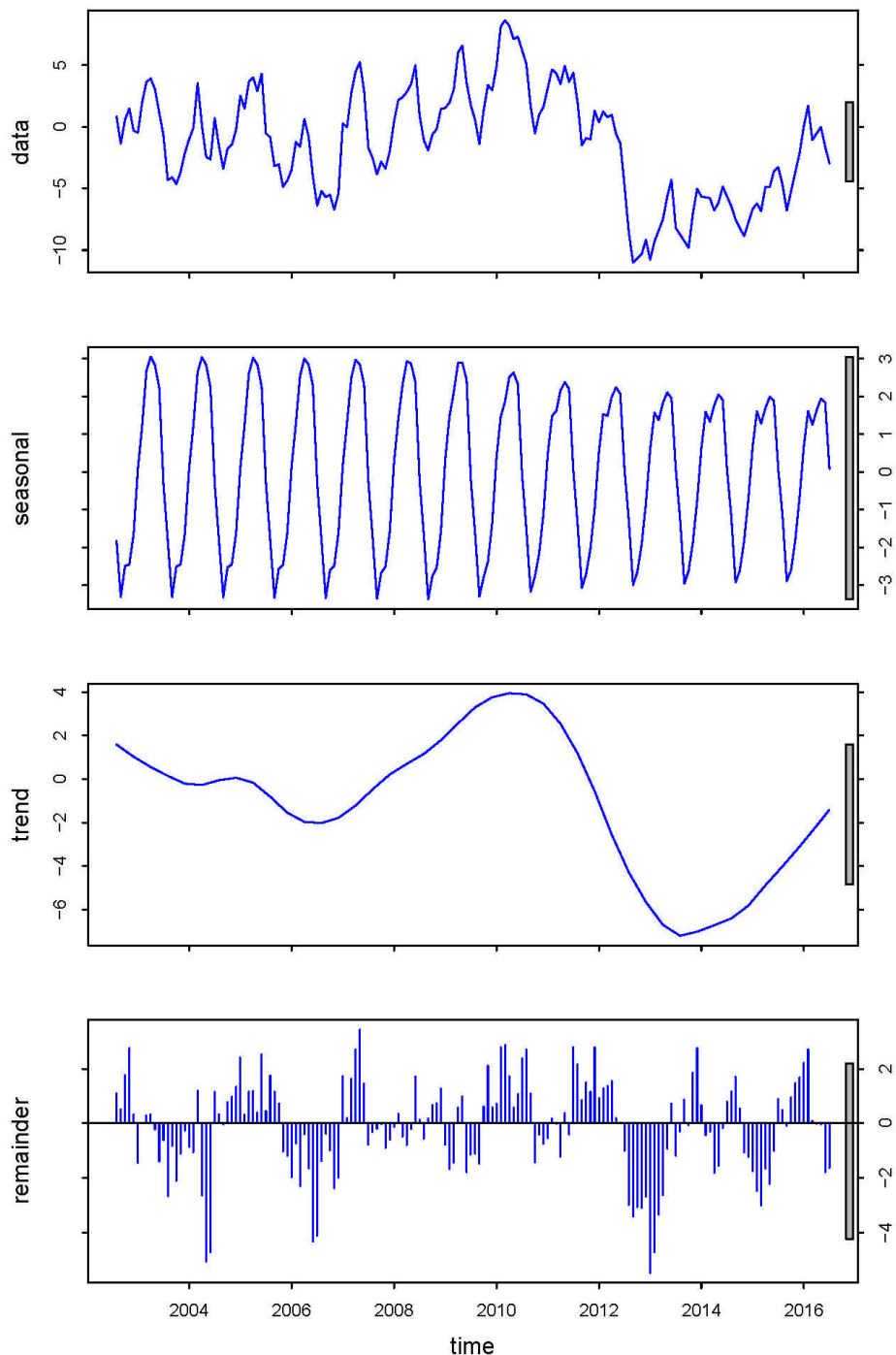
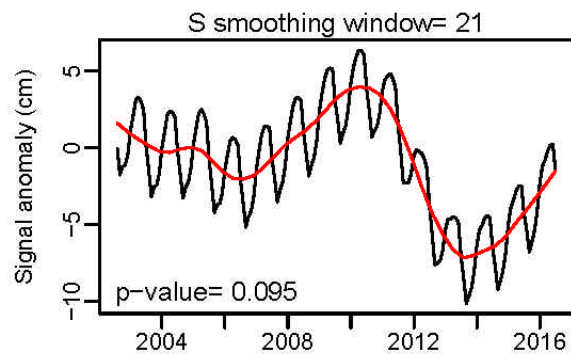
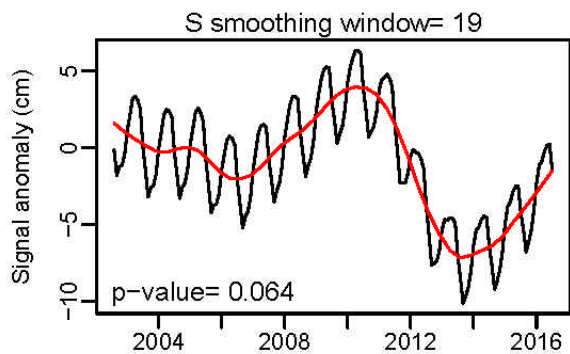
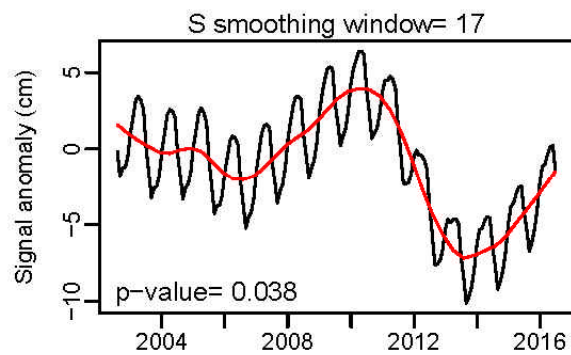
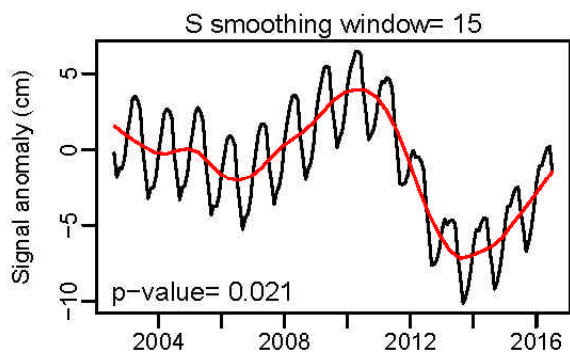
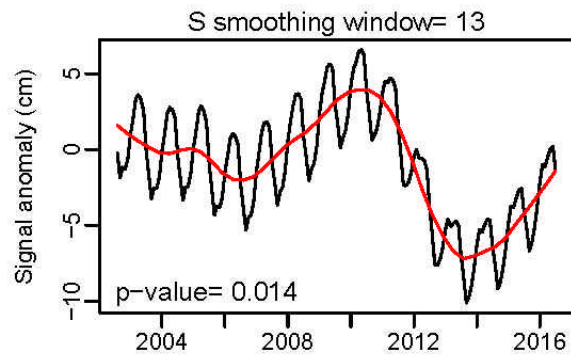
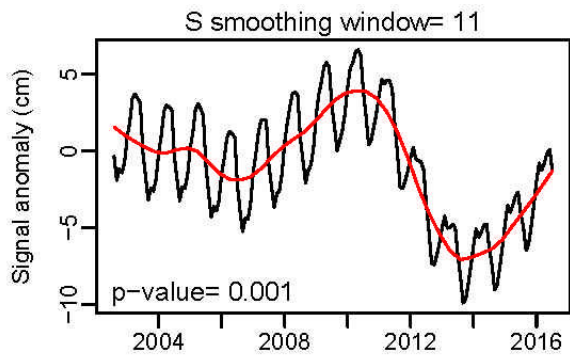


Fig. S37: (a) STL decomposition of ensemble GRACE-TWS signal High Plains Aquifer System (17); (b) various S window smoothing parameters; and (c) various T window parameters and fitted. The *p*-value in each panel derives from a Shapiro-Wilk normality test of the residuals after fitting the STL line.

(a)



(b)



(c)

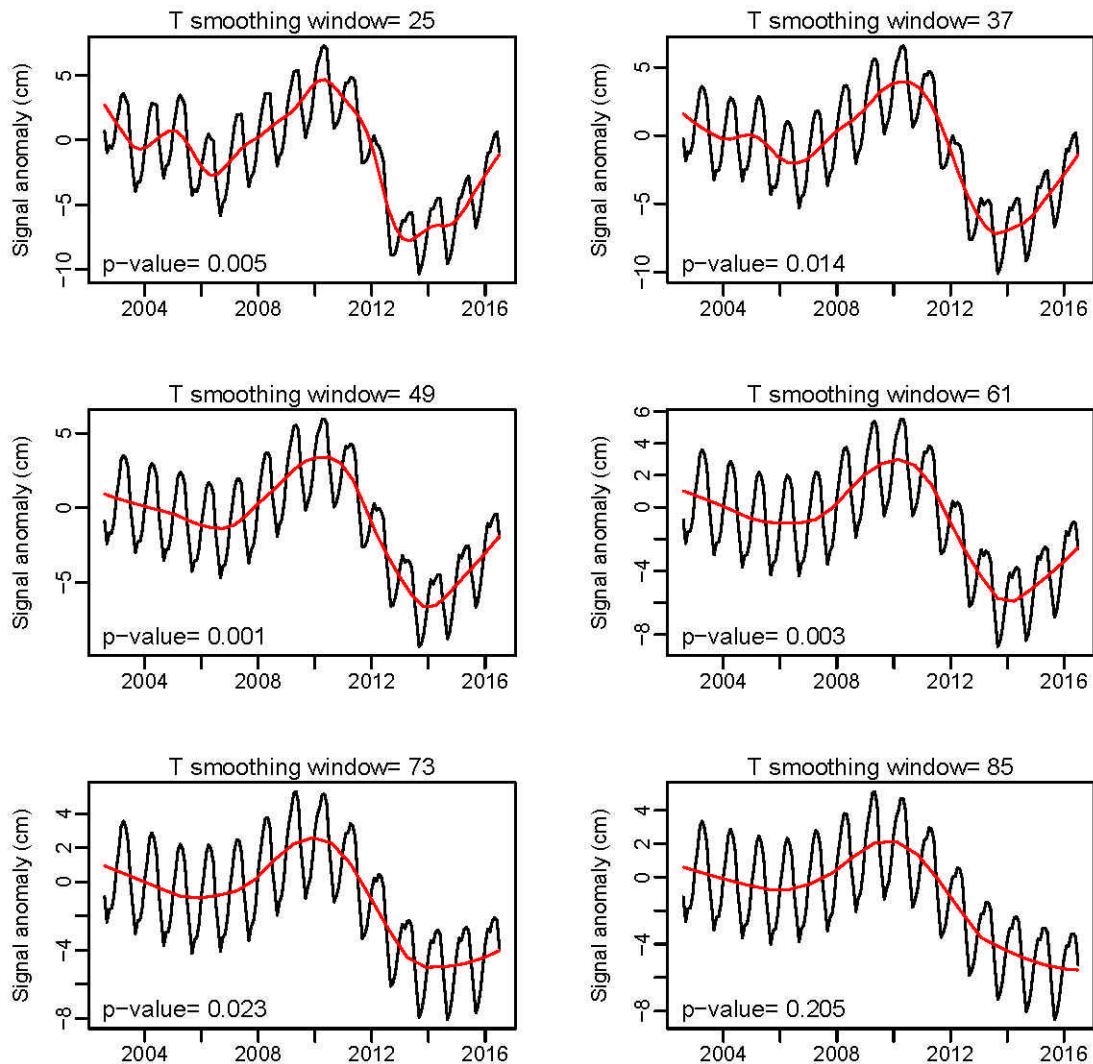


Fig. S38

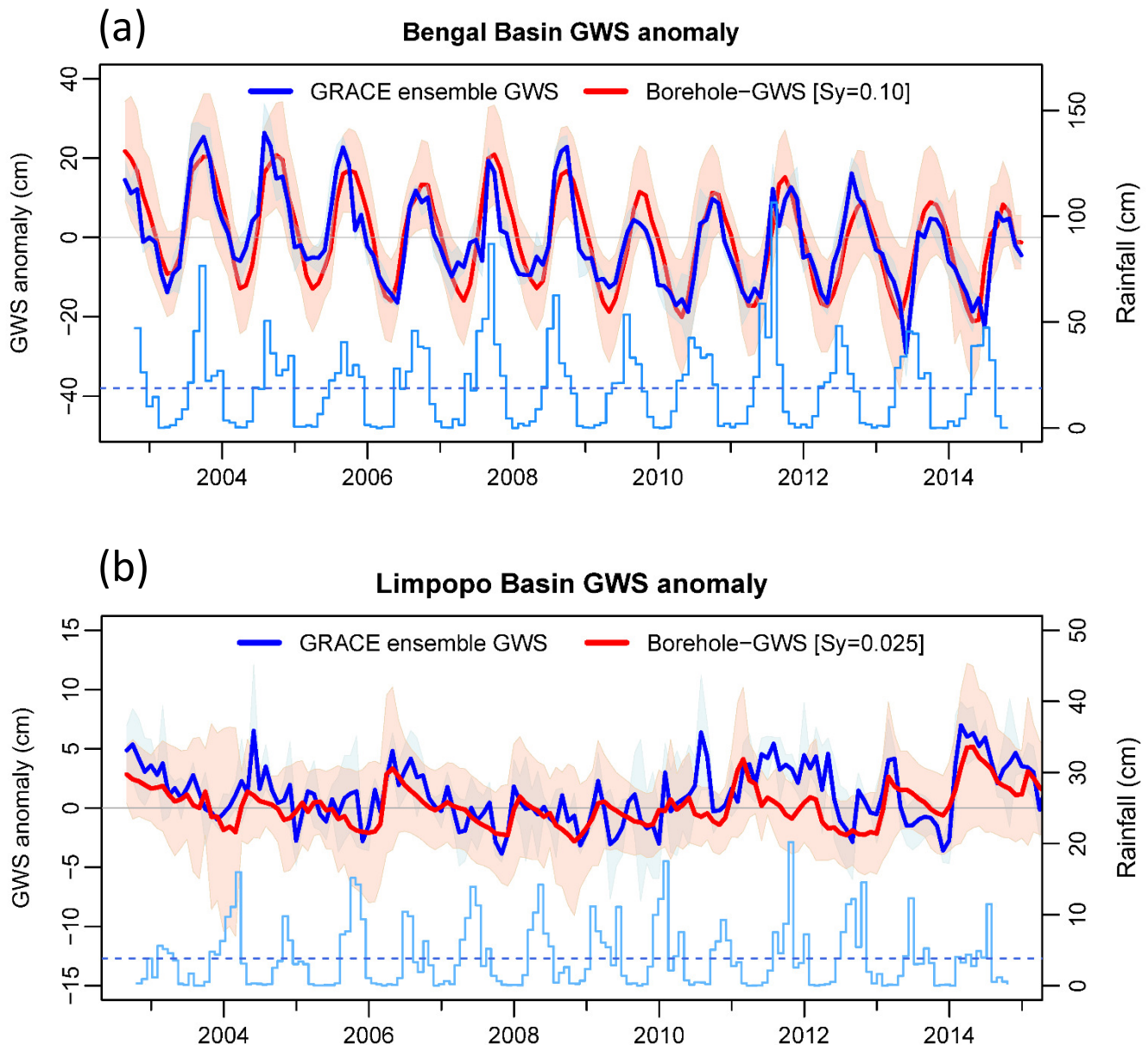


Fig. S39: Bengal Basin

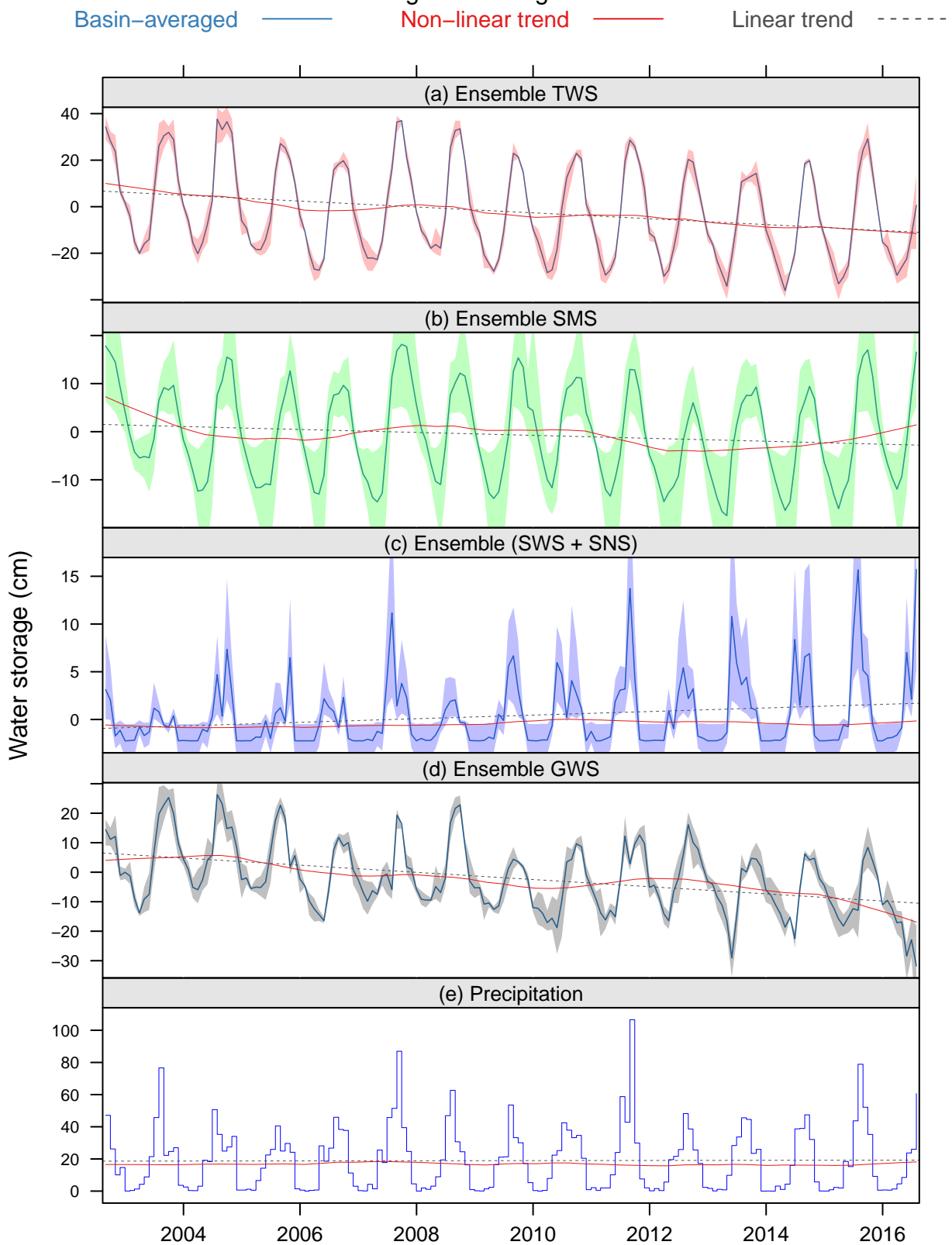


Fig. S40: Limpopo Basin

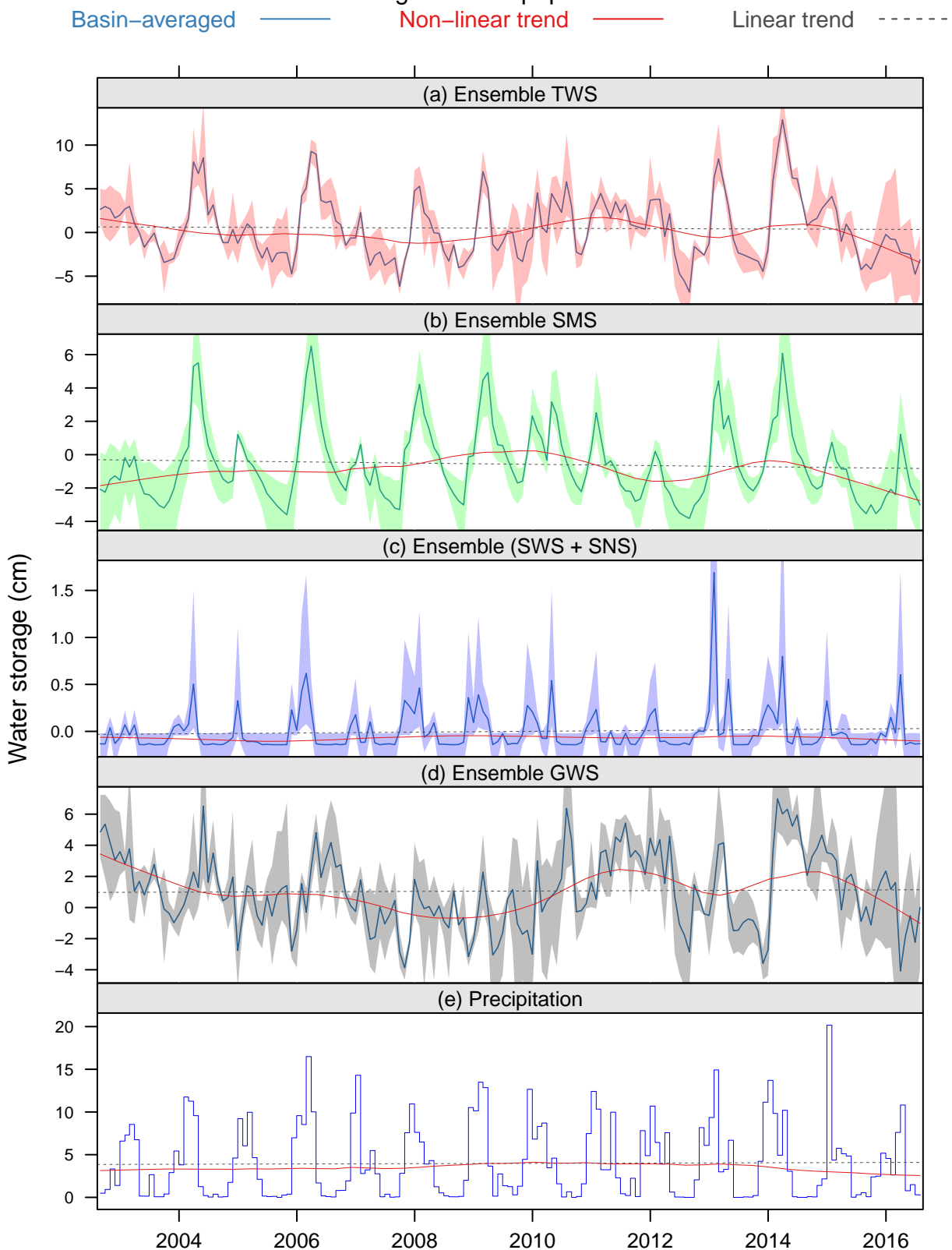
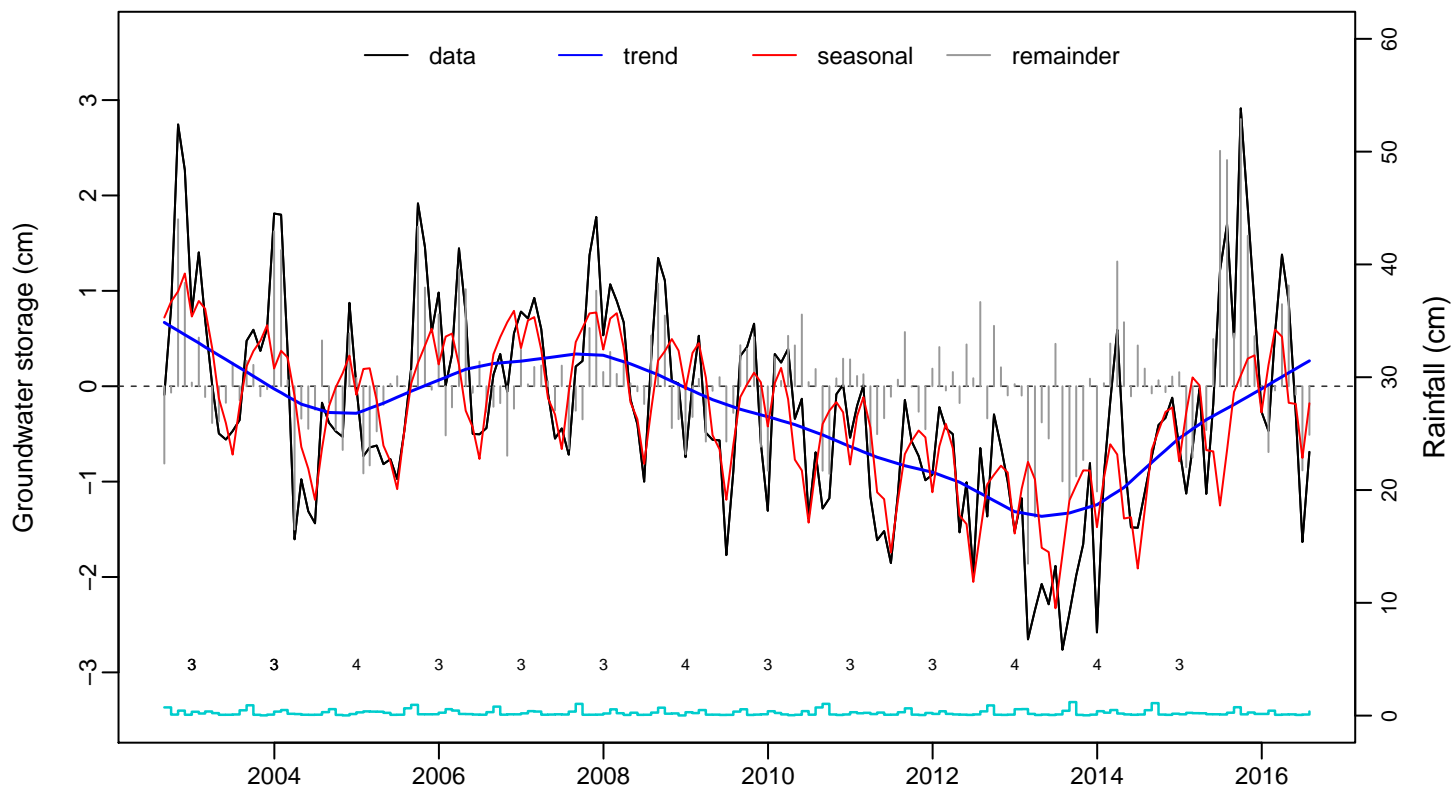


Fig. S41: Nubian Sandstone Aquifer System (1)



**Seasonal–Trend–Remainder (GRACE GWS)
Proportion of variance**

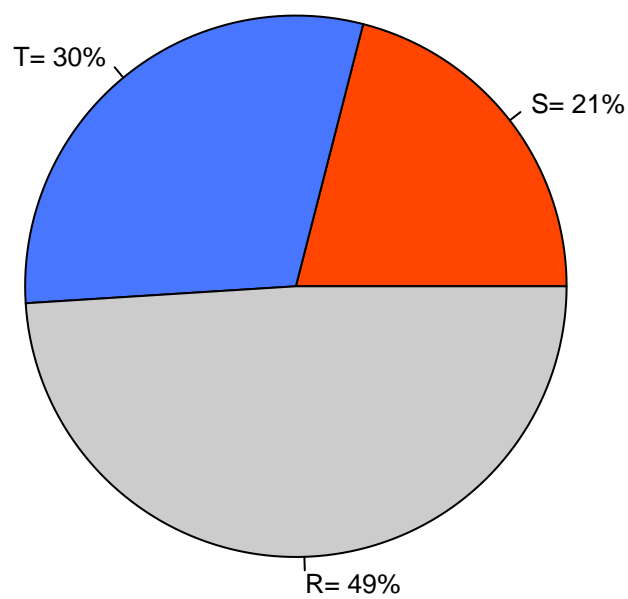
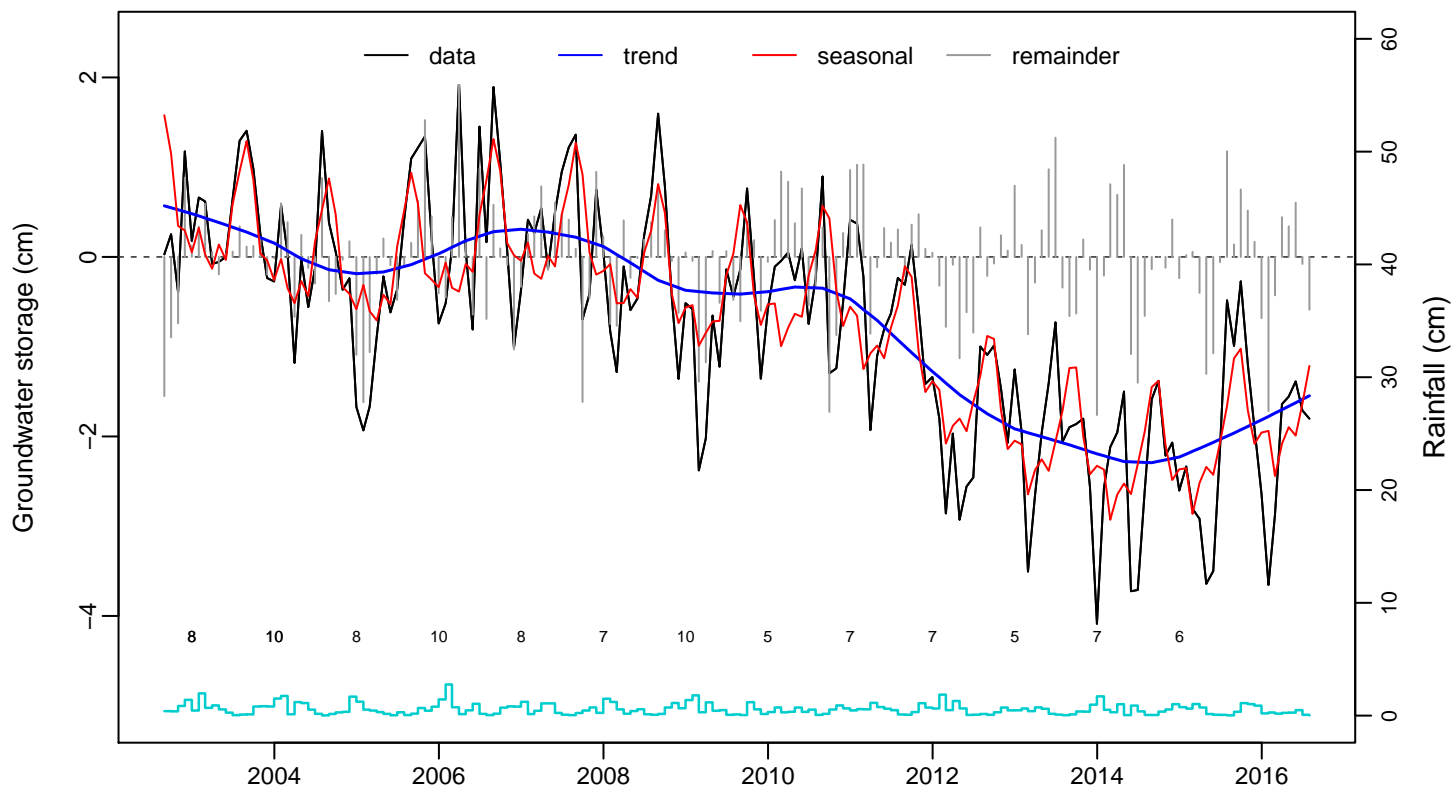


Fig. S42: Northwestern Sahara Aquifer System (2)



**Seasonal–Trend–Remainder (GRACE GWS)
Proportion of variance**

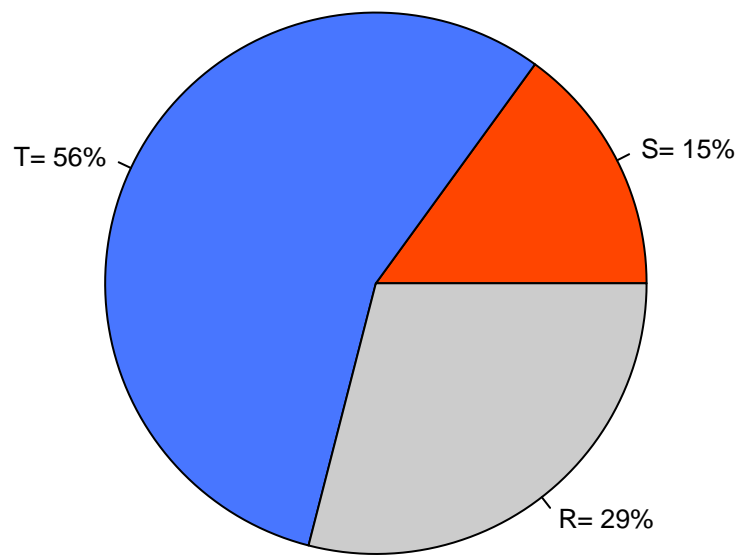
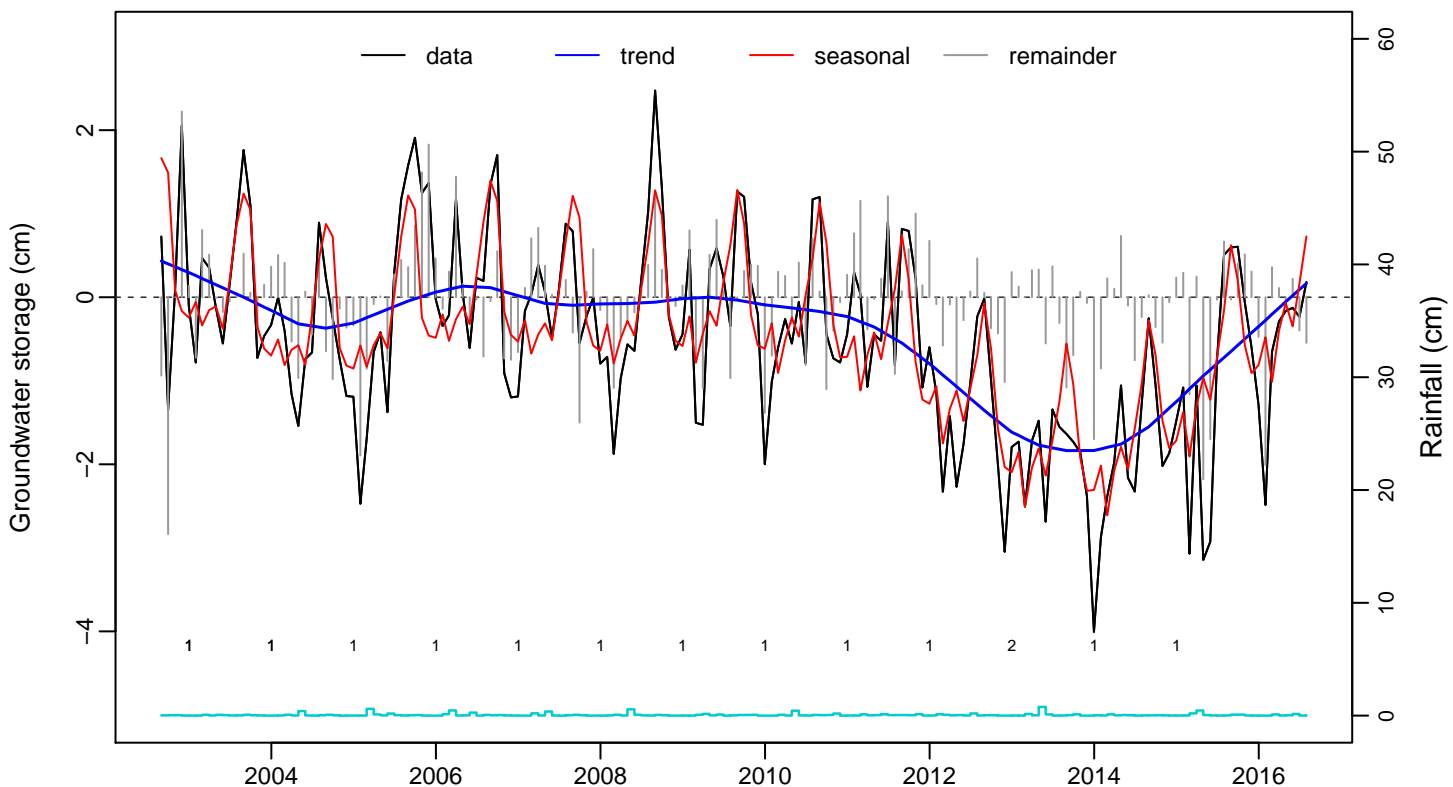


Fig. S43: Murzuk–Djado Basin (3)



**Seasonal–Trend–Remainder (GRACE GWS)
Proportion of variance**

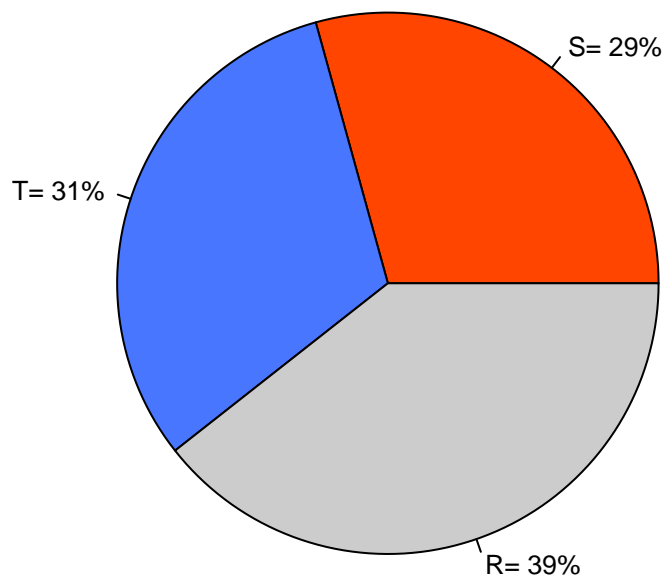
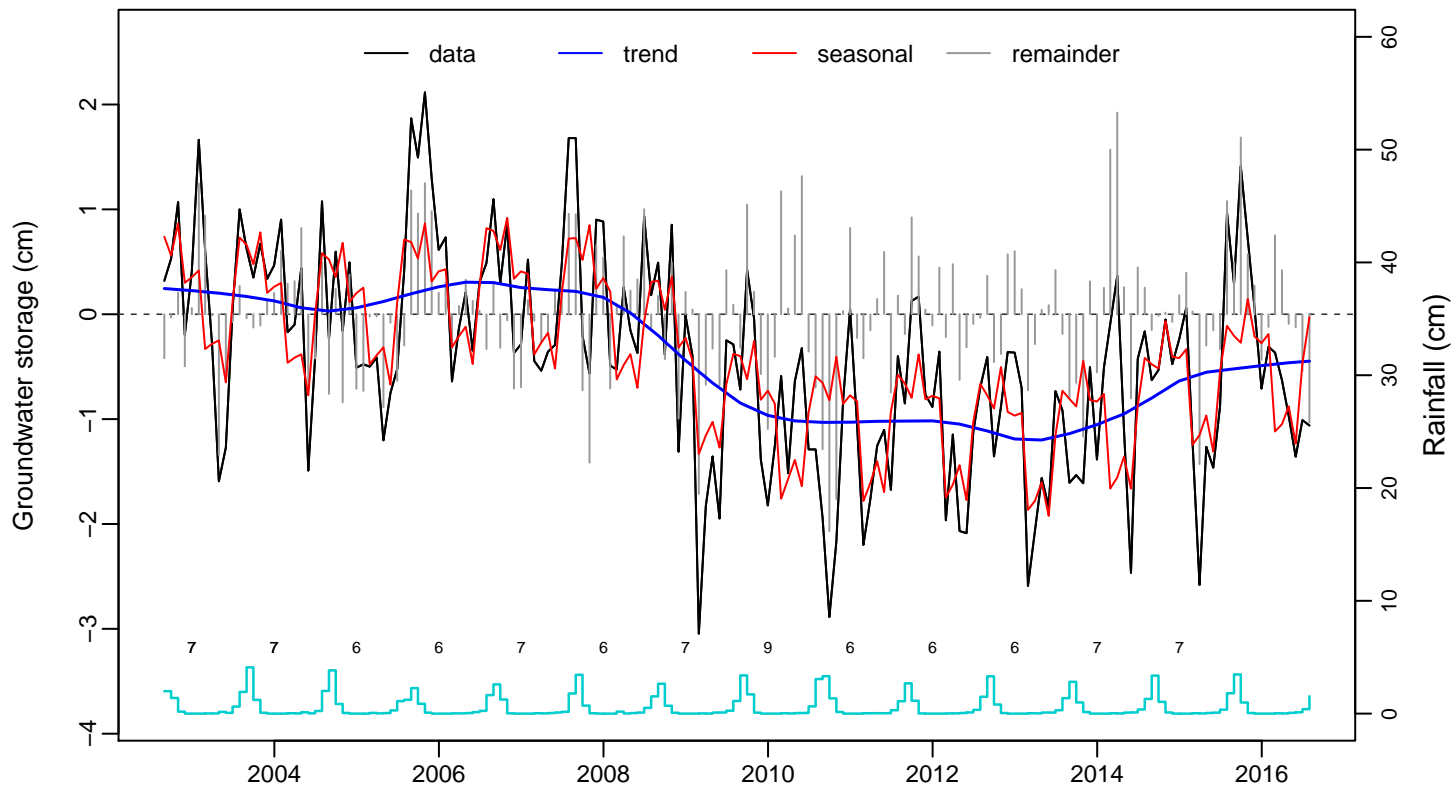


Fig. S44: Taoudeni–Tanezrouft Basin (4)



**Seasonal–Trend–Remainder (GRACE GWS)
Proportion of variance**

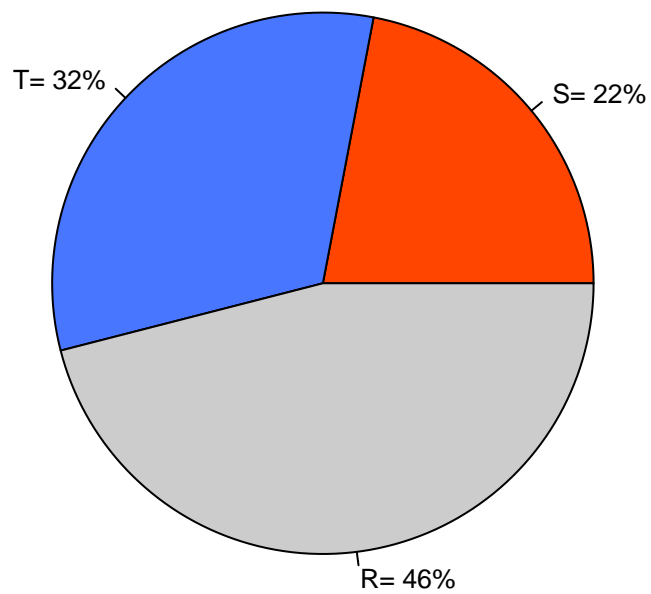
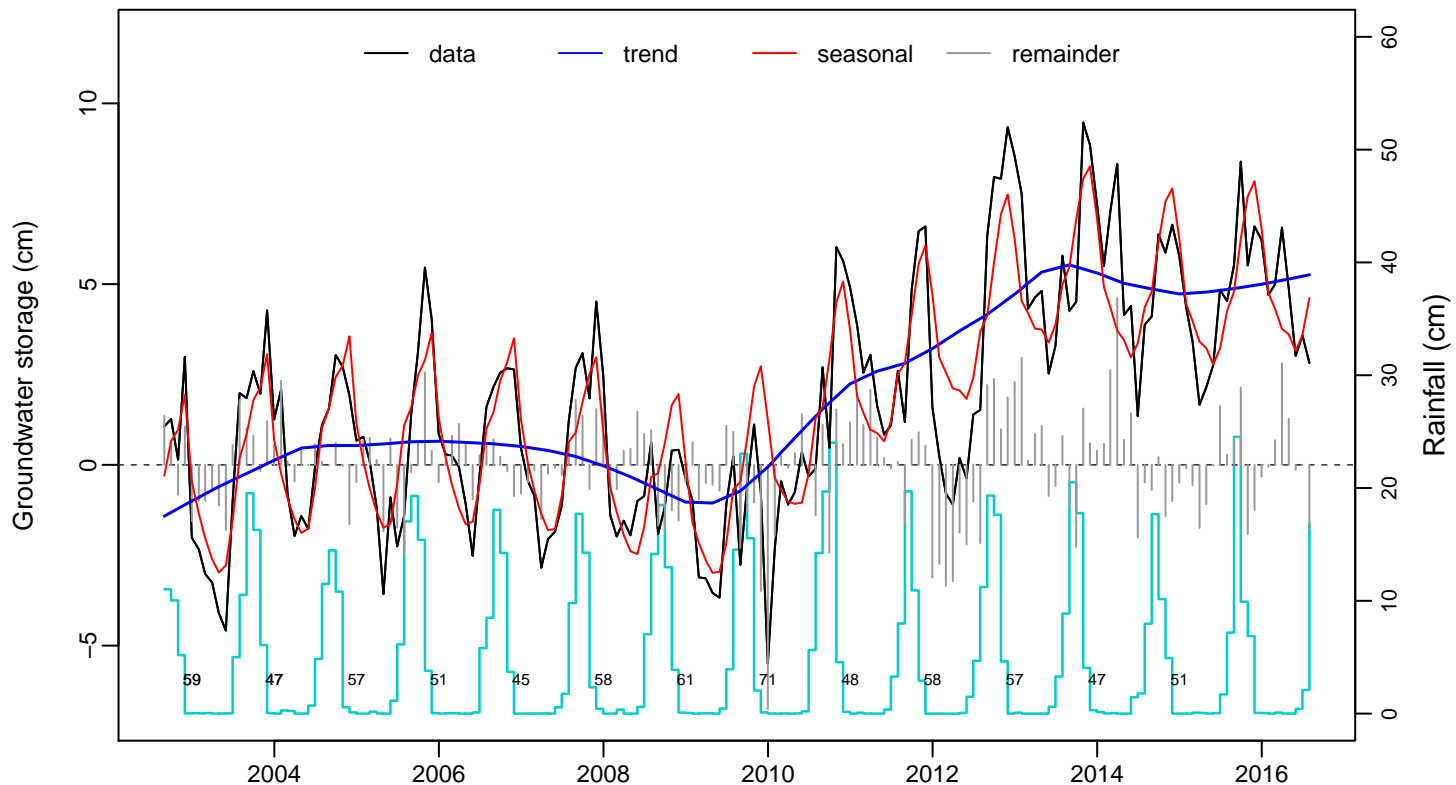


Fig. S45: Senegal–Mauritanian Basin (5)



**Seasonal–Trend–Remainder (GRACE GWS)
Proportion of variance**

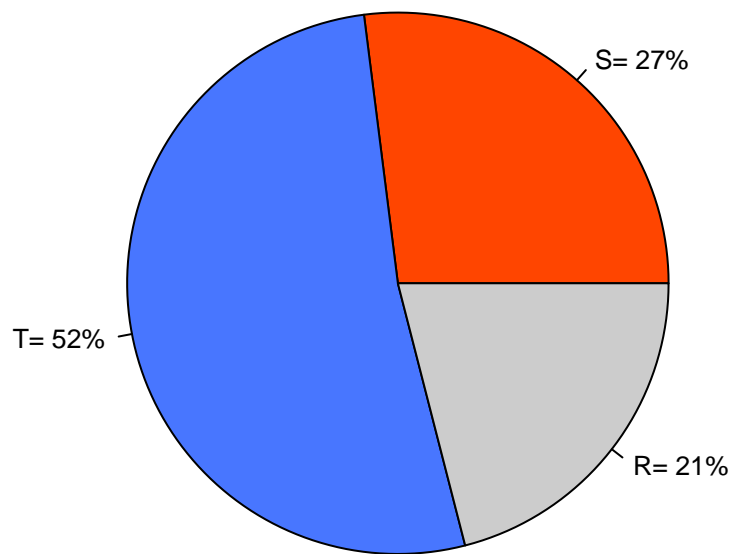
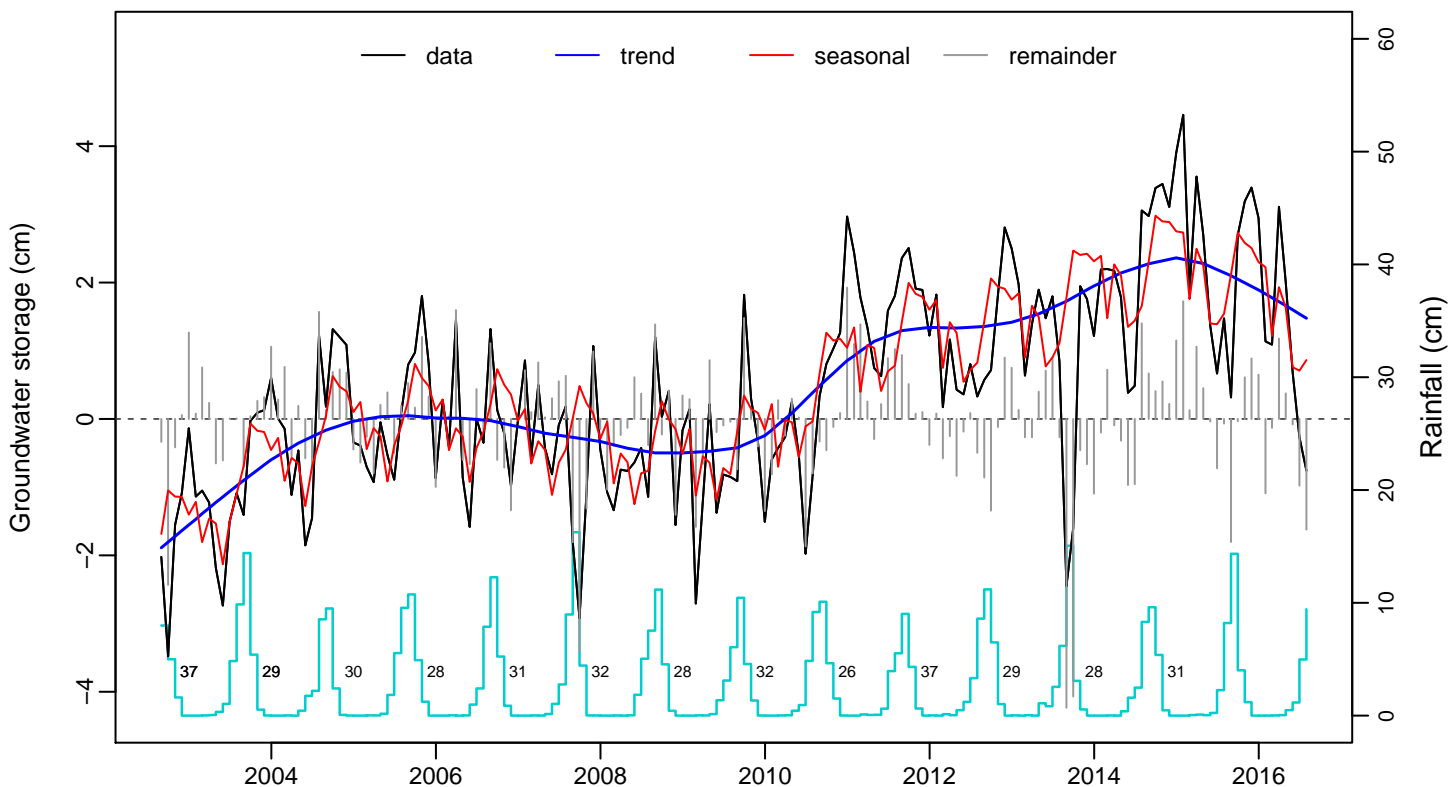


Fig. S46: IJllemmeden–Irhazer Aquifer System (6)



**Seasonal–Trend–Remainder (GRACE GWS)
Proportion of variance**

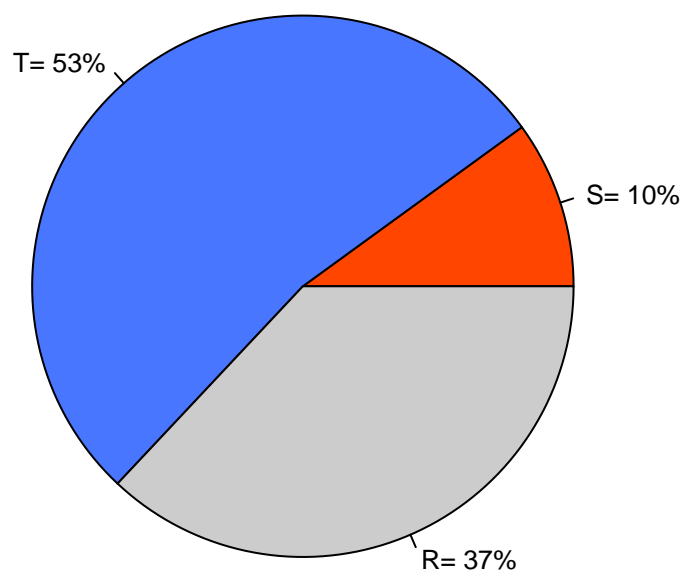
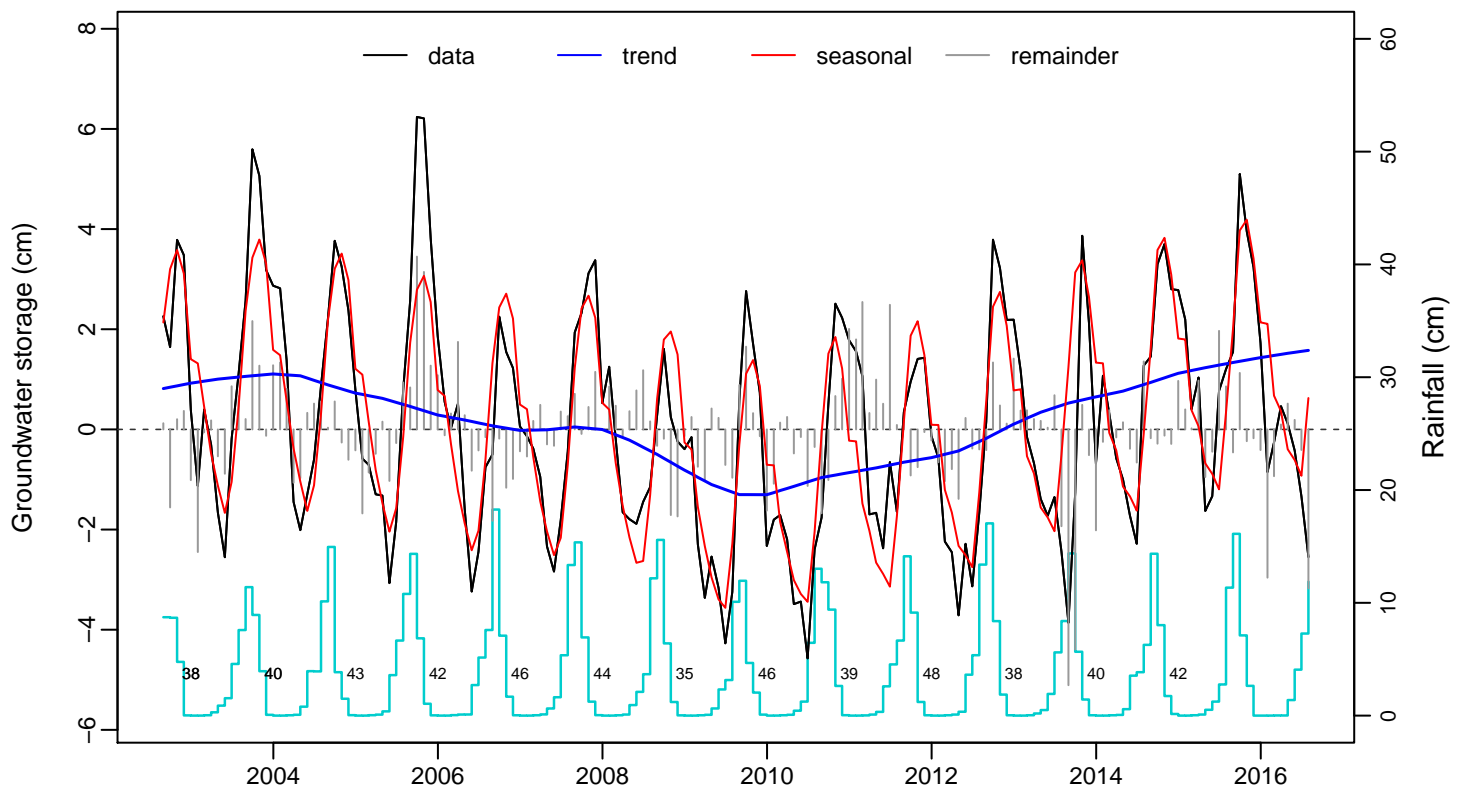


Fig. S47: Lake Chad Basin (7)



**Seasonal-Trend-Remainder (GRACE GWS)
Proportion of variance**

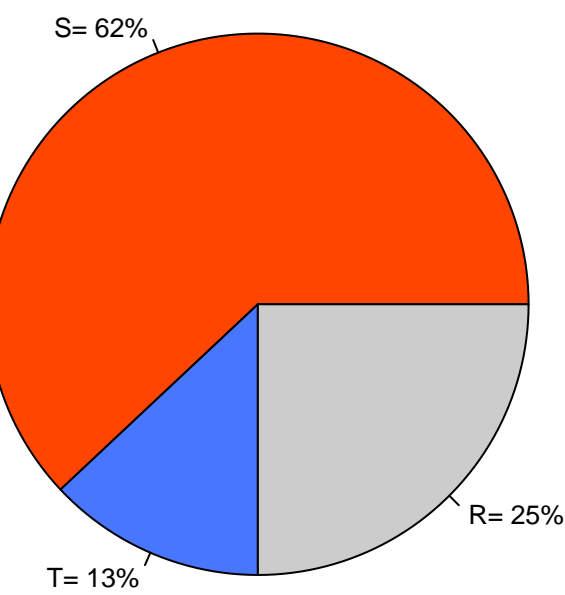
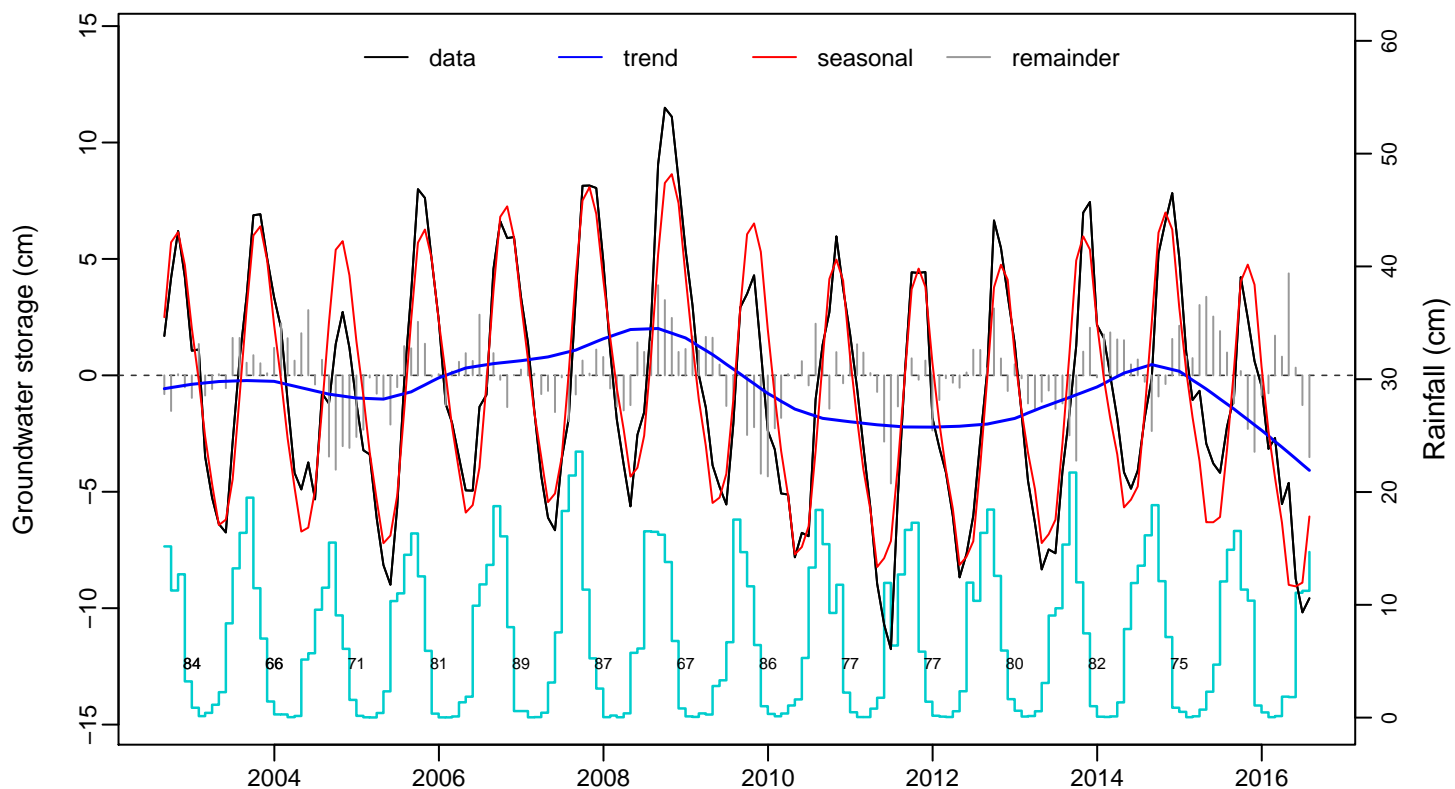


Fig. S48: Umm Ruwaba Aquifer (Sudd Basin) (8)



**Seasonal-Trend-Remainder (GRACE GWS)
Proportion of variance**

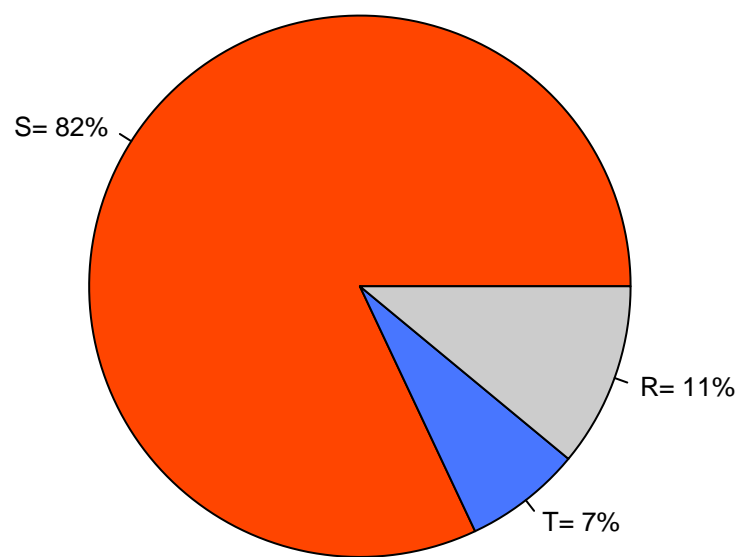
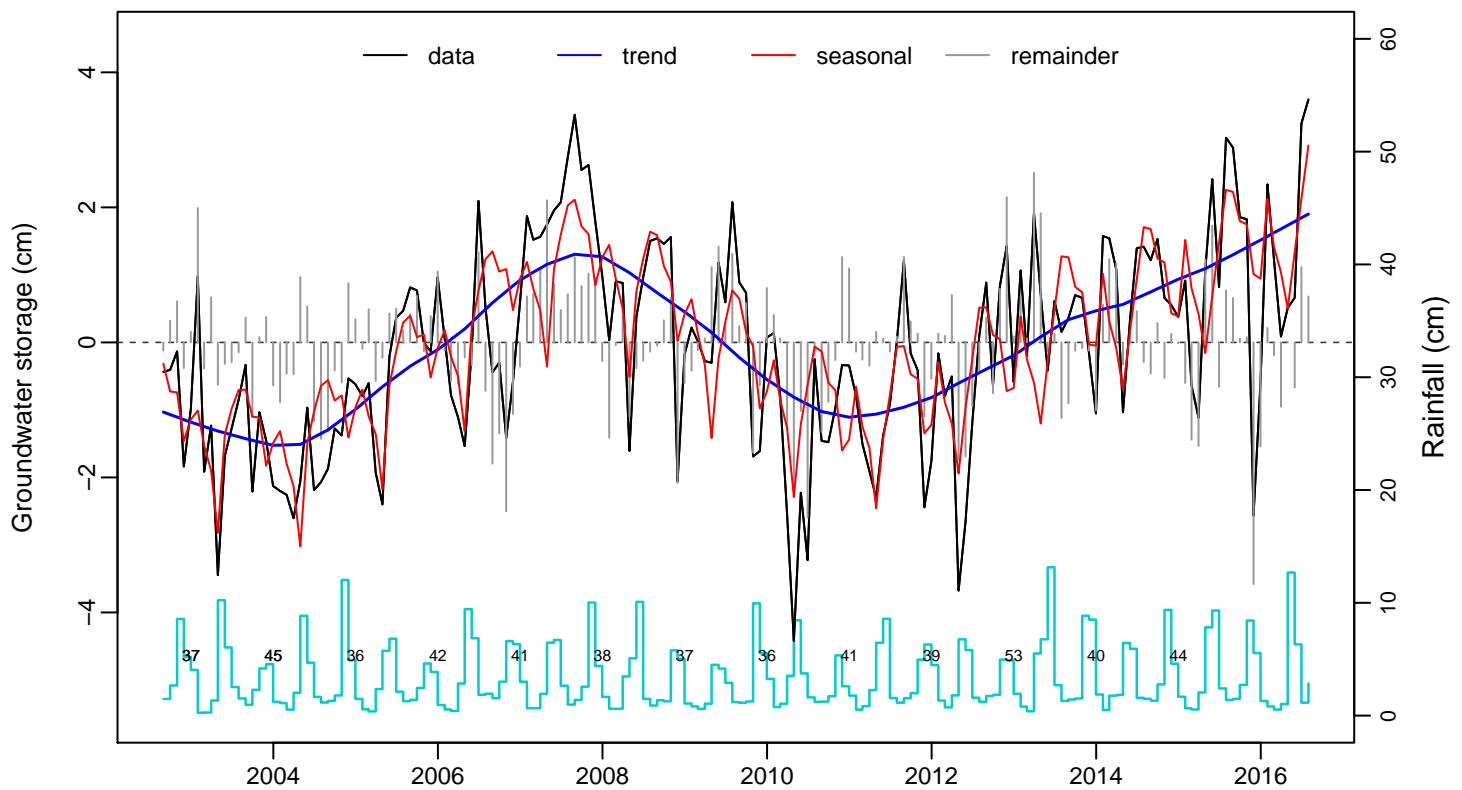


Fig. S49: Ogaden–Juba Basin (9)



**Seasonal–Trend–Remainder (GRACE GWS)
Proportion of variance**

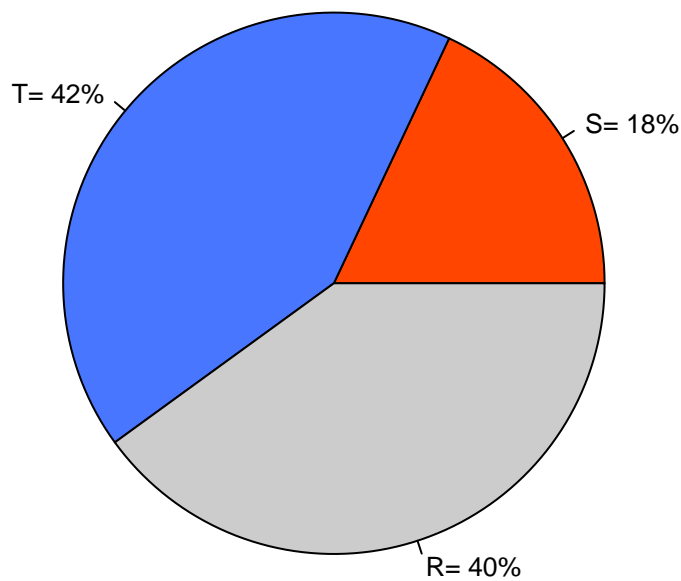
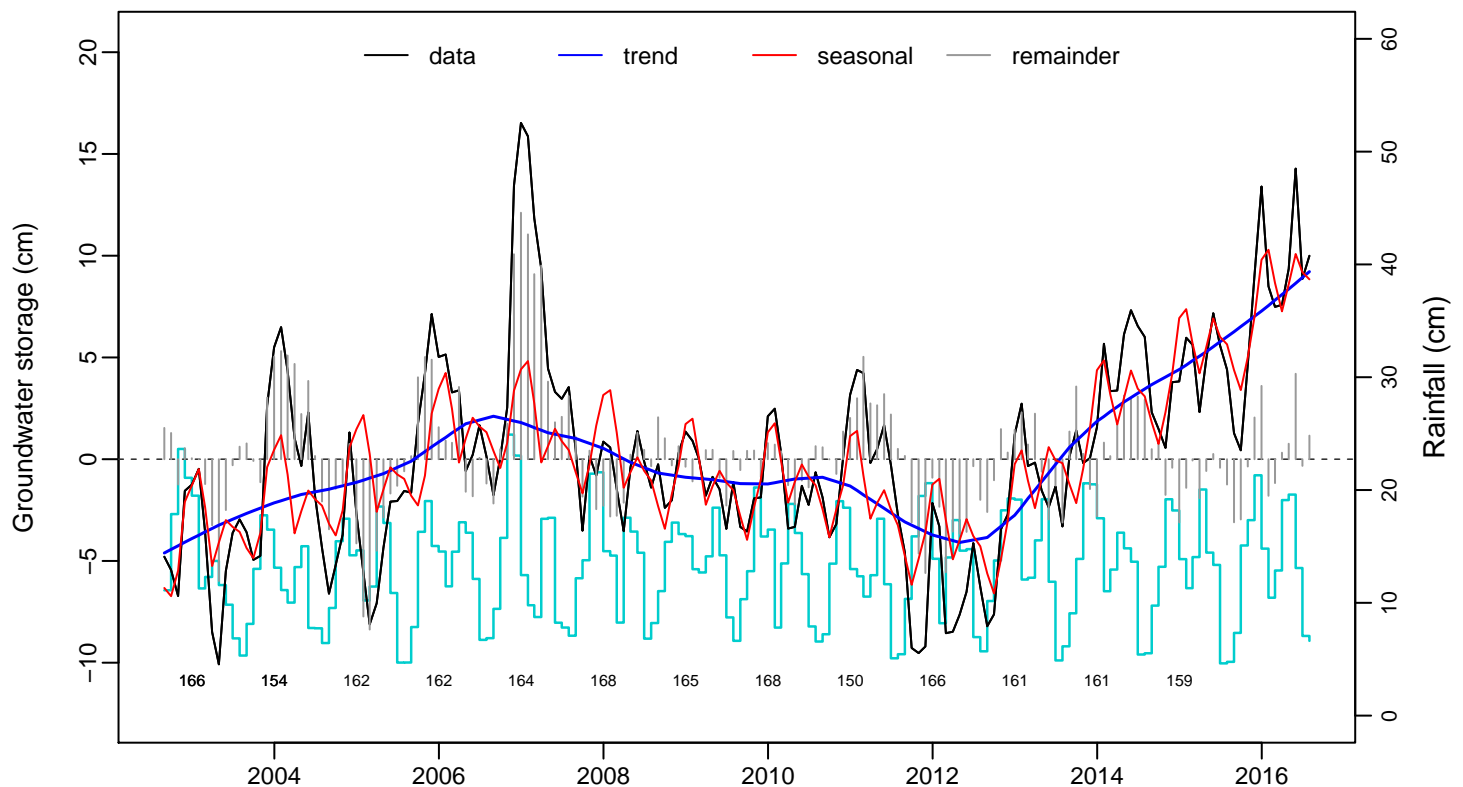


Fig. S50: Congo Basin (10)



**Seasonal–Trend–Remainder (GRACE GWS)
Proportion of variance**

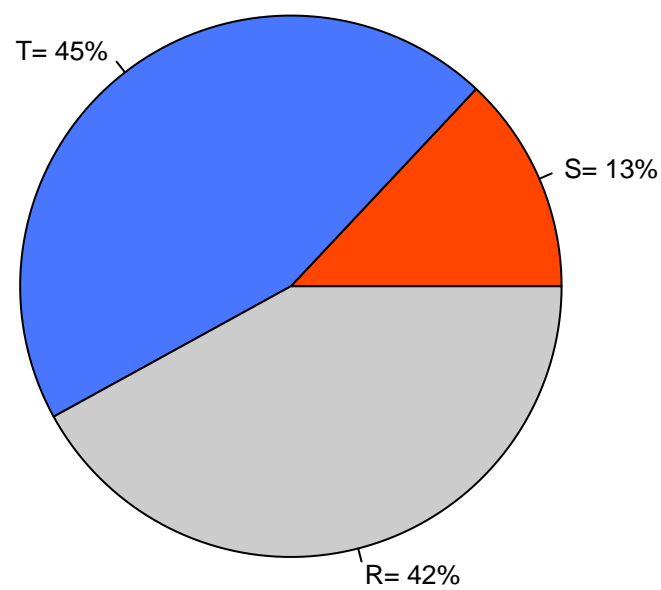
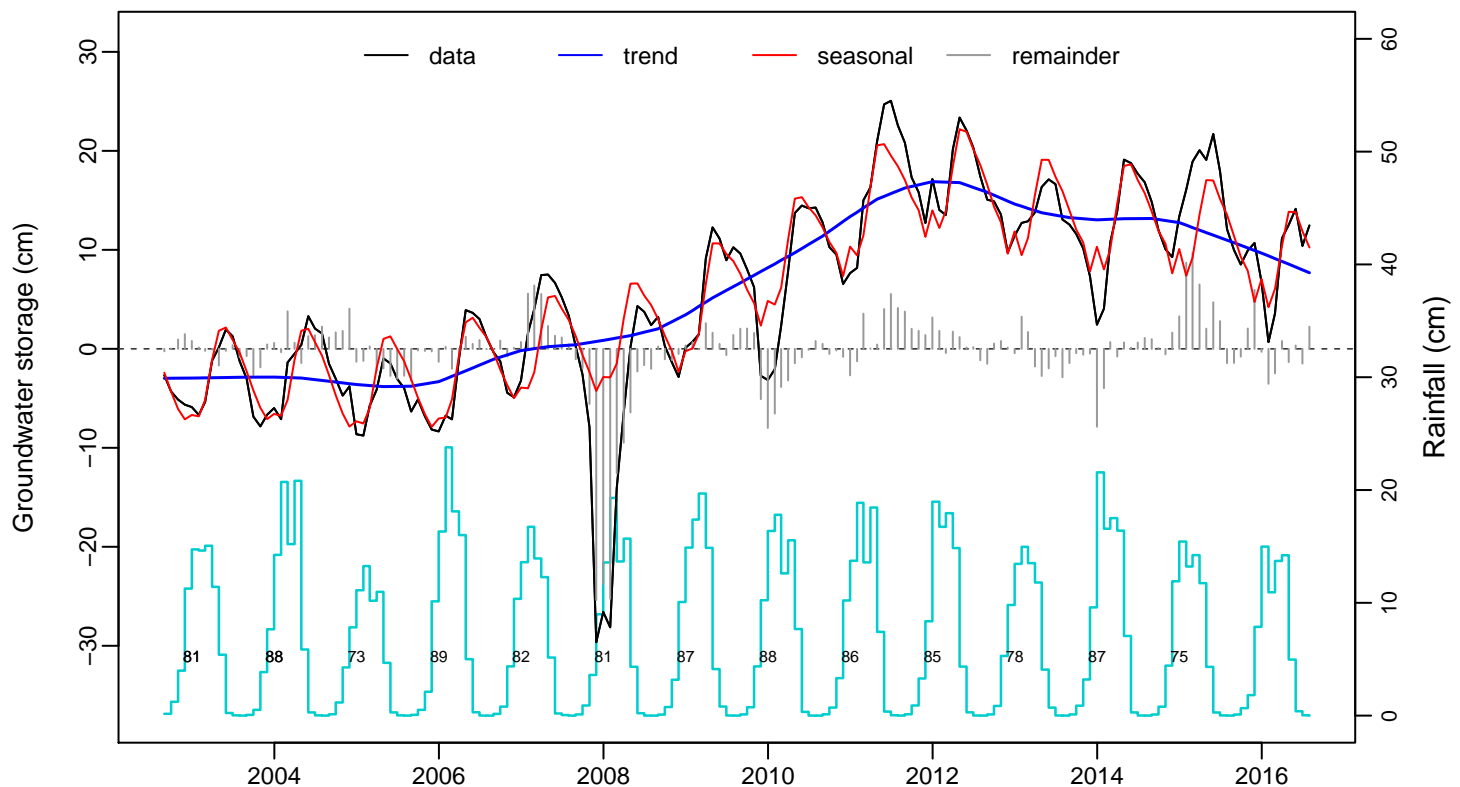


Fig. S51: Upper Kalahari–Cuvelai–Zambezi Basin (11)



**Seasonal–Trend–Remainder (GRACE GWS)
Proportion of variance**

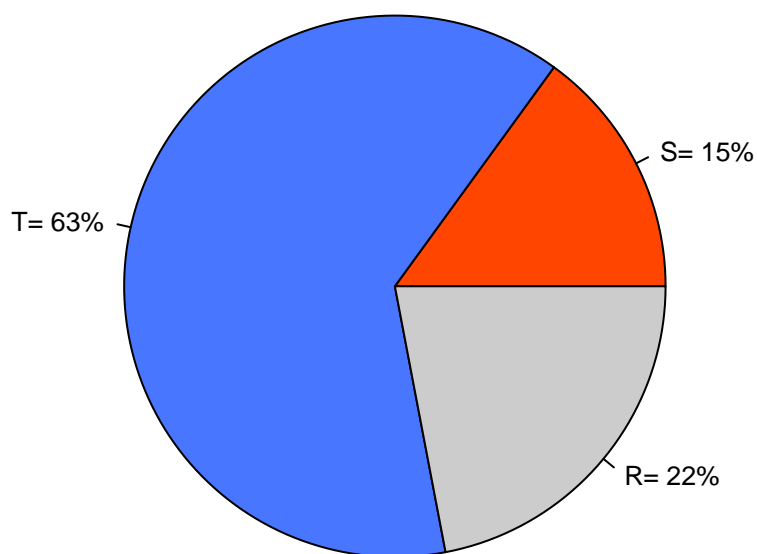
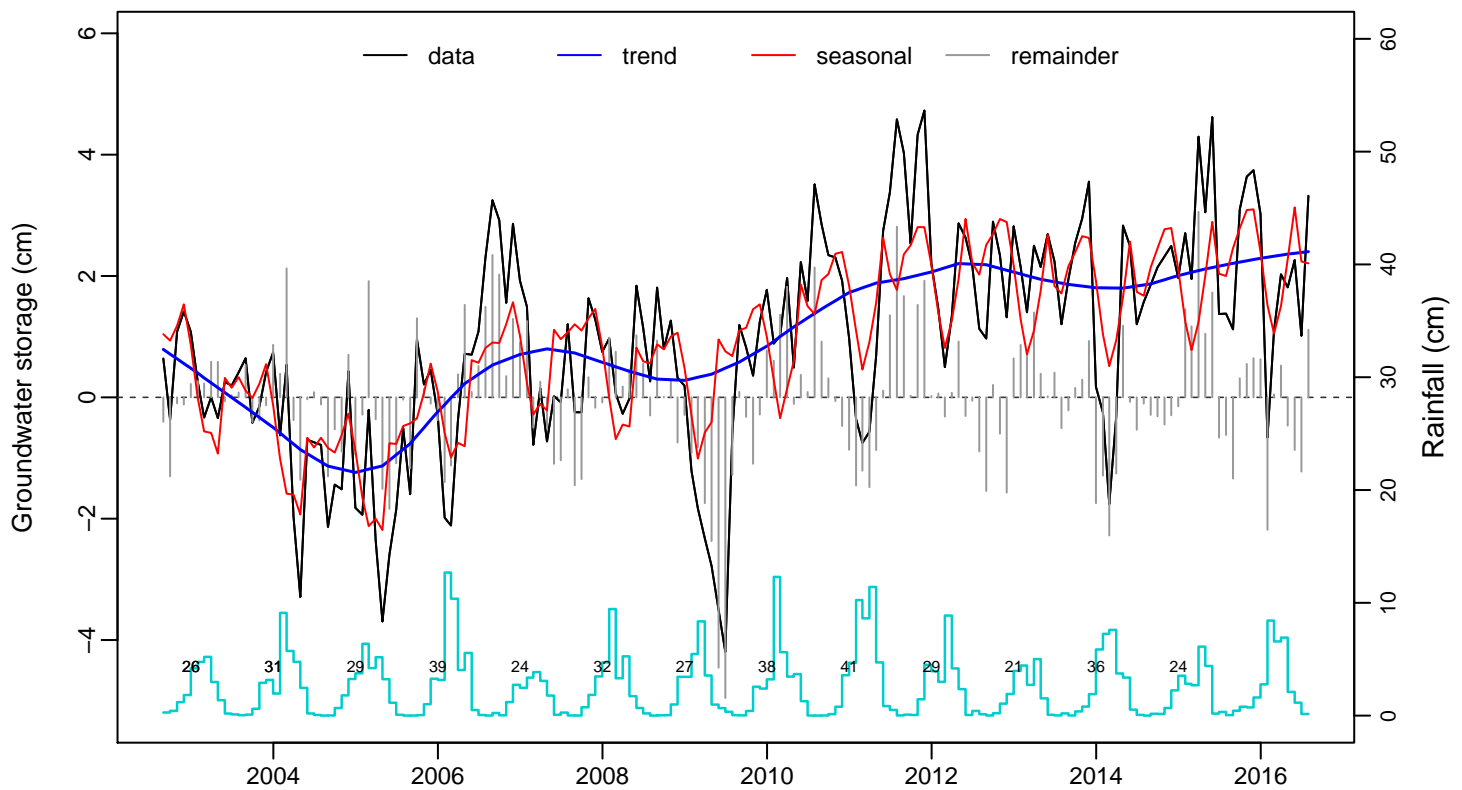


Fig. S52: Lower Kalahari–Stampriet Basin (12)



**Seasonal-Trend-Remainder (GRACE GWS)
Proportion of variance**

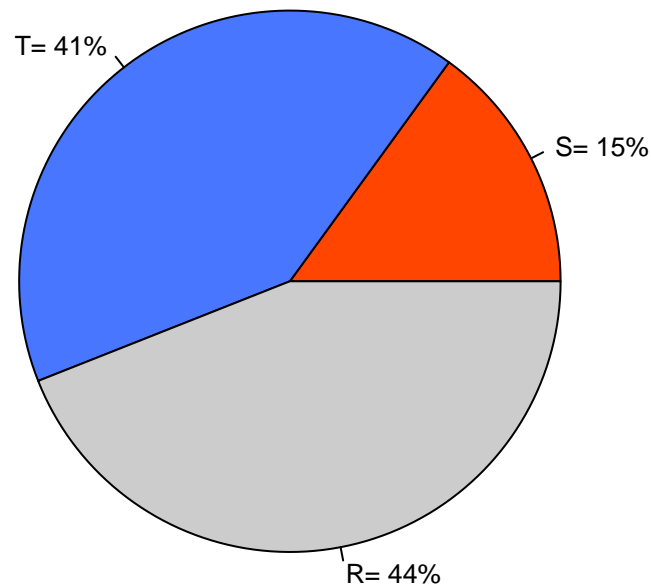
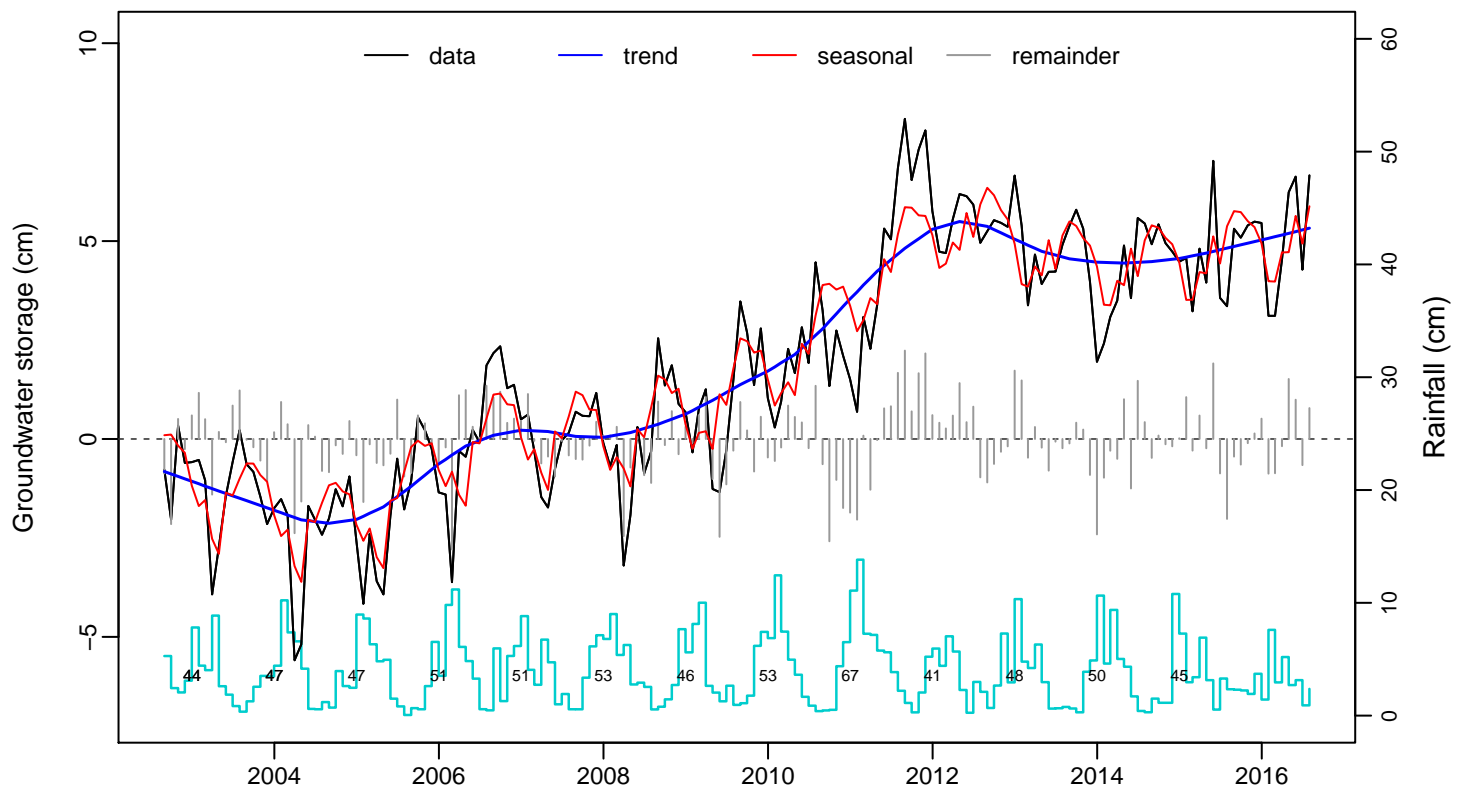


Fig. S53: Karoo Basin (13)



**Seasonal–Trend–Remainder (GRACE GWS)
Proportion of variance**

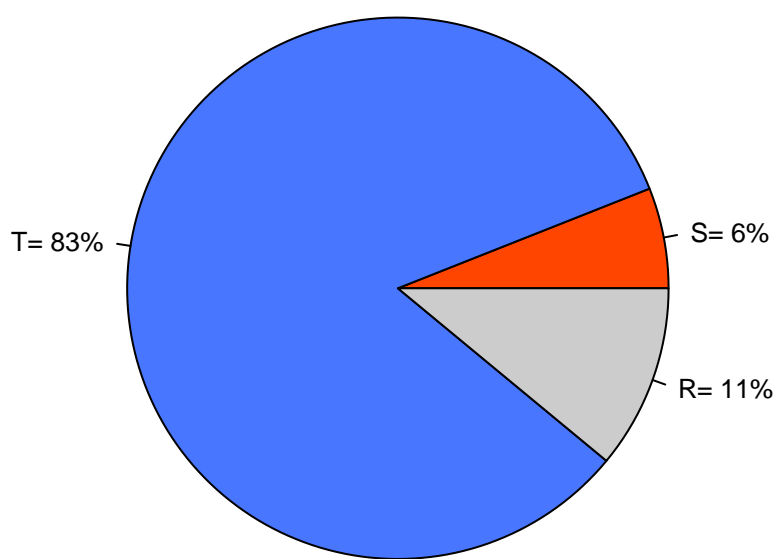
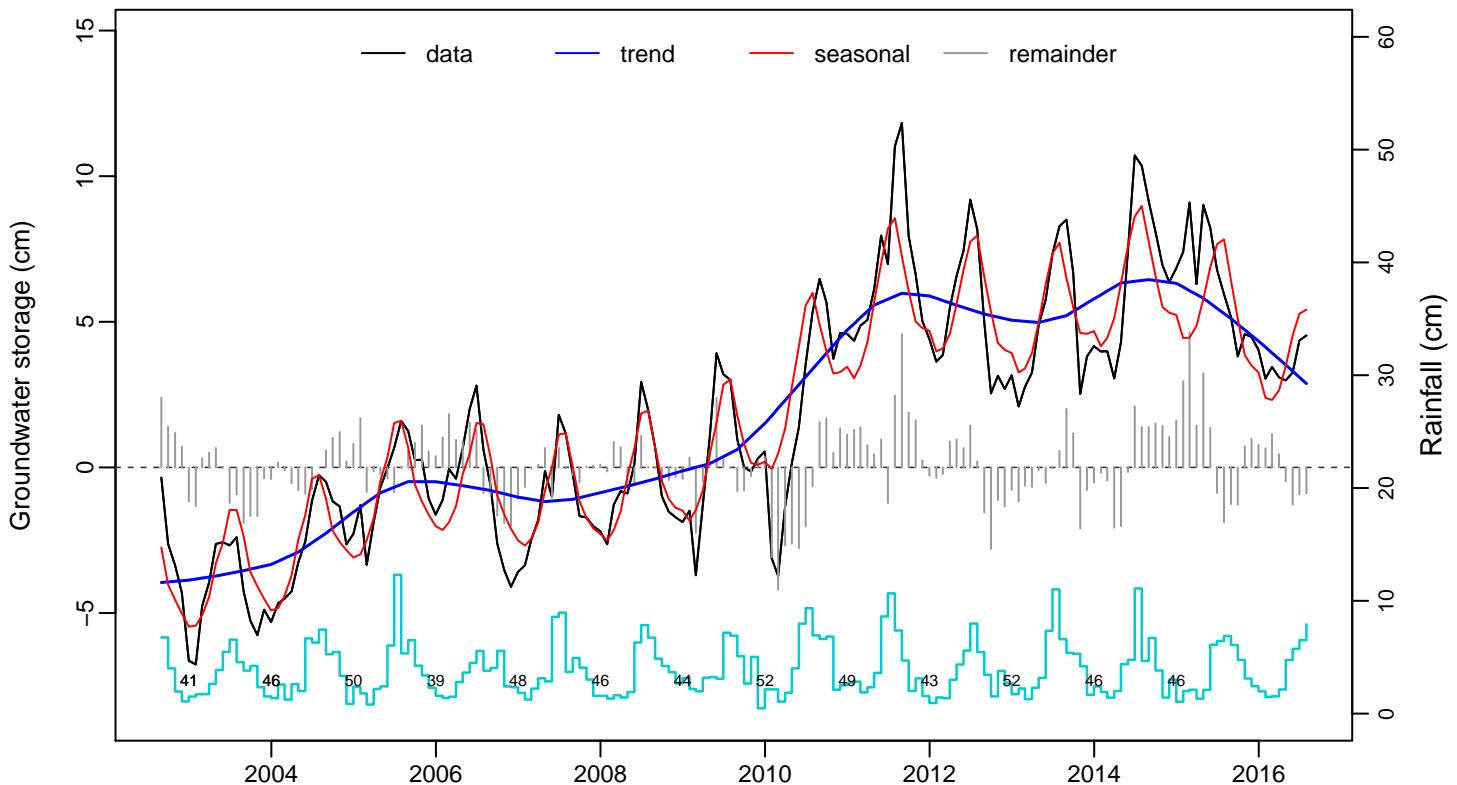


Fig. S54: Northern Great Plains Aquifer (14)



**Seasonal-Trend-Remainder (GRACE GWS)
Proportion of variance**

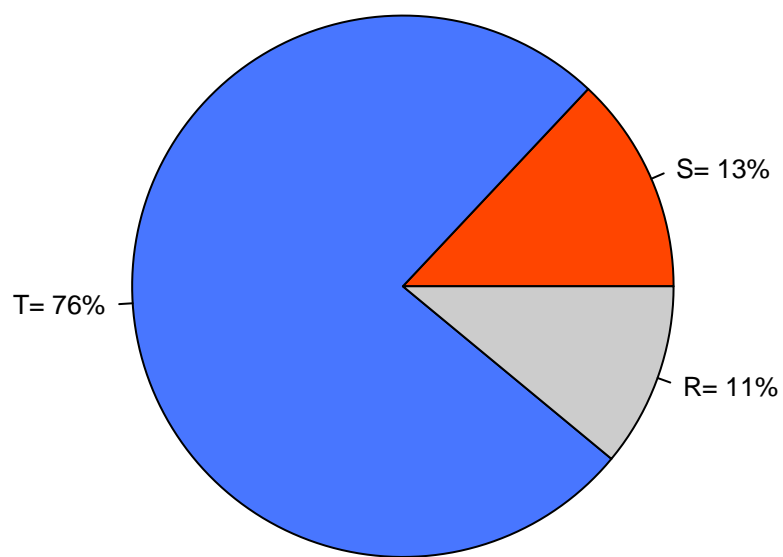
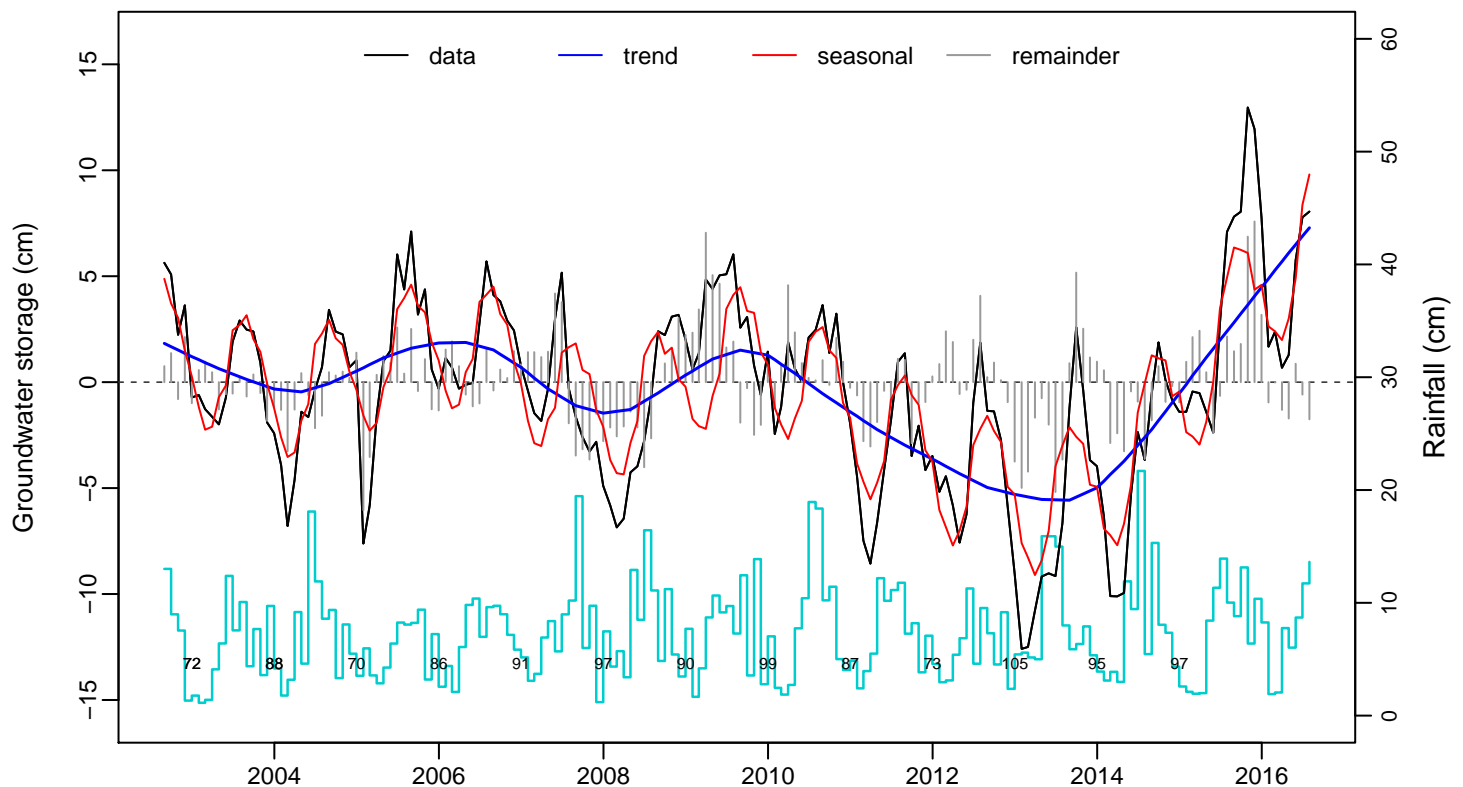


Fig. S55: Cambro–Ordovician Aquifer System (15)



**Seasonal–Trend–Remainder (GRACE GWS)
Proportion of variance**

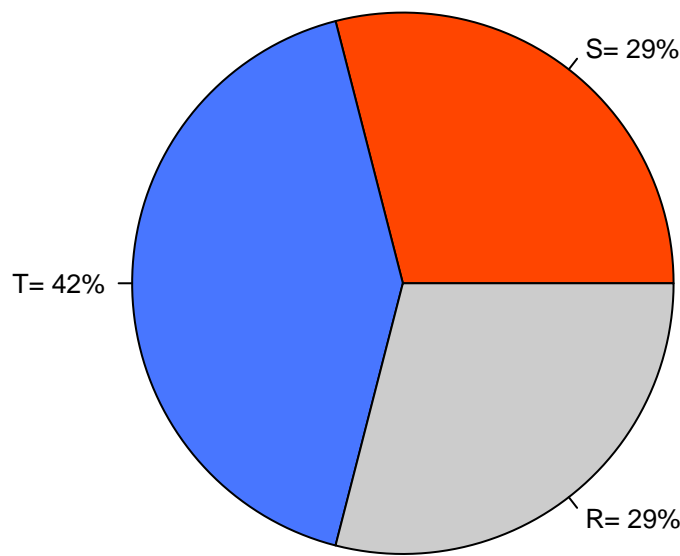
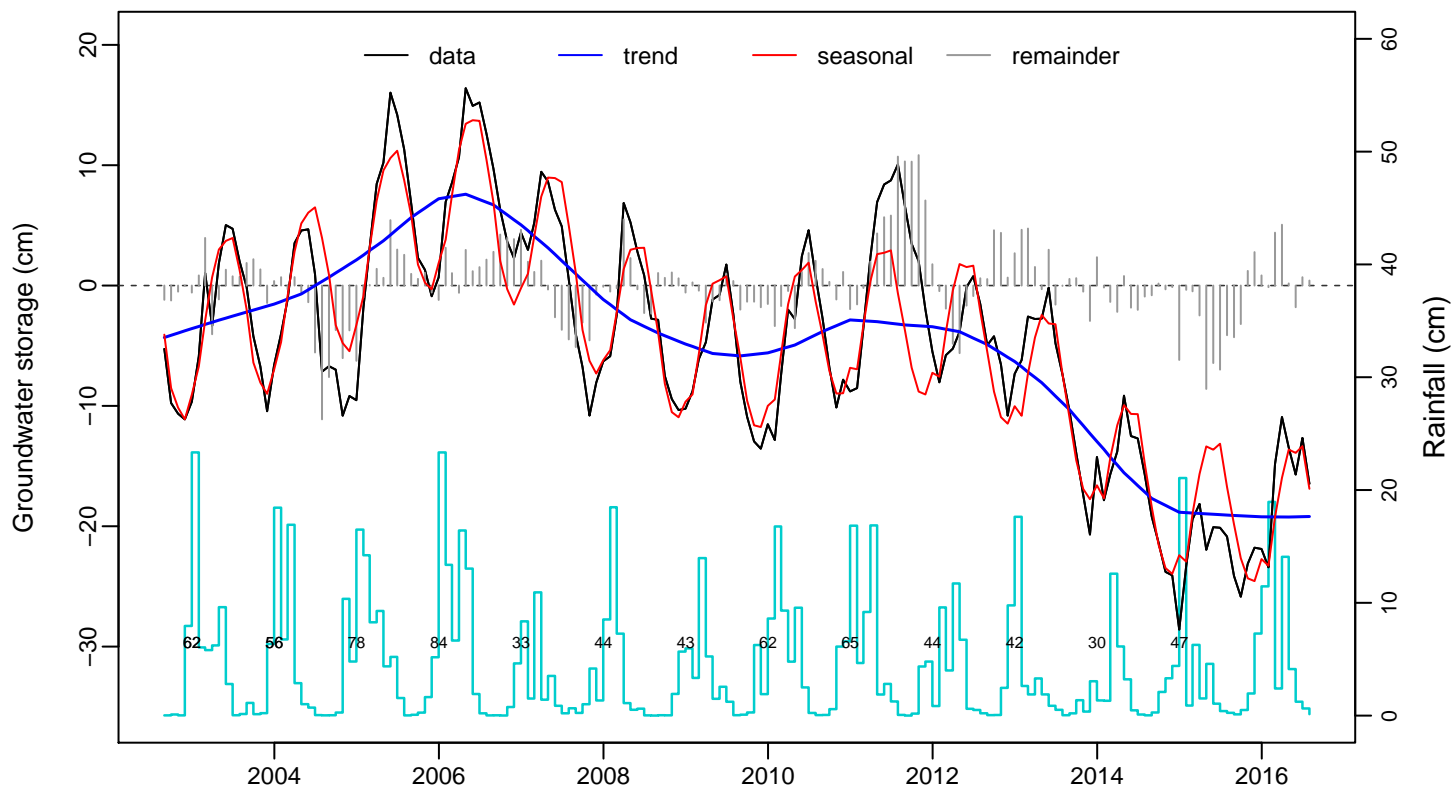


Fig. S56: California Central Valley Aquifer System (16)



**Seasonal-Trend-Remainder (GRACE GWS)
Proportion of variance**

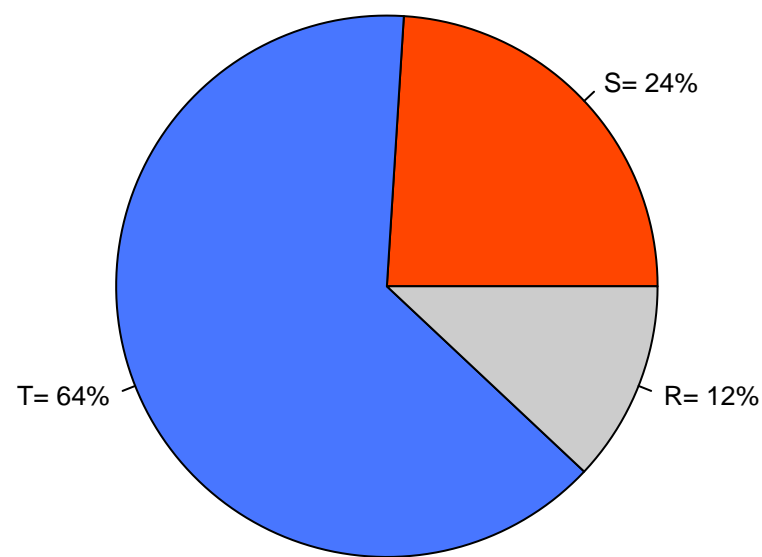
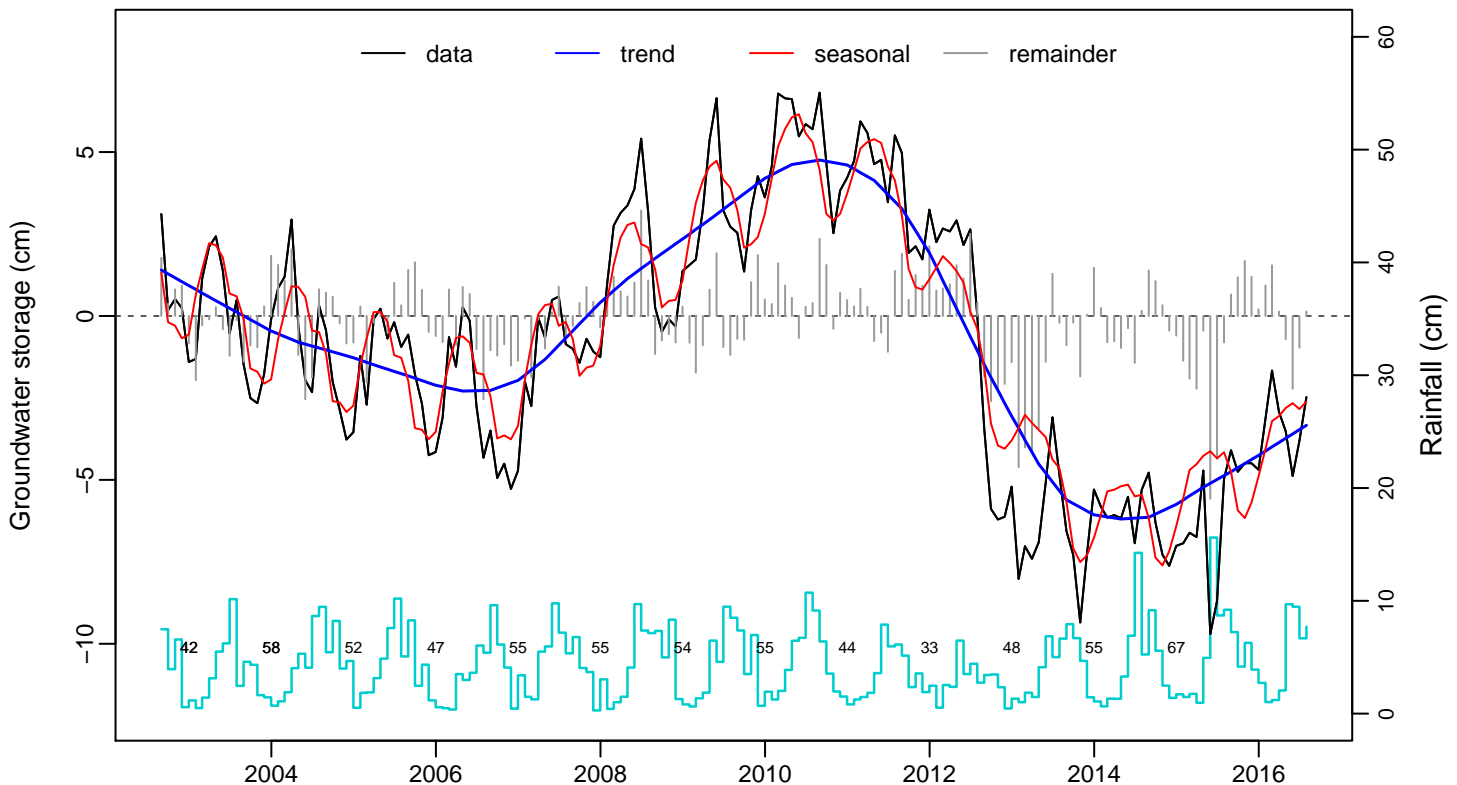


Fig. S57: Ogallala Aquifer (High Plains) (17)



**Seasonal–Trend–Remainder (GRACE GWS)
Proportion of variance**

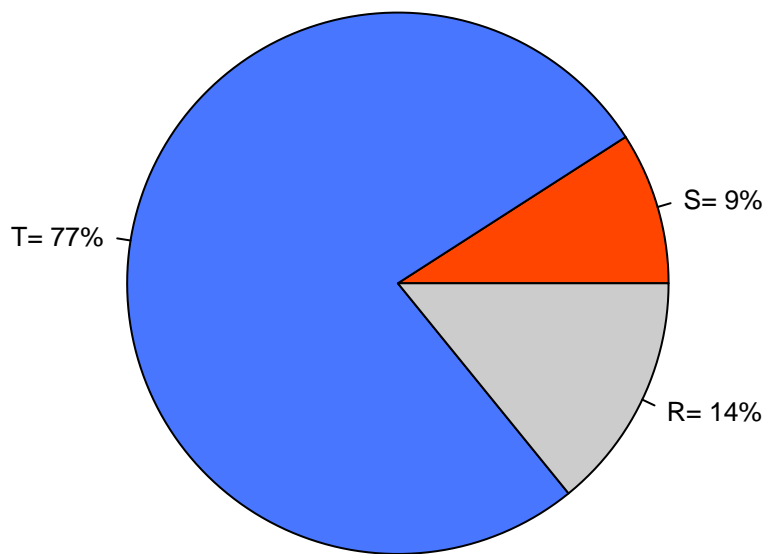
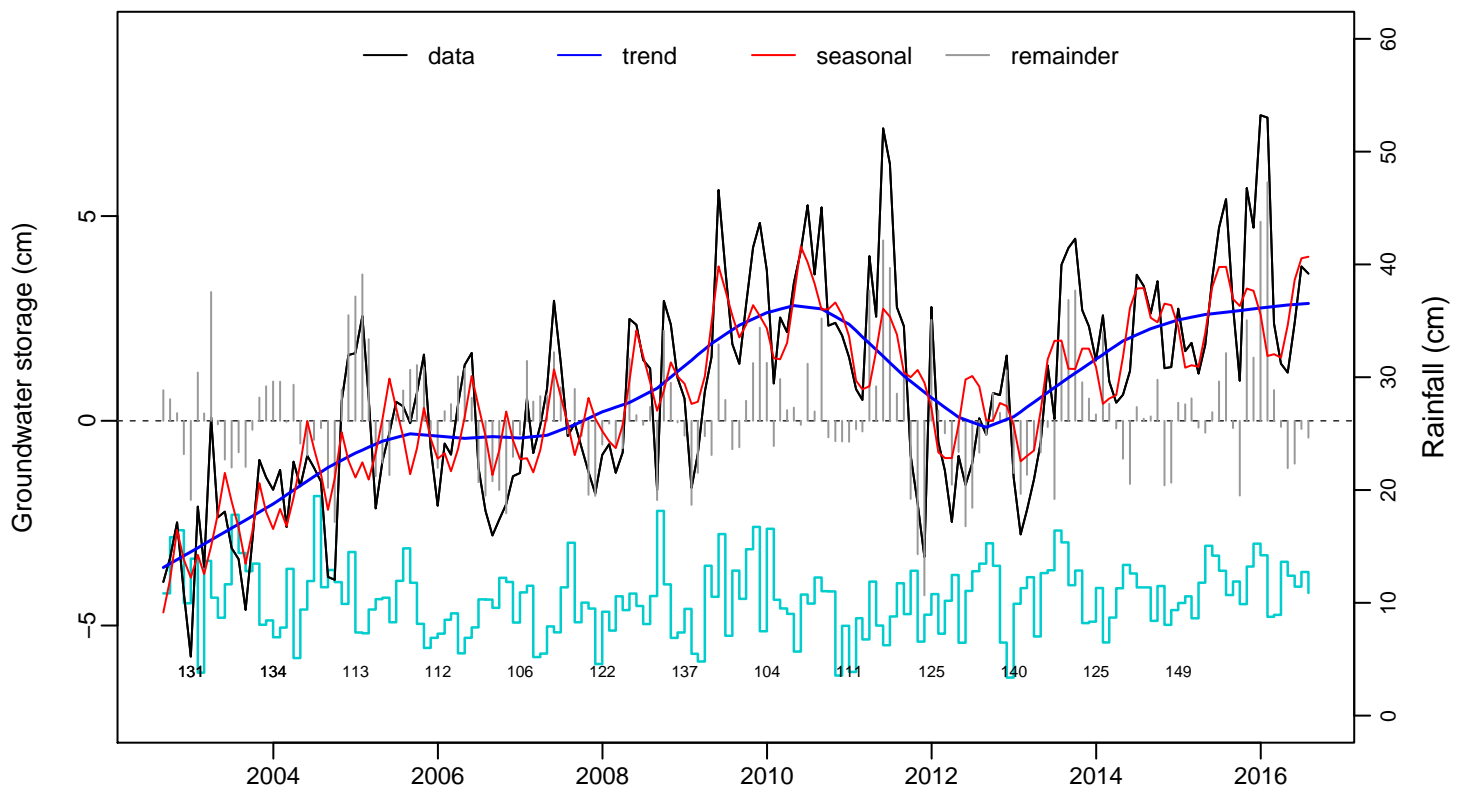


Fig. S58: Atlantic and Gulf Coastal Plains Aquifer (18)



**Seasonal–Trend–Remainder (GRACE GWS)
Proportion of variance**

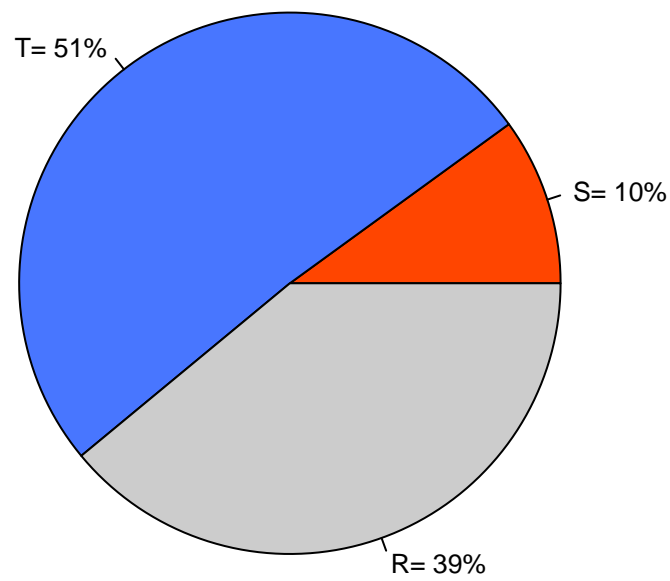
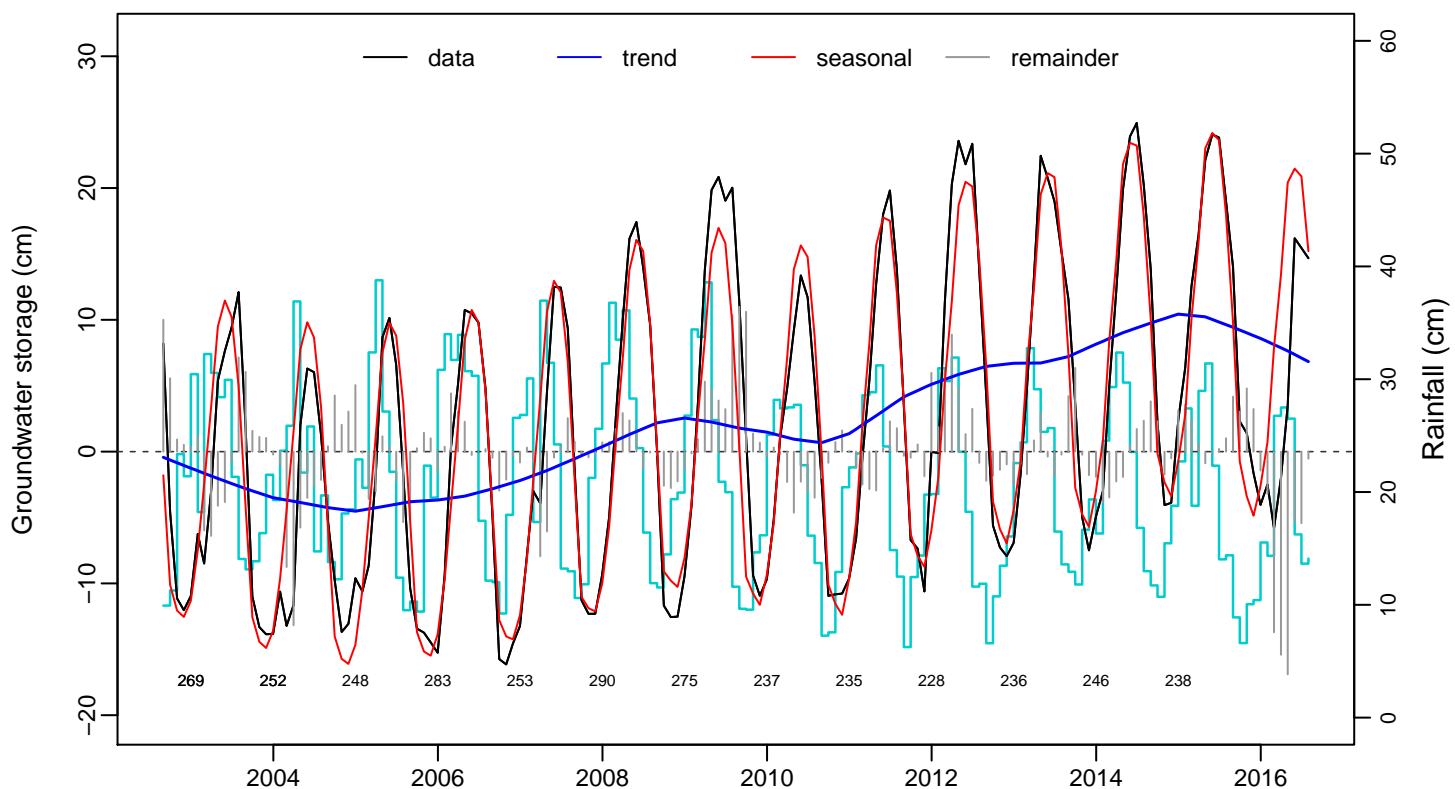


Fig. S59: Amazon Basin (19)



**Seasonal–Trend–Remainder (GRACE GWS)
Proportion of variance**

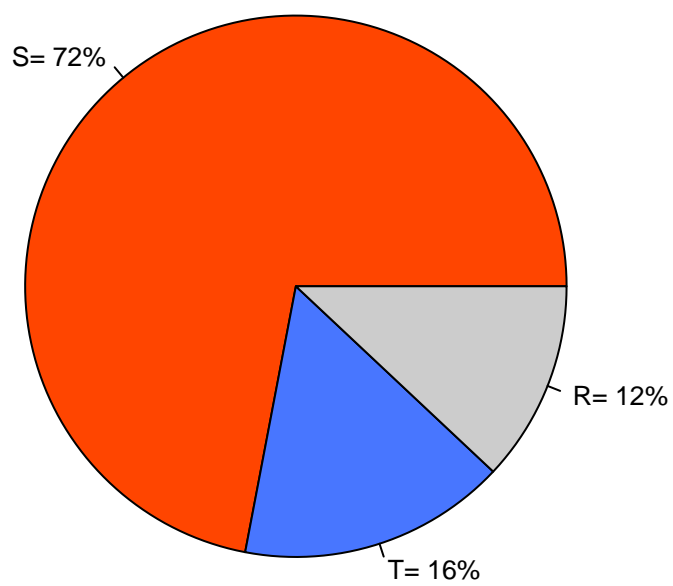
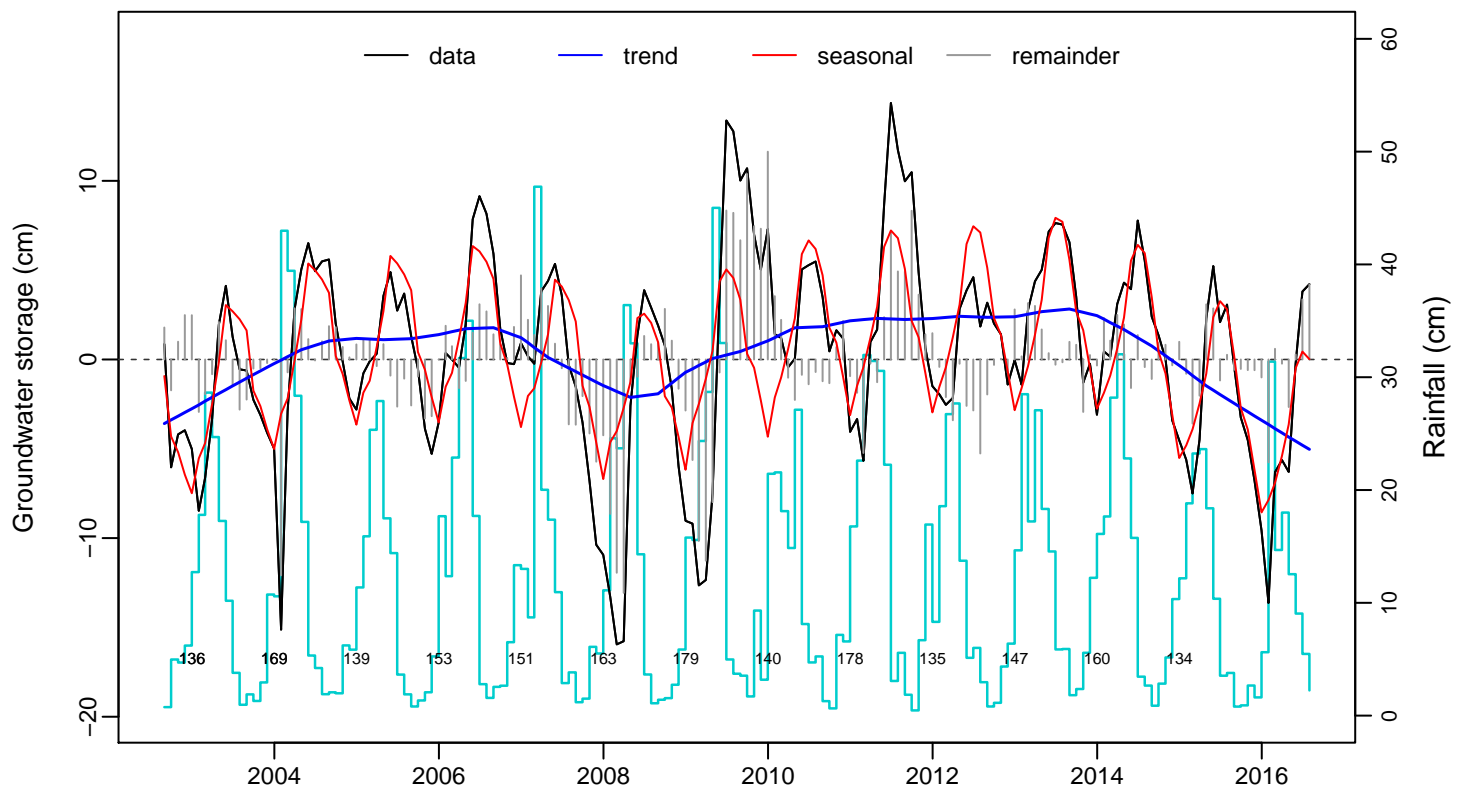


Fig. S60: Maranhao Basin (20)



**Seasonal-Trend-Remainder (GRACE GWS)
Proportion of variance**

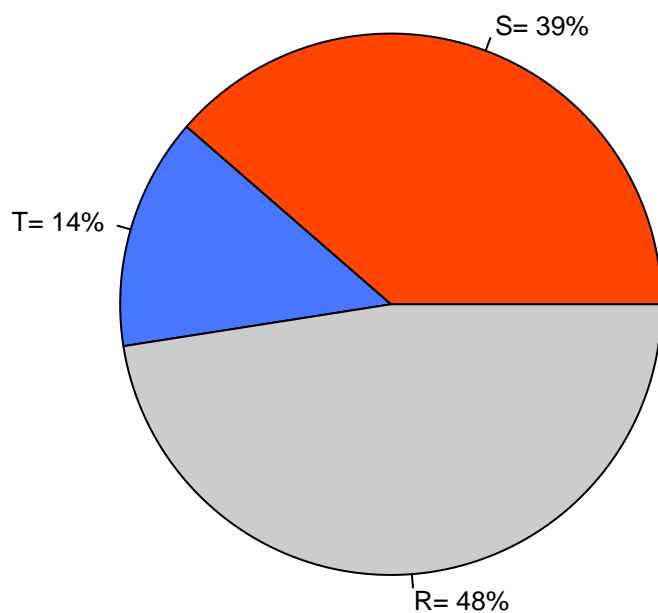
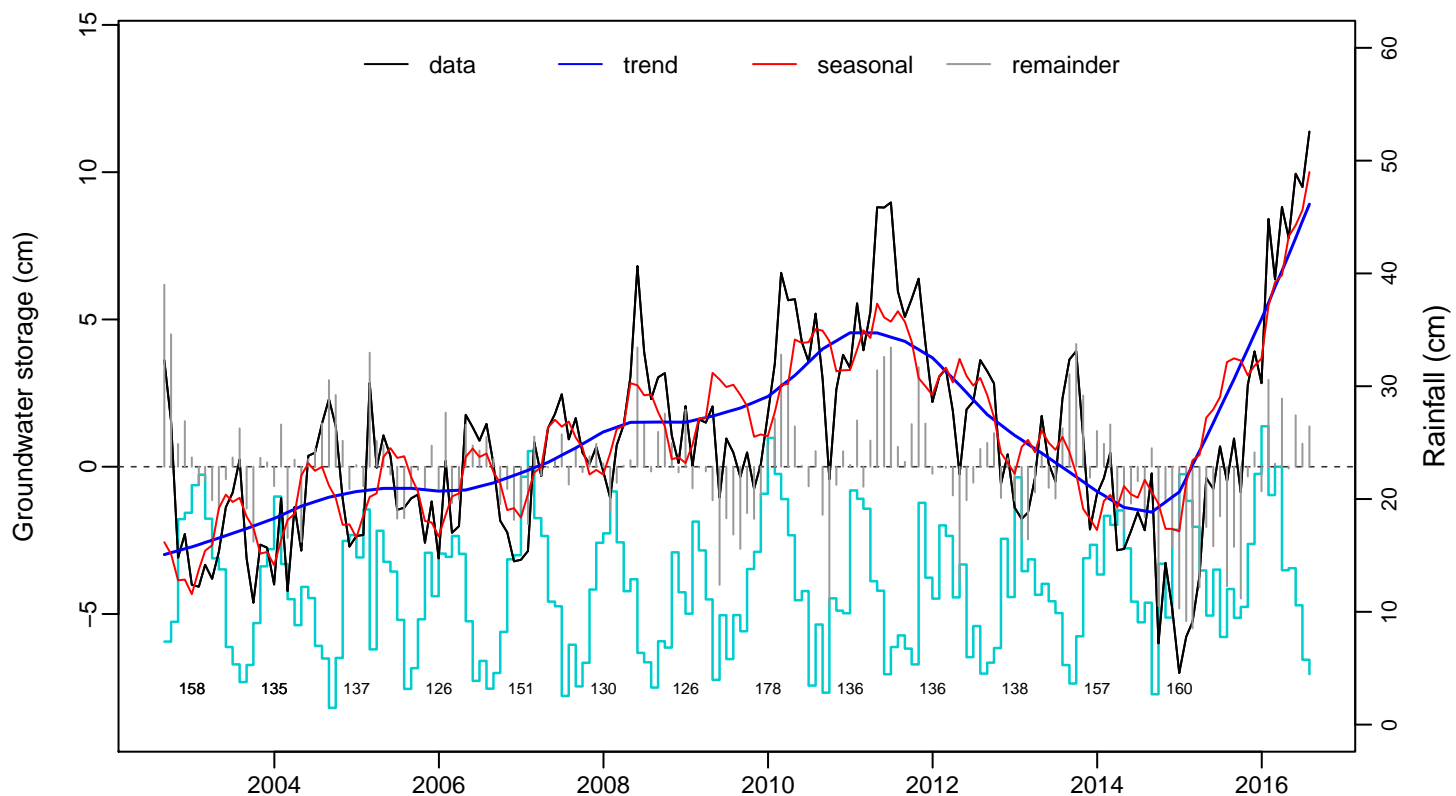


Fig. S61: Guarani Aquifer System (Parana Basin) (21)



**Seasonal–Trend–Remainder (GRACE GWS)
Proportion of variance**

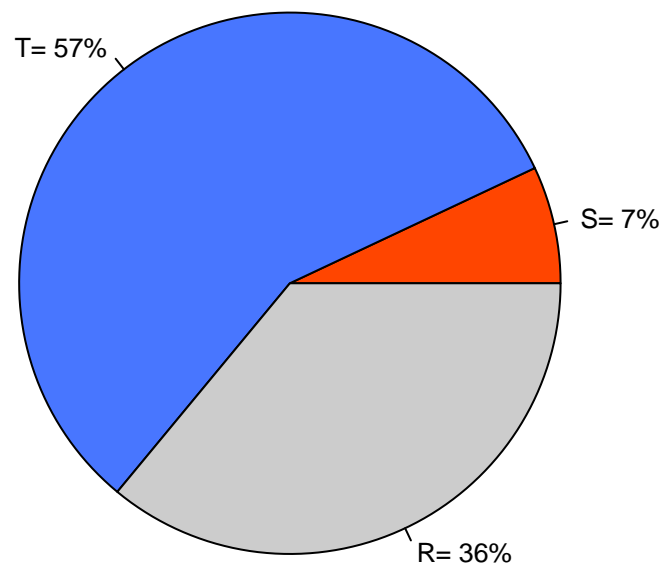
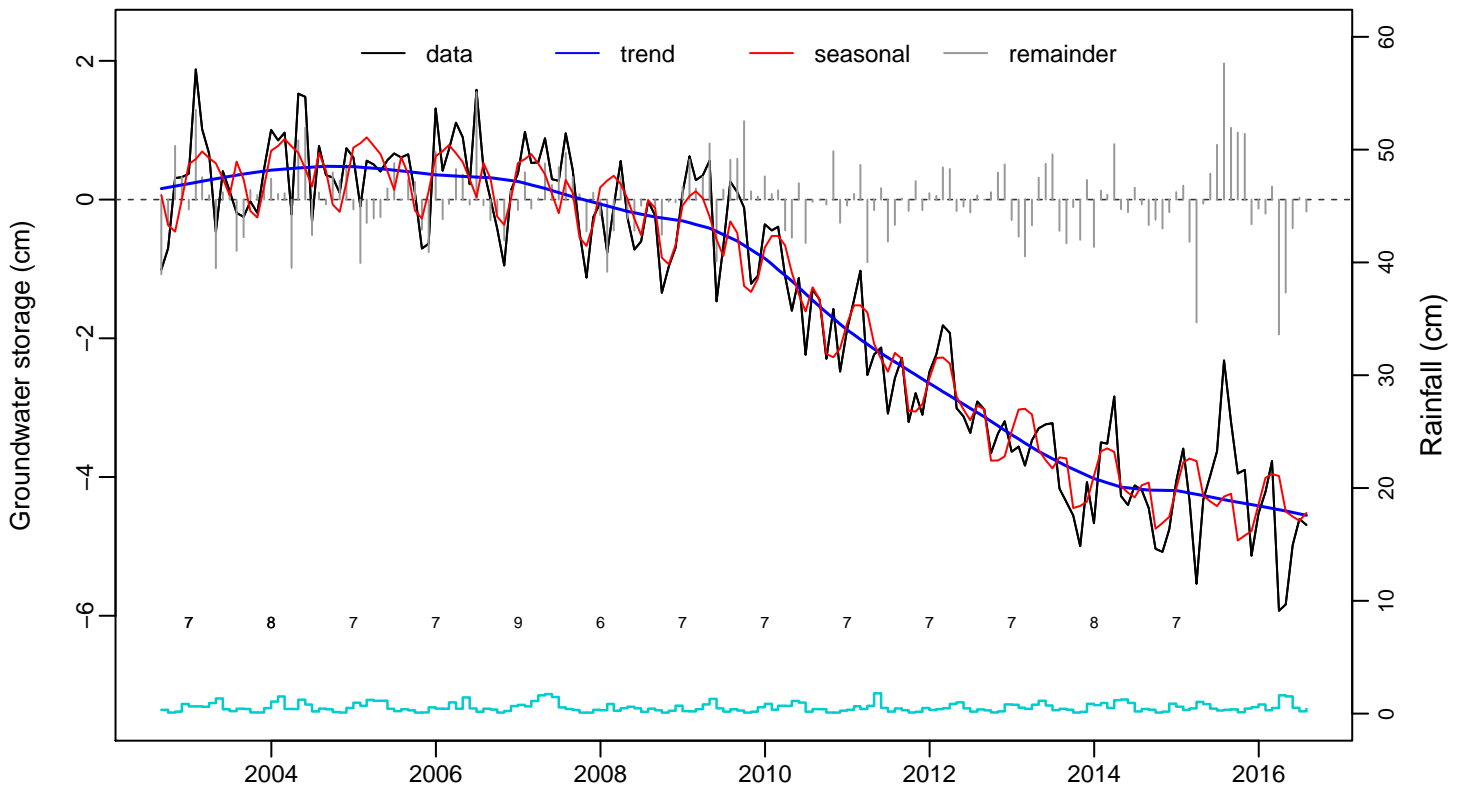


Fig. S62: Arabian Aquifer System (22)



**Seasonal–Trend–Remainder (GRACE GWS)
Proportion of variance**

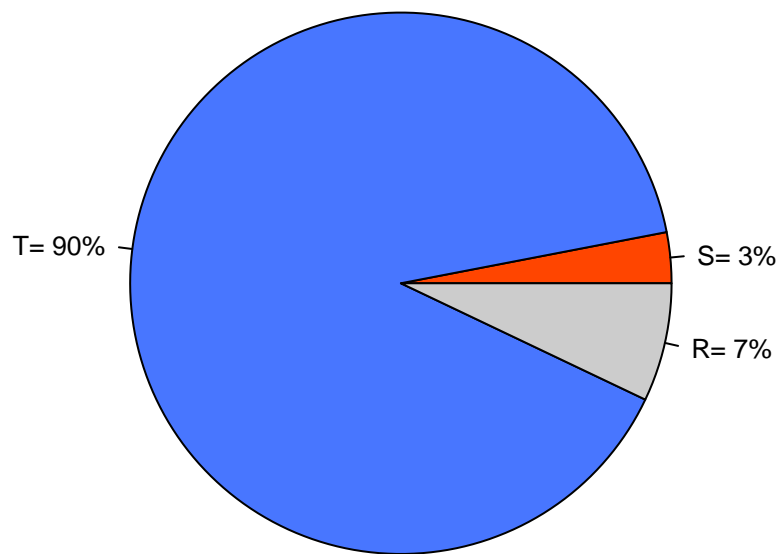
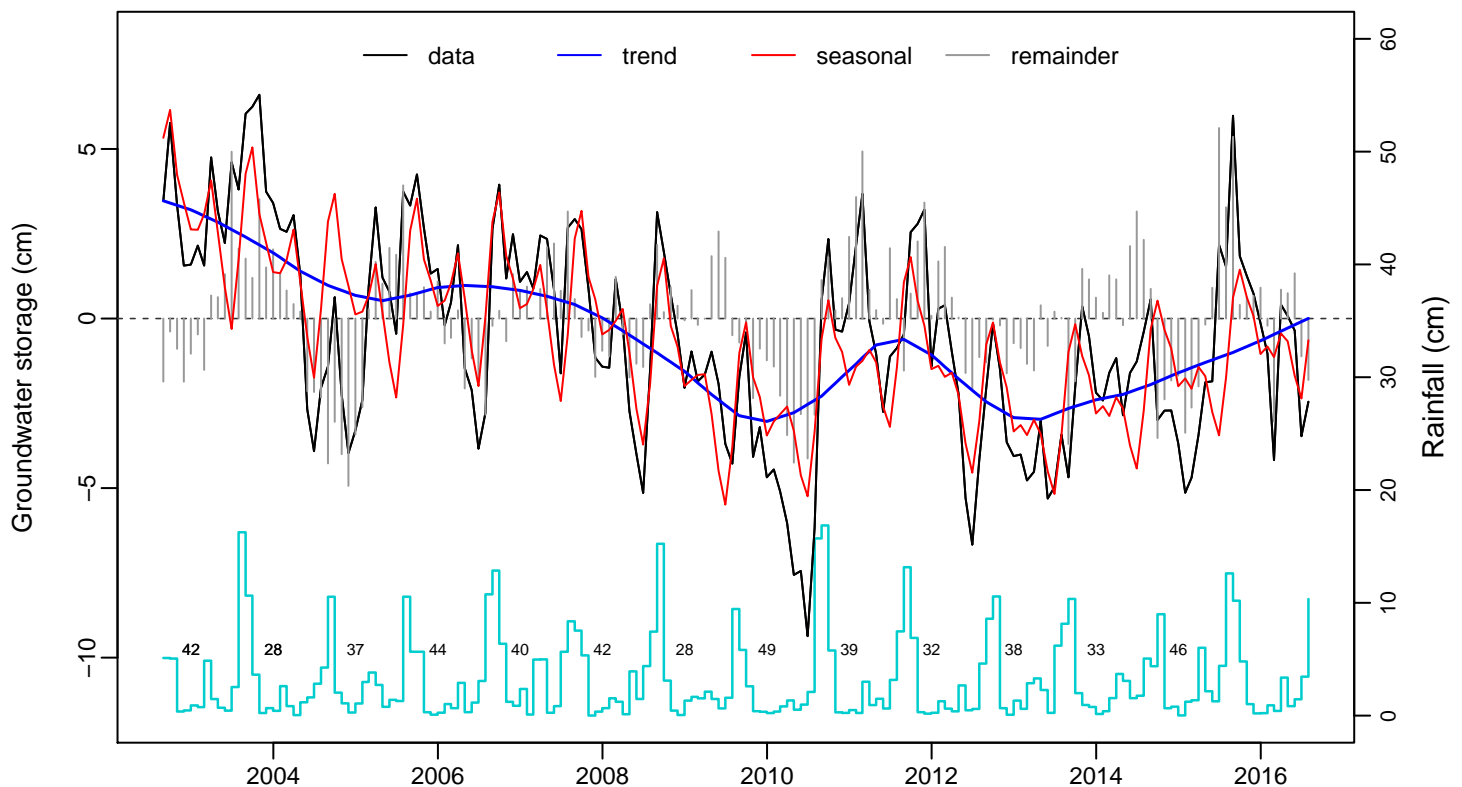


Fig. S63: Indus River Basin (23)



**Seasonal-Trend-Remainder (GRACE GWS)
Proportion of variance**

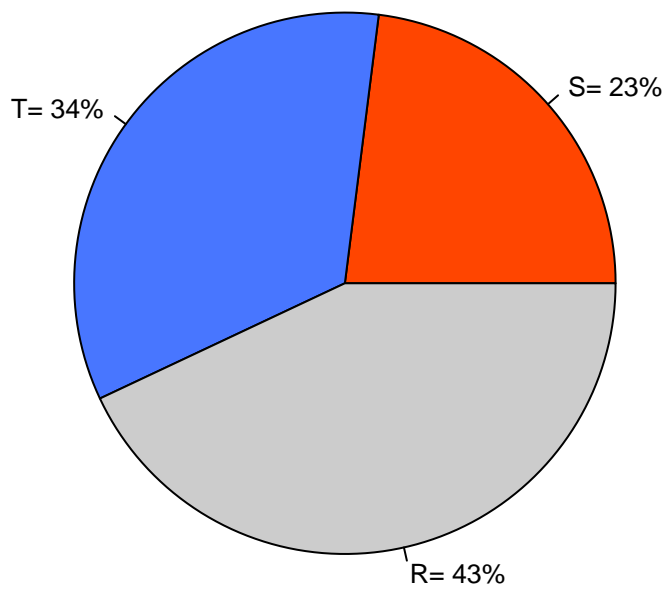
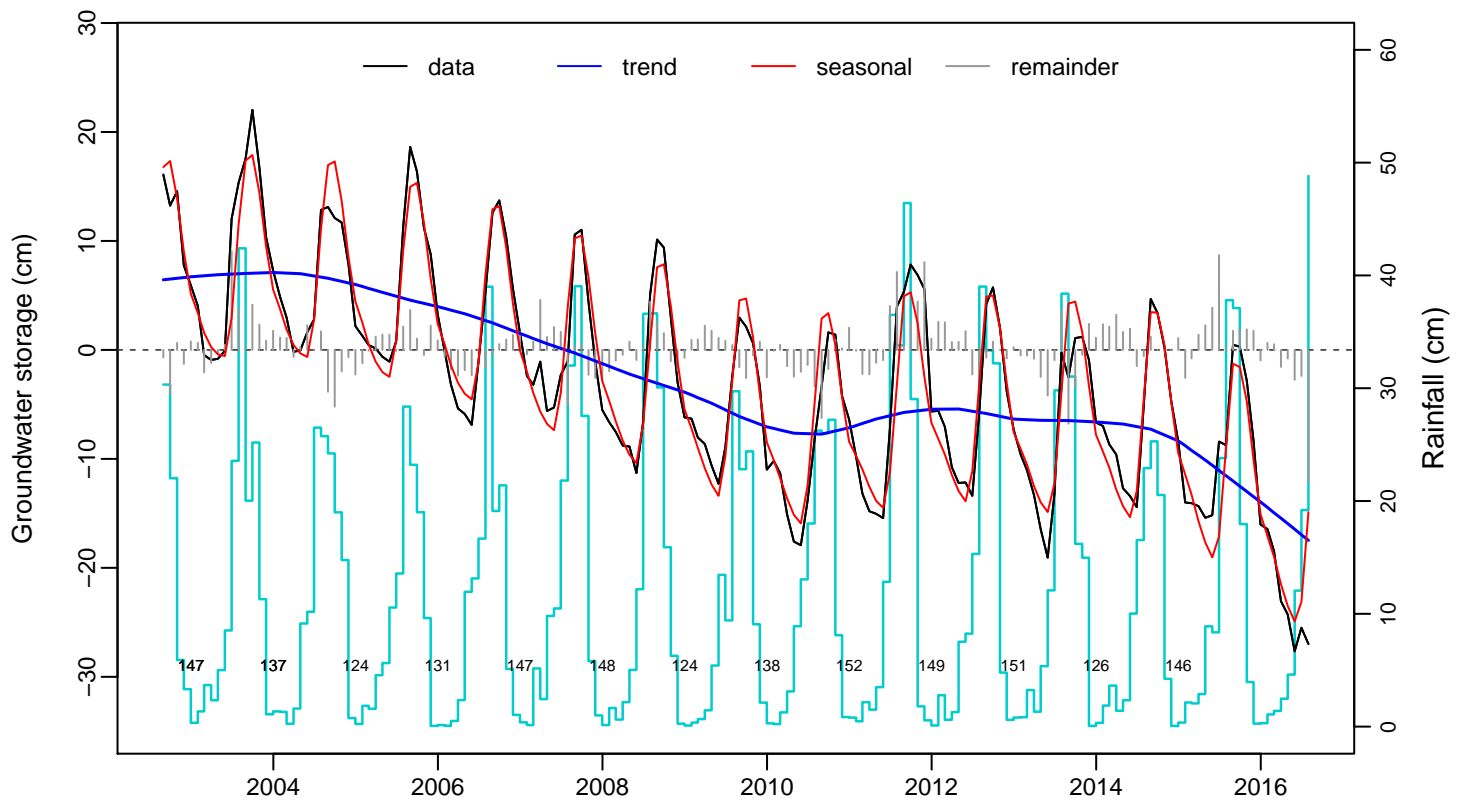


Fig. S64: Ganges–Brahmaputra River Basin (IGB) (24)



**Seasonal–Trend–Remainder (GRACE GWS)
Proportion of variance**

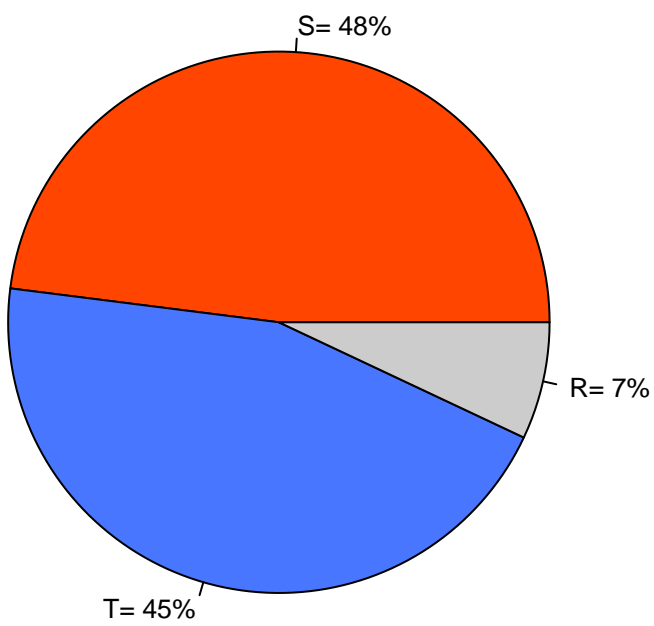
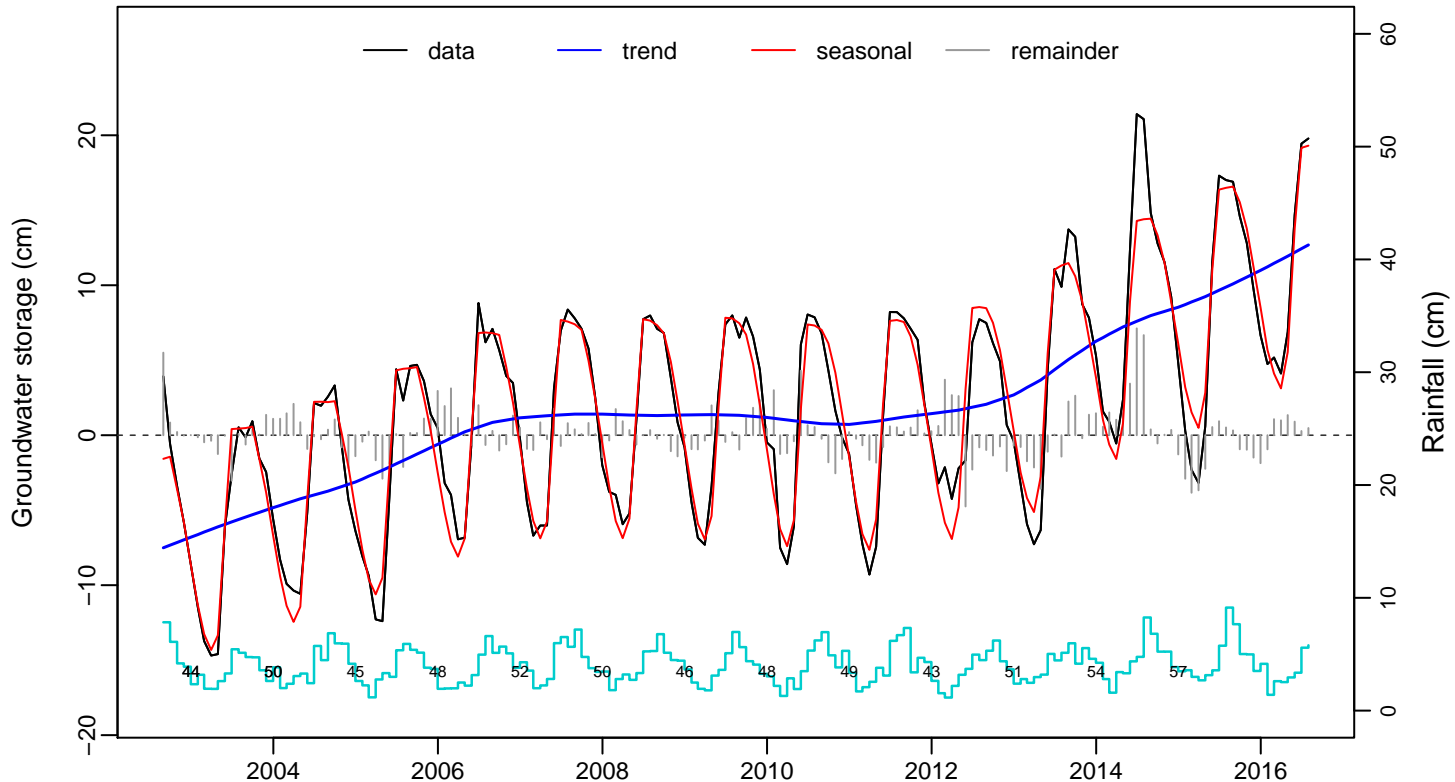


Fig. S65: West Siberian Artesian Basin (25)



**Seasonal–Trend–Remainder (GRACE GWS)
Proportion of variance**

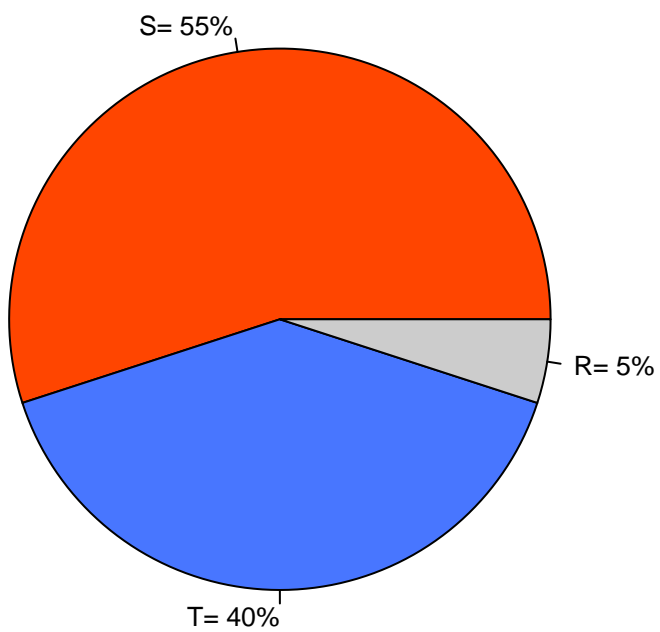
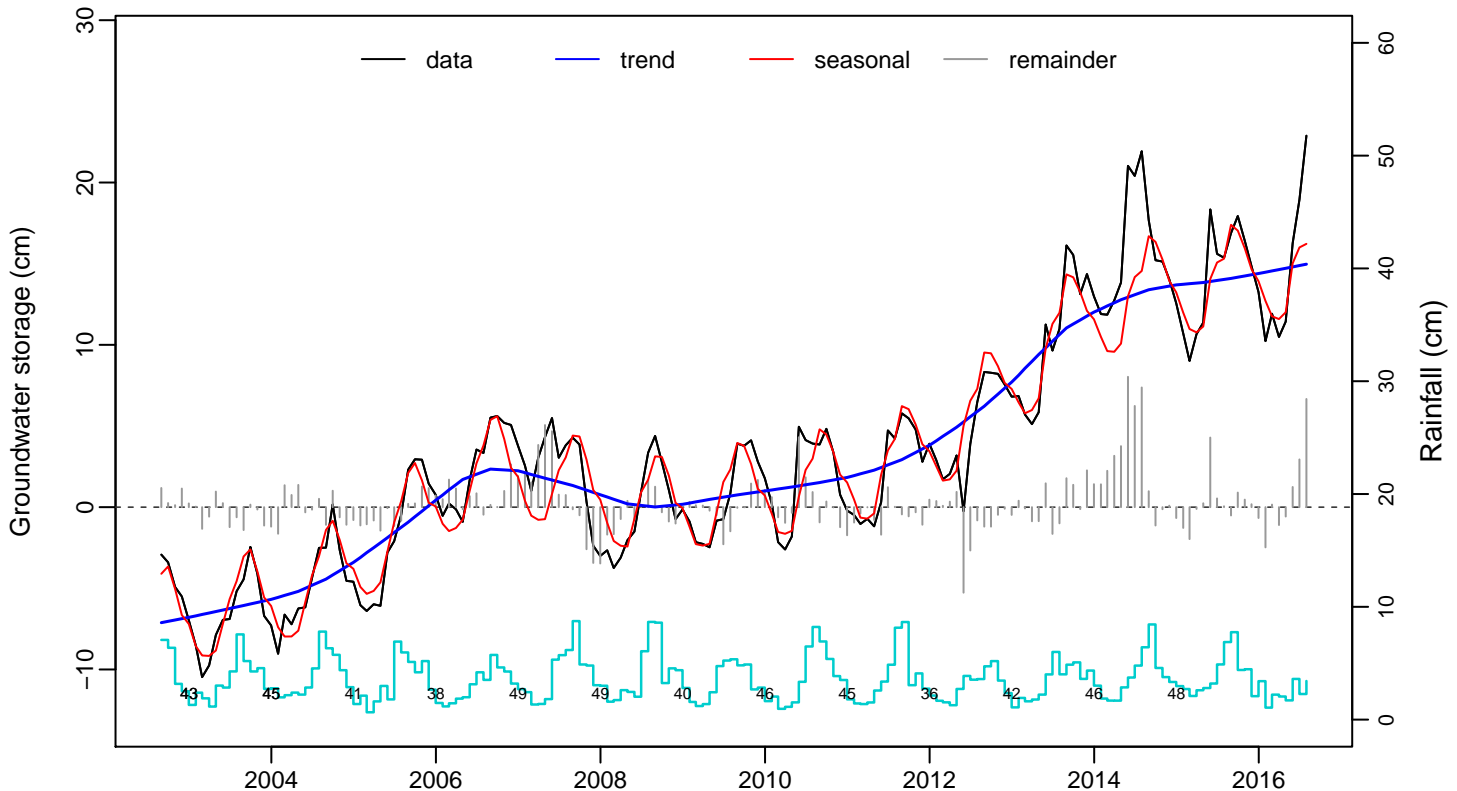


Fig. S66: Tunguss Basin (26)



**Seasonal–Trend–Remainder (GRACE GWS)
Proportion of variance**

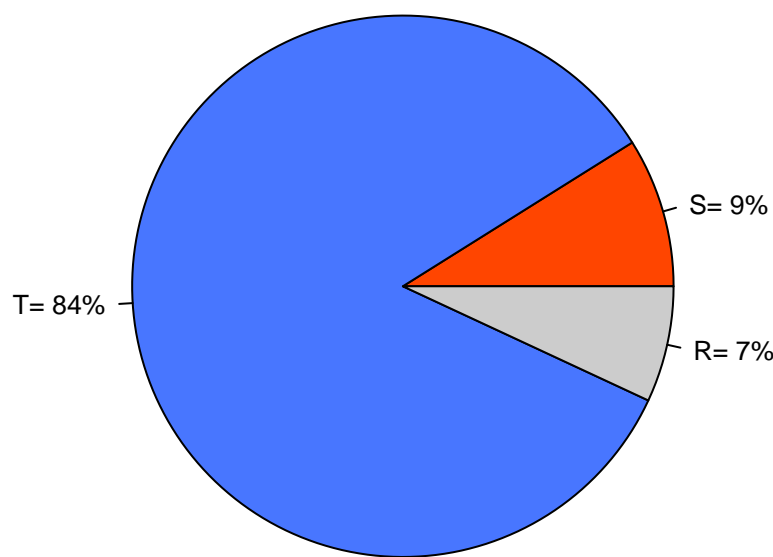
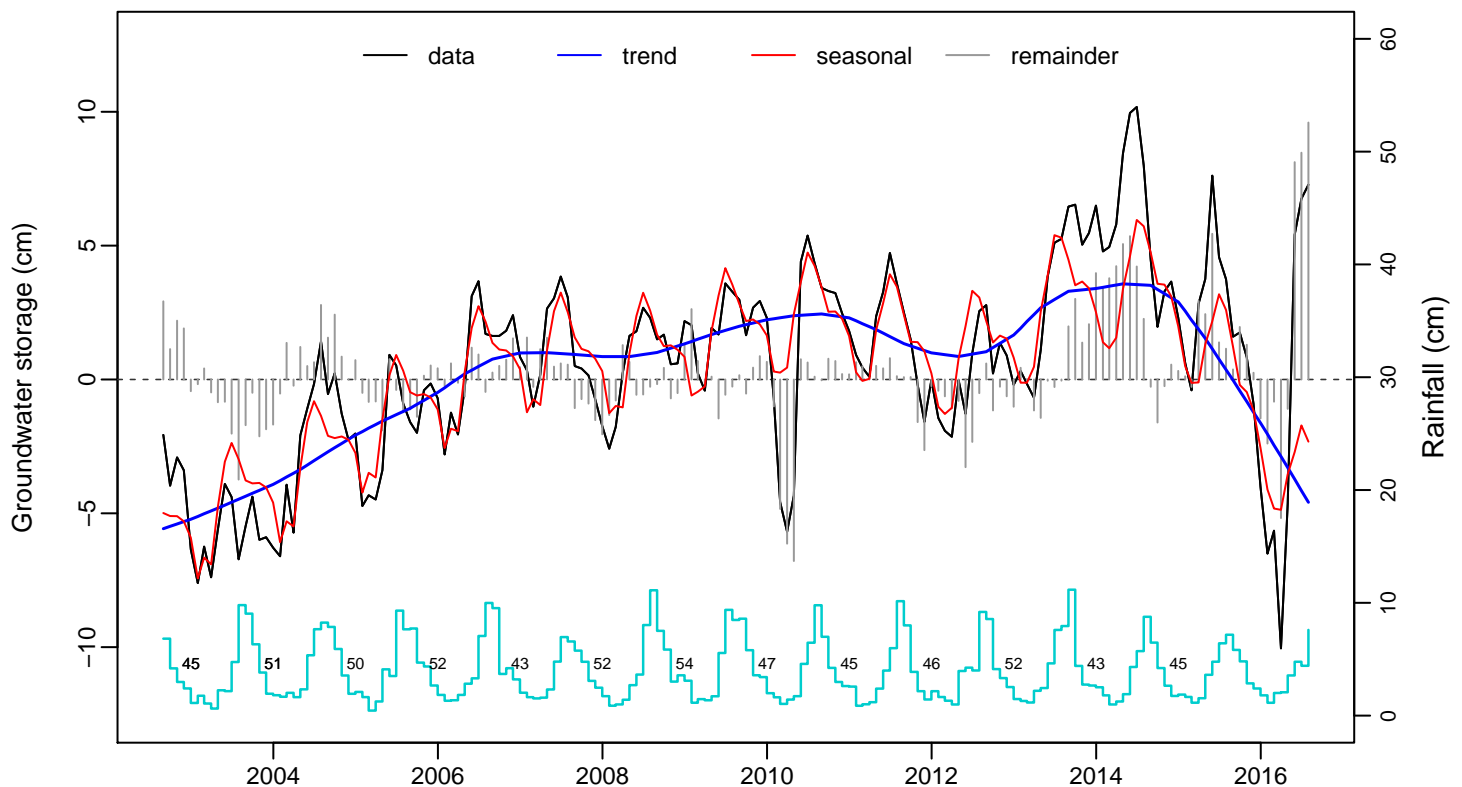


Fig. S67: Angara–Lena Basin (27)



**Seasonal–Trend–Remainder (GRACE GWS)
Proportion of variance**

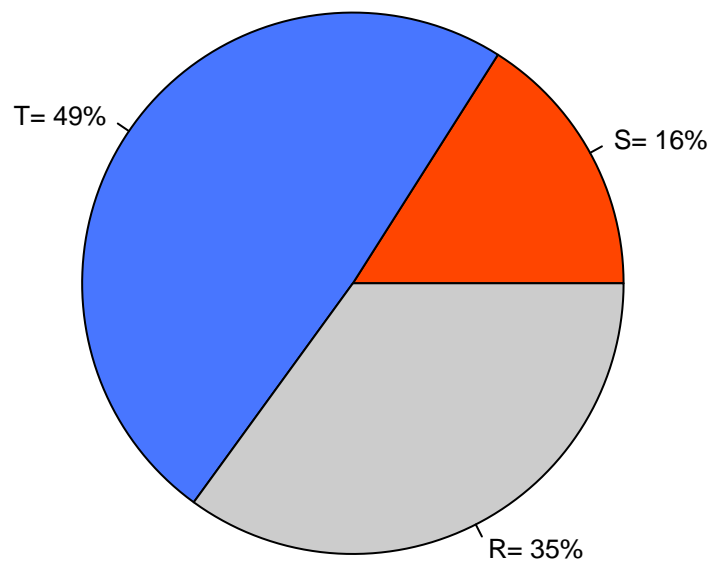
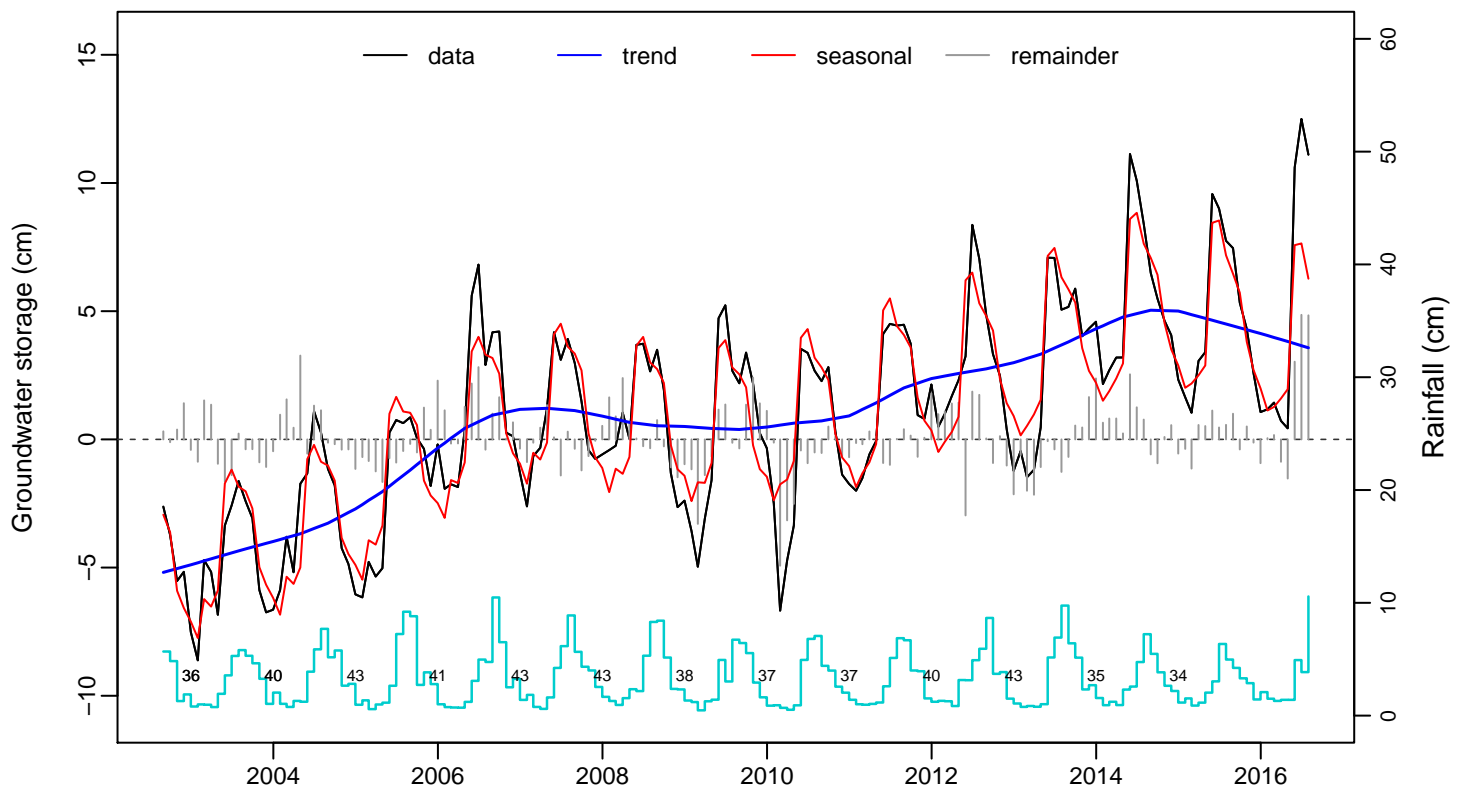


Fig. S68: Yakut Basin (28)



**Seasonal-Trend-Remainder (GRACE GWS)
Proportion of variance**

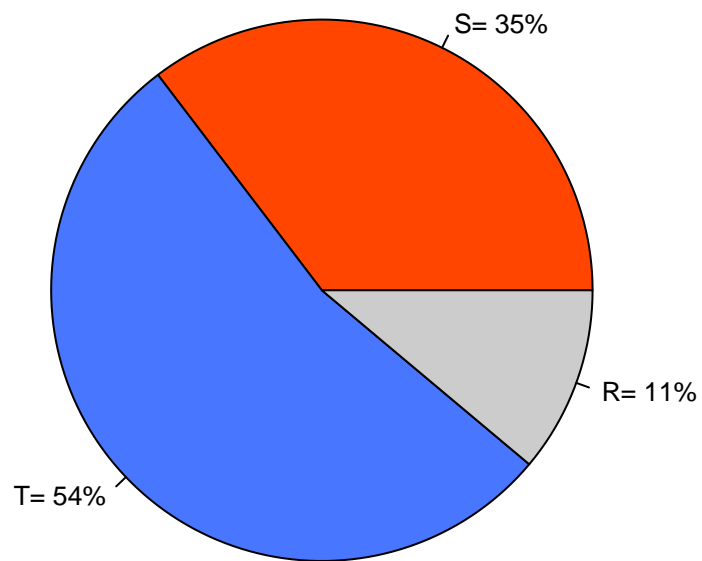
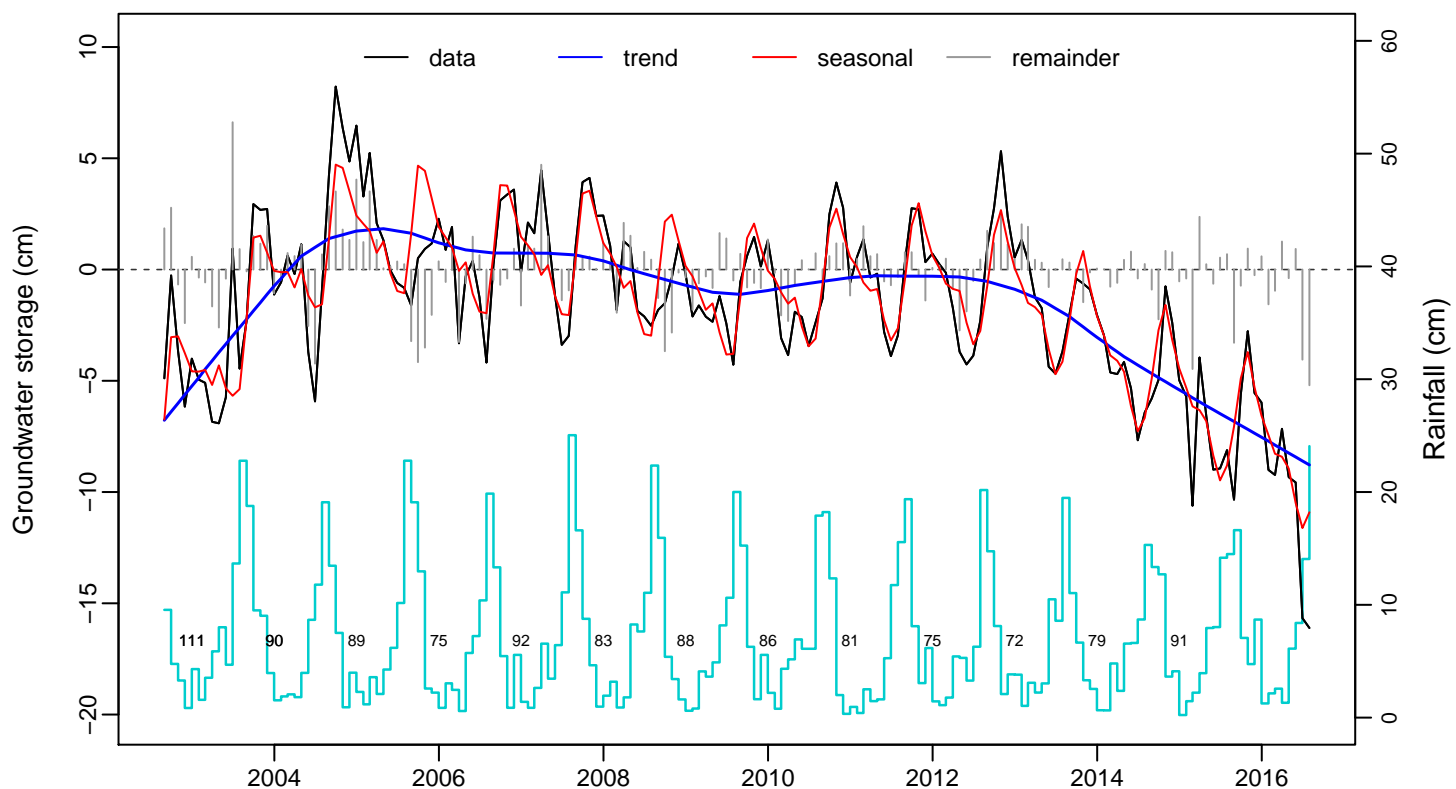


Fig. S69: North China Plains Aquifer System (29)



**Seasonal–Trend–Remainder (GRACE GWS)
Proportion of variance**

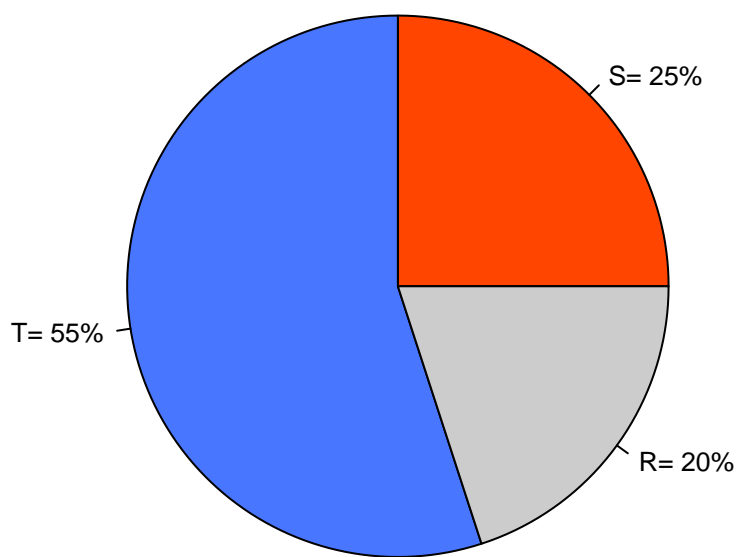
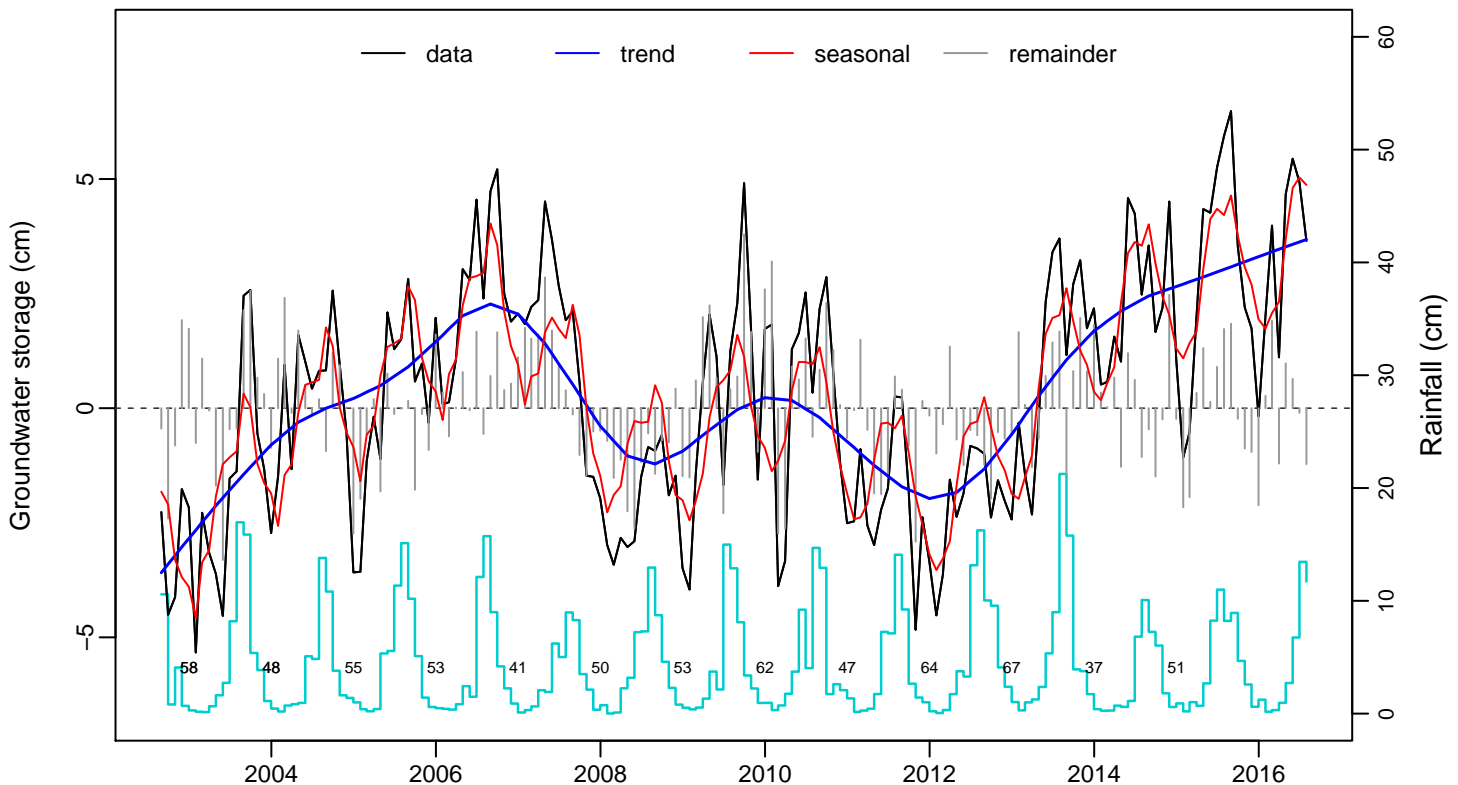


Fig. S70: Song-Liao Plain (30)



**Seasonal-Trend-Remainder (GRACE GWS)
Proportion of variance**

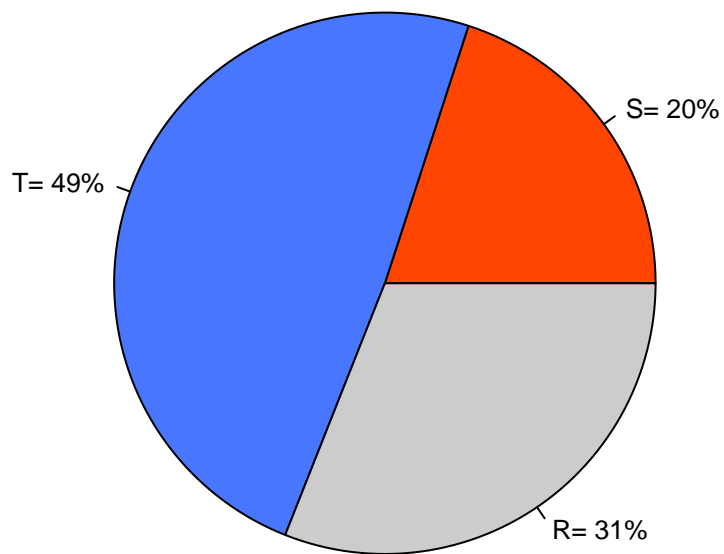
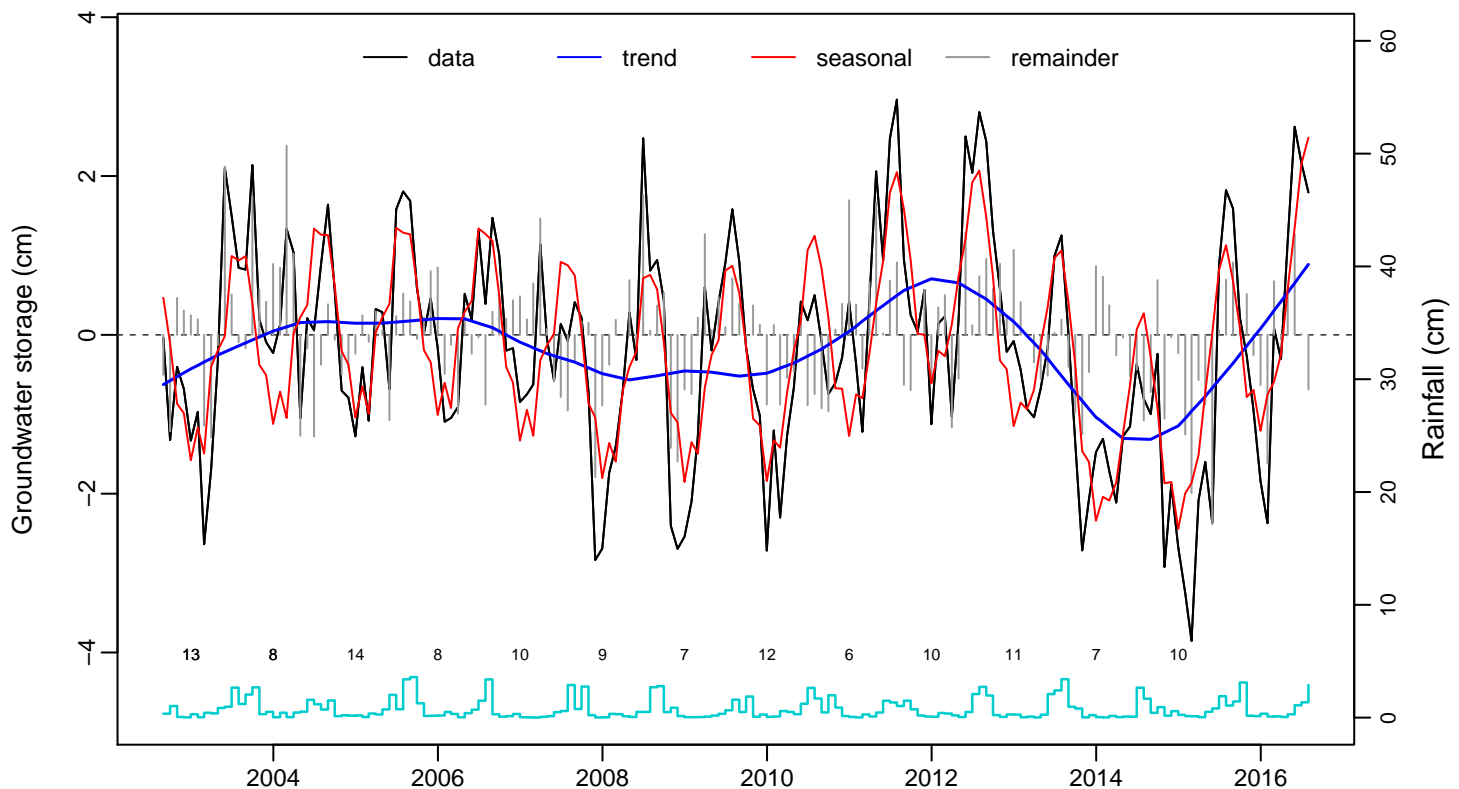


Fig. S71: Tarim Basin (31)



**Seasonal-Trend-Remainder (GRACE GWS)
Proportion of variance**

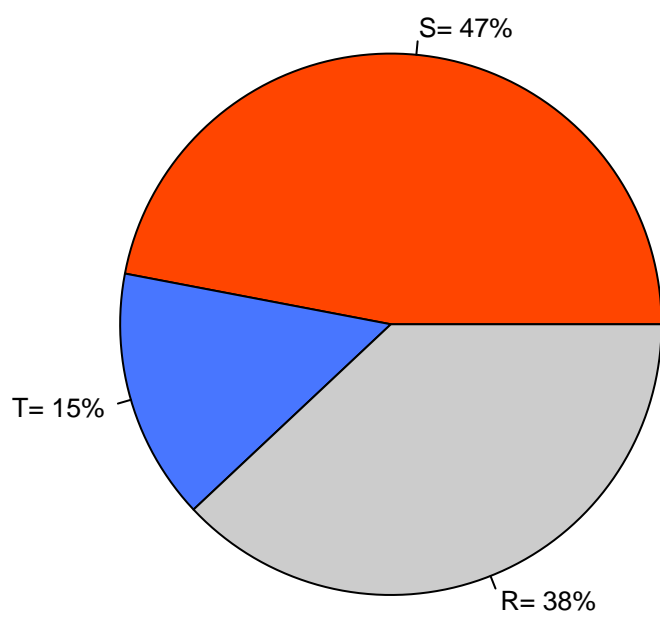
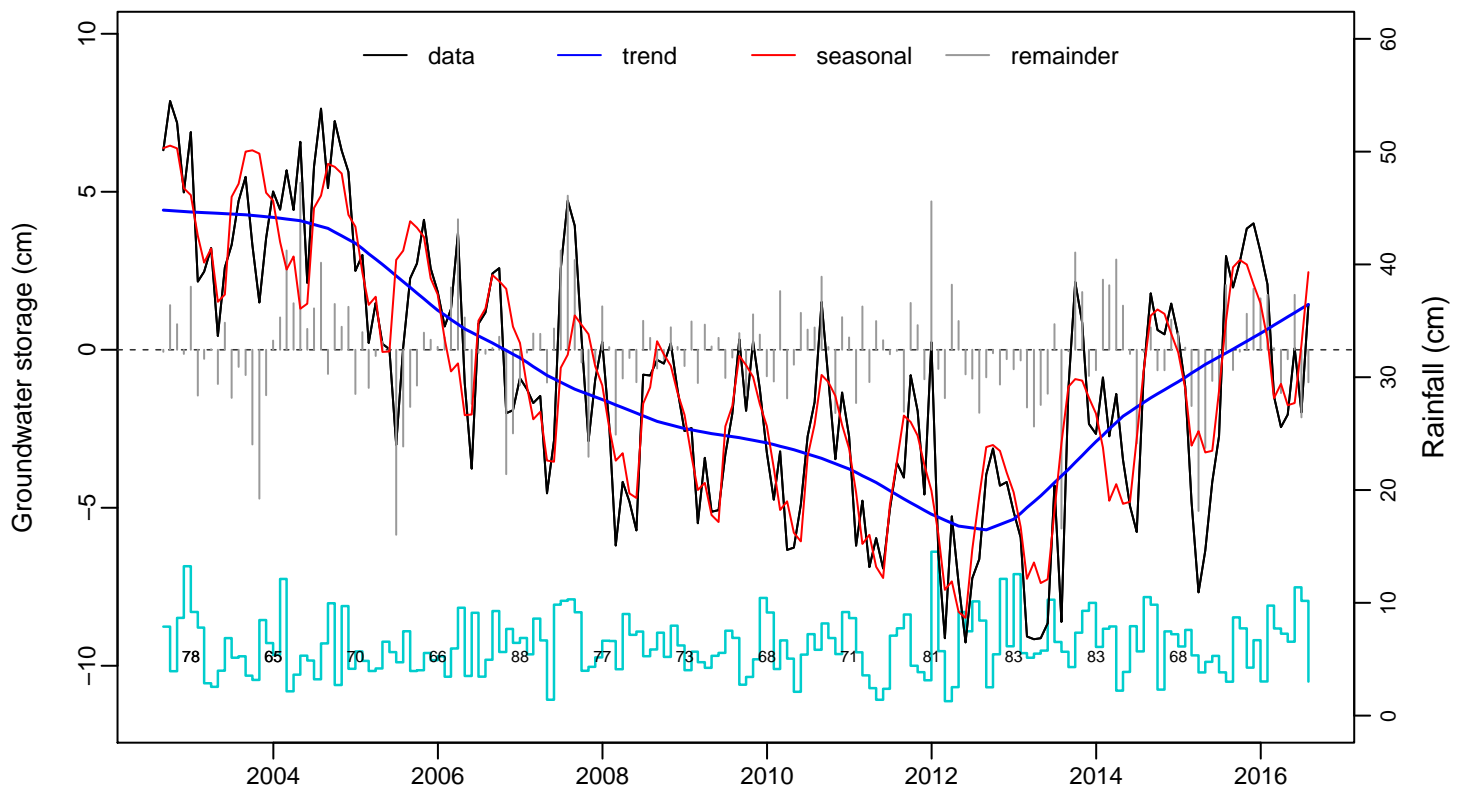


Fig. S72: Paris Basin (32)



**Seasonal–Trend–Remainder (GRACE GWS)
Proportion of variance**

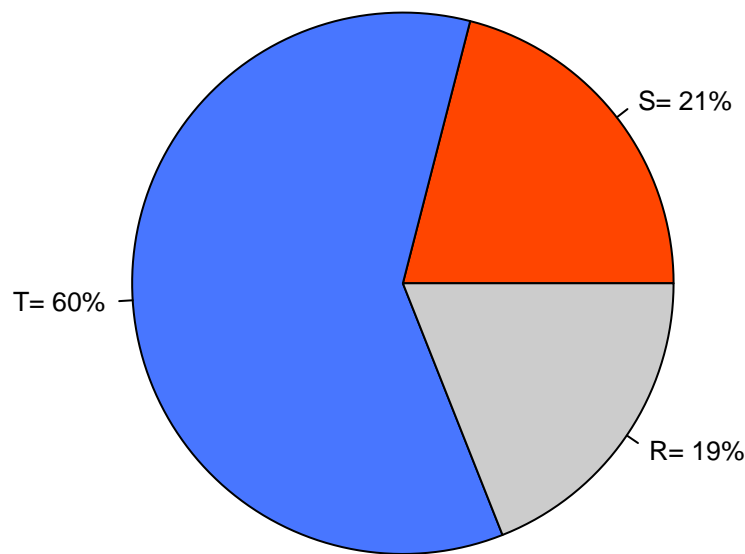
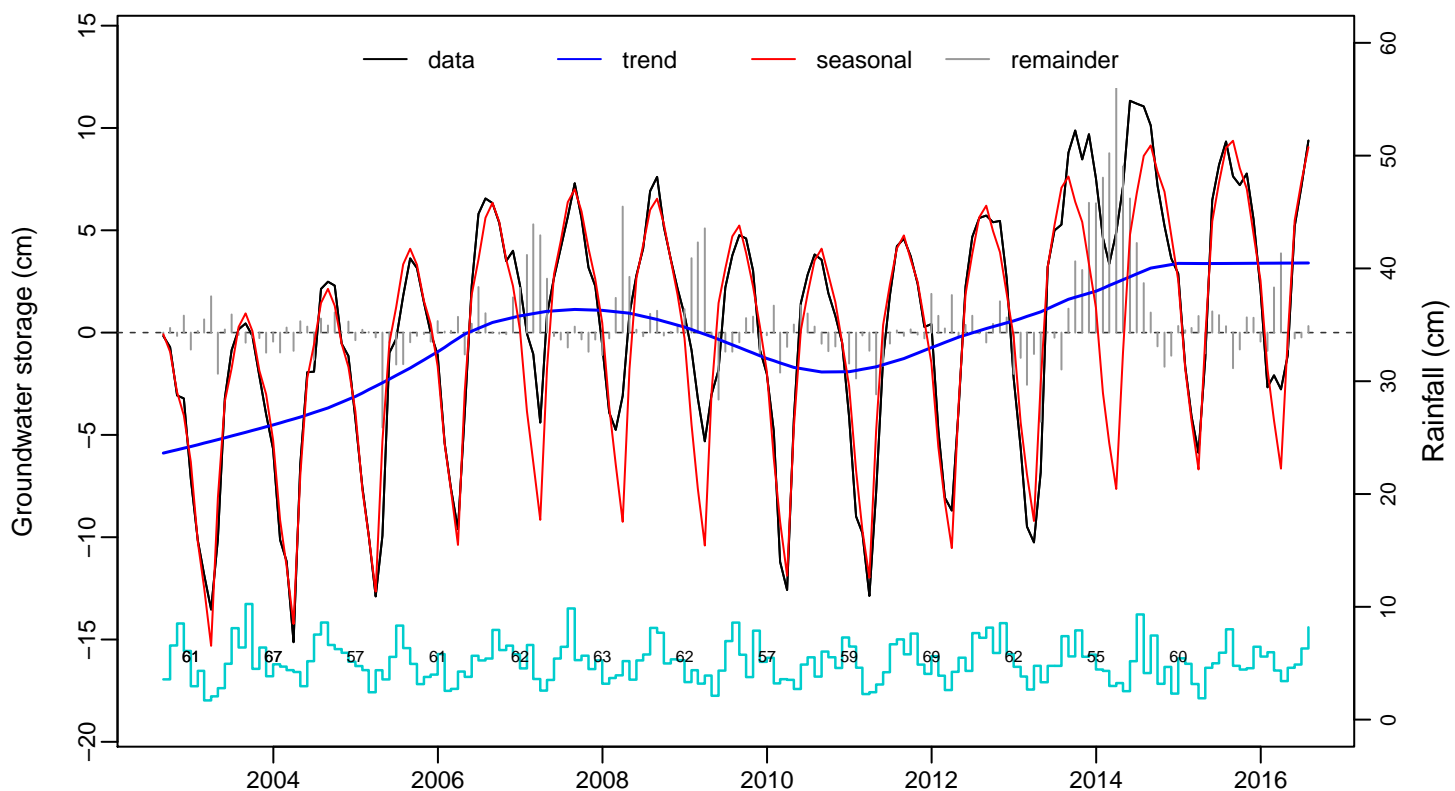


Fig. S73: East European Aquifer System (33)



**Seasonal–Trend–Remainder (GRACE GWS)
Proportion of variance**

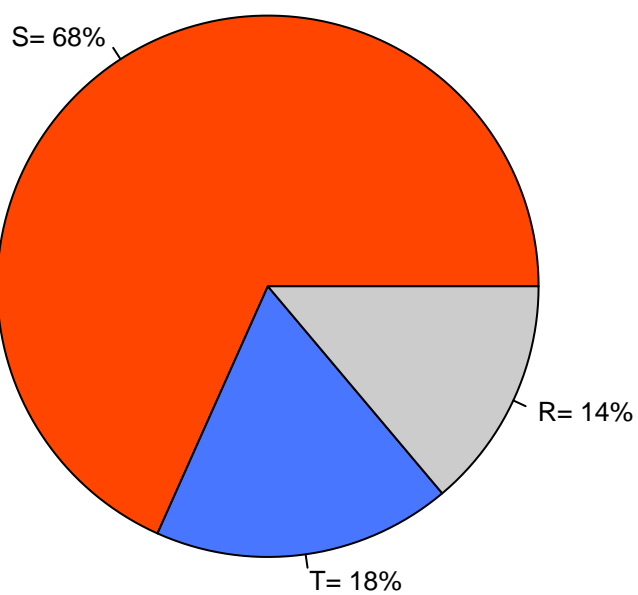
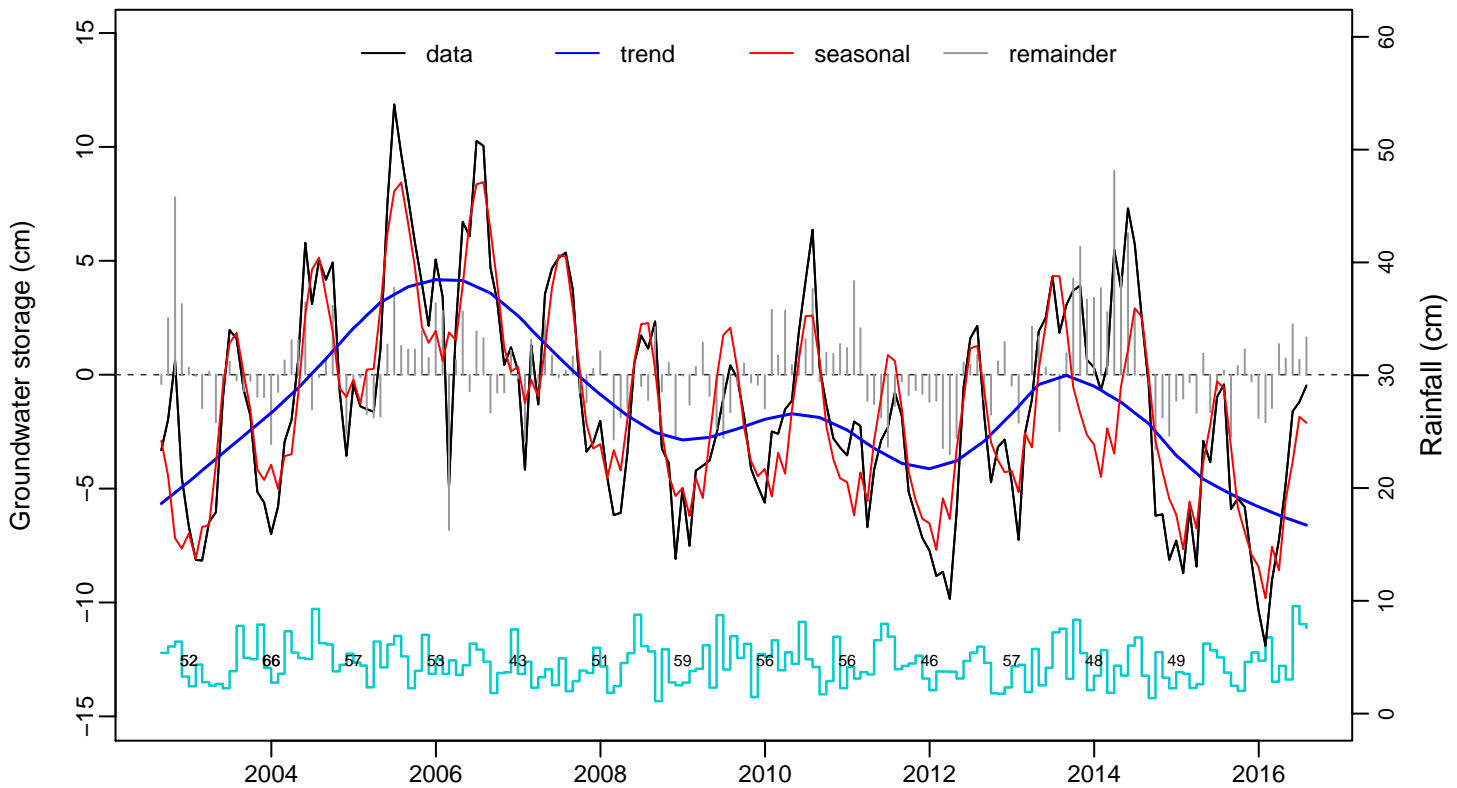


Fig. S74: North Caucasus Basin (34)



**Seasonal–Trend–Remainder (GRACE GWS)
Proportion of variance**

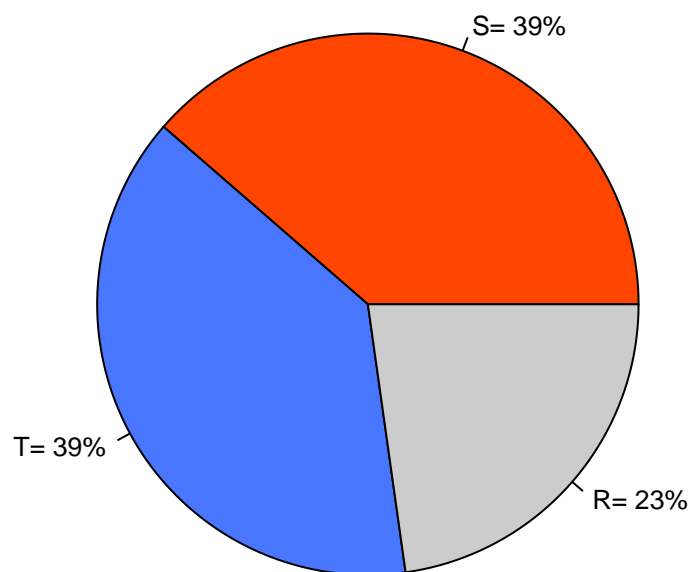
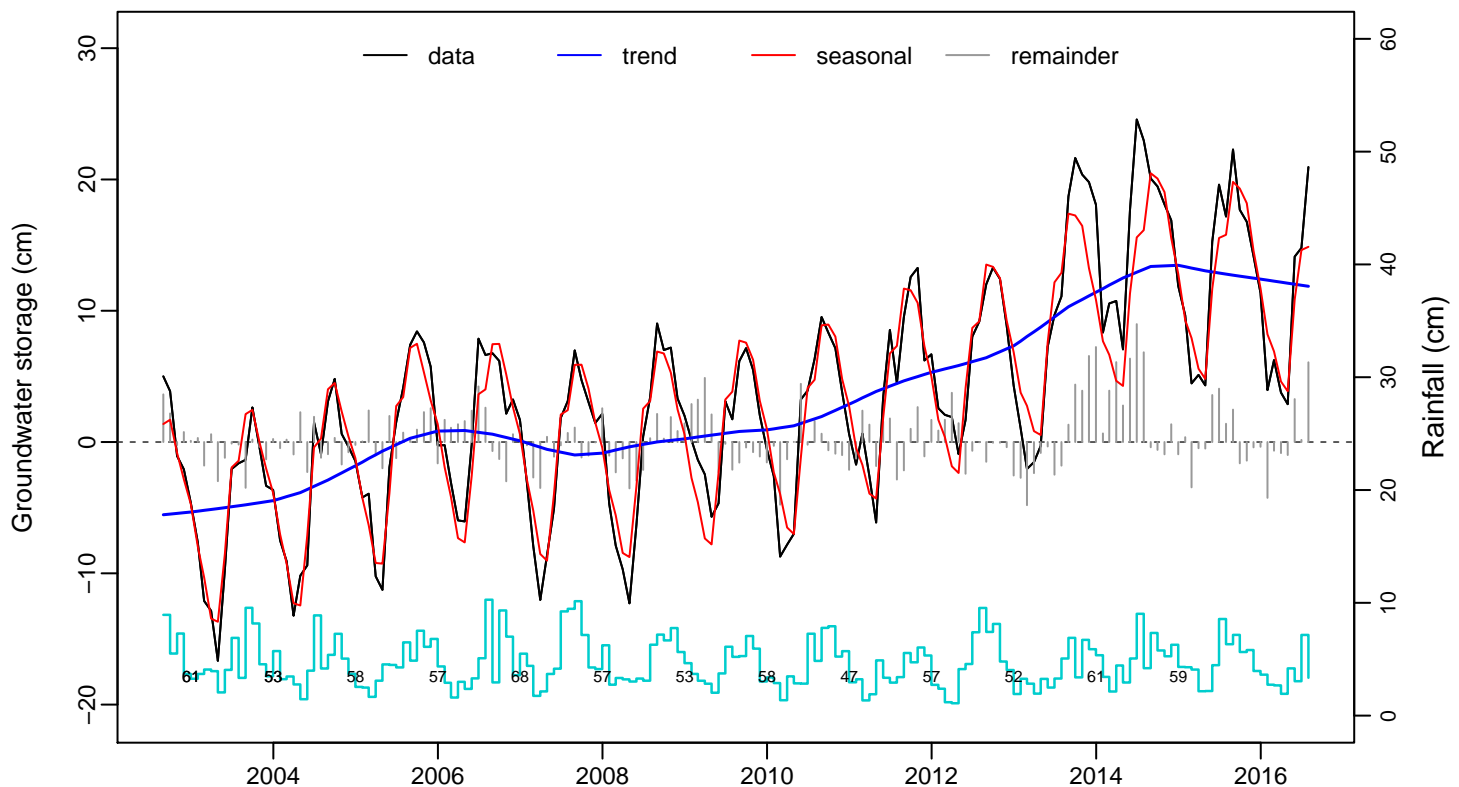


Fig. S75: Pechora Basin (35)



**Seasonal-Trend-Remainder (GRACE GWS)
Proportion of variance**

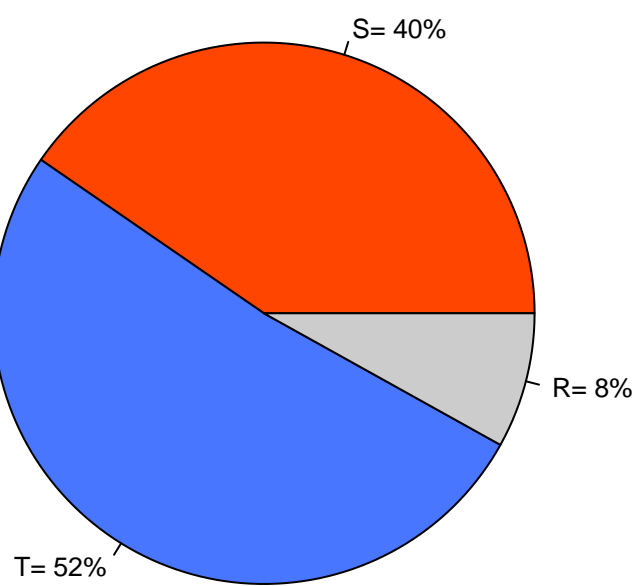
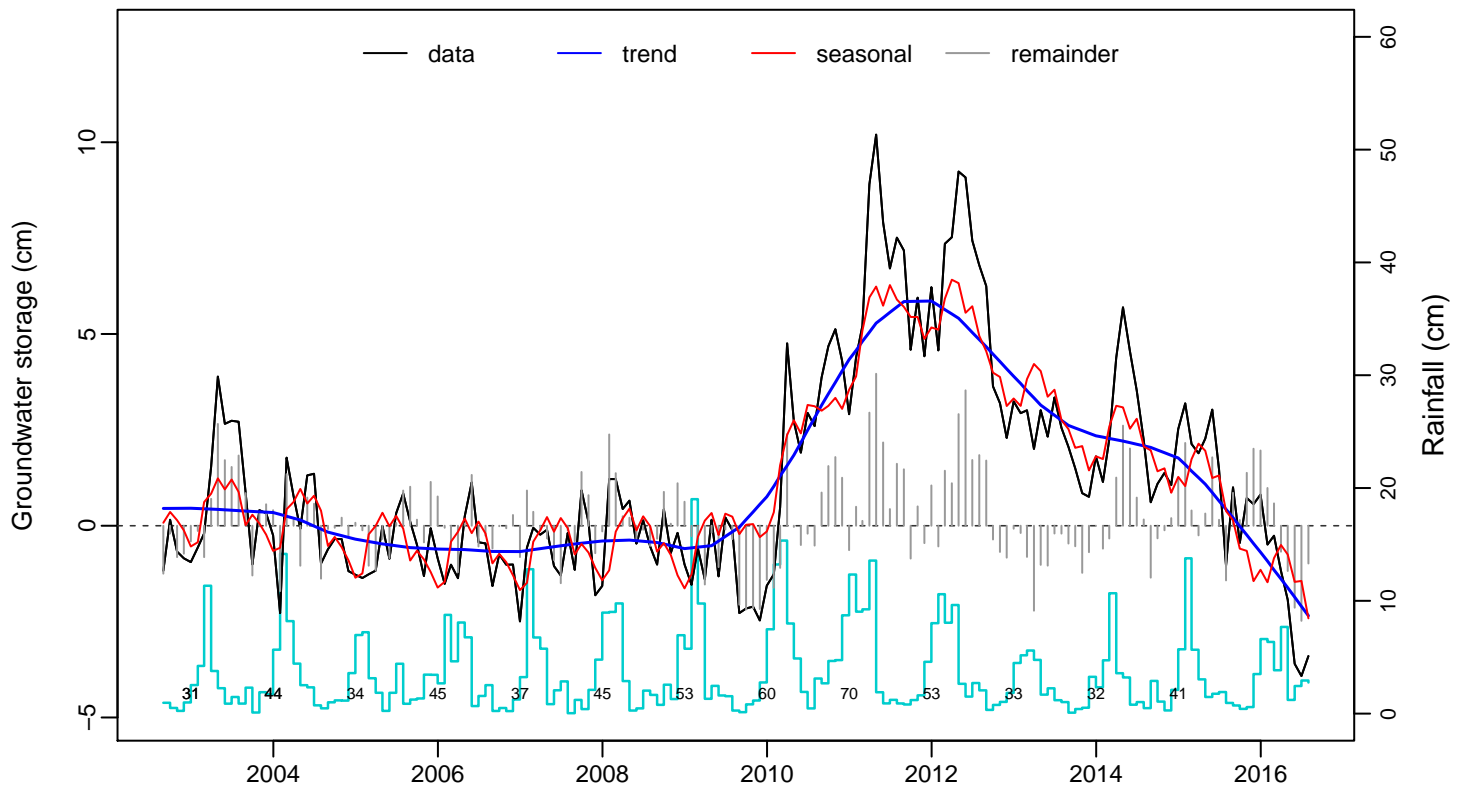


Fig. S76: Great Artesian Basin (36)



**Seasonal–Trend–Remainder (GRACE GWS)
Proportion of variance**

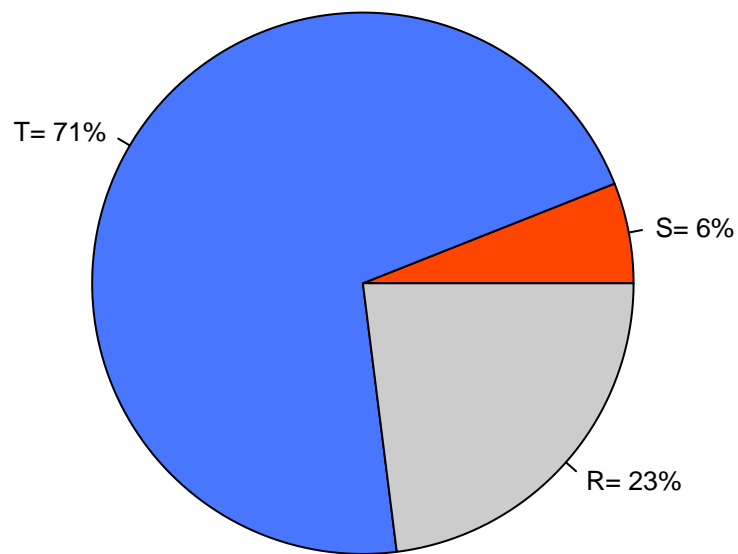
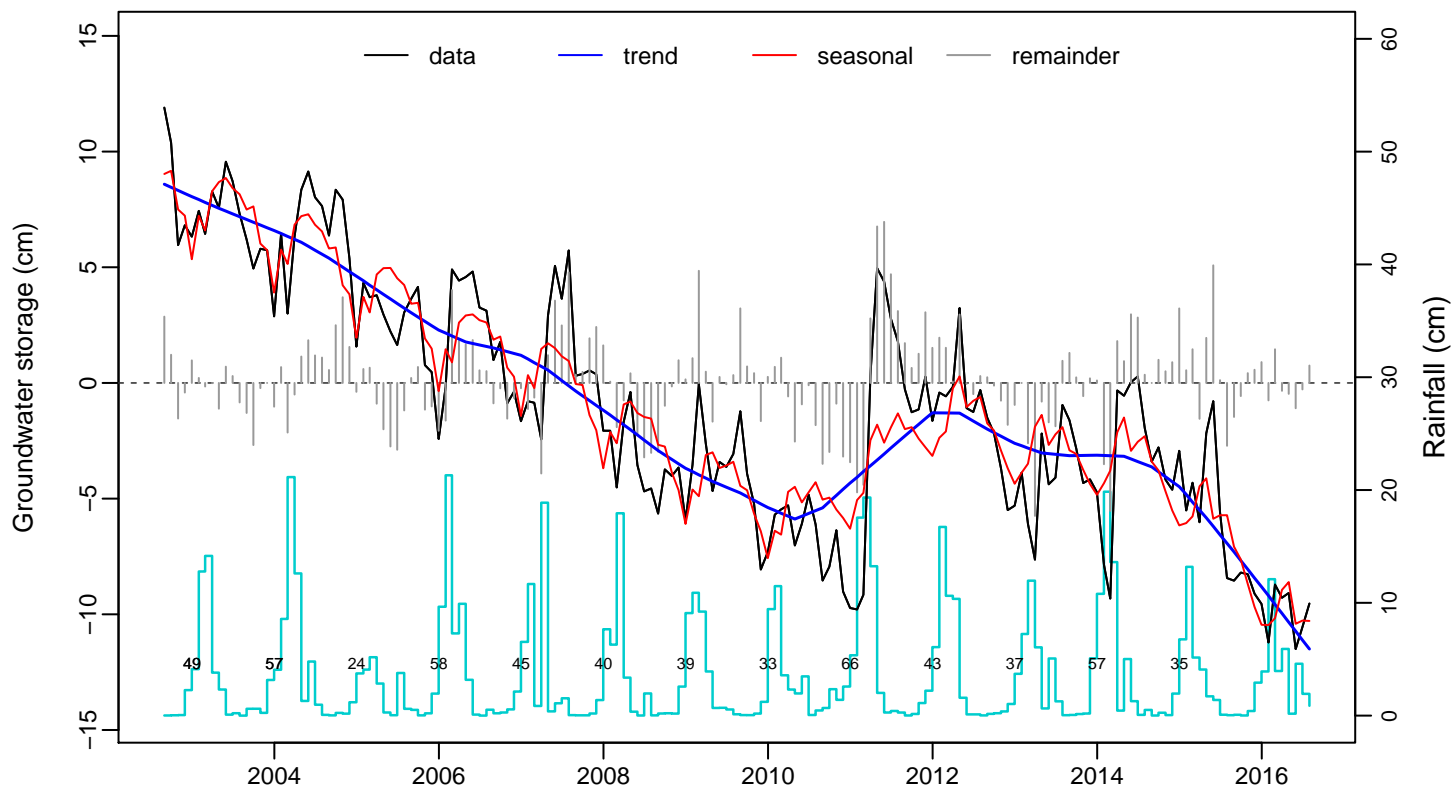


Fig. S77: Canning Basin (37)



**Seasonal–Trend–Remainder (GRACE GWS)
Proportion of variance**

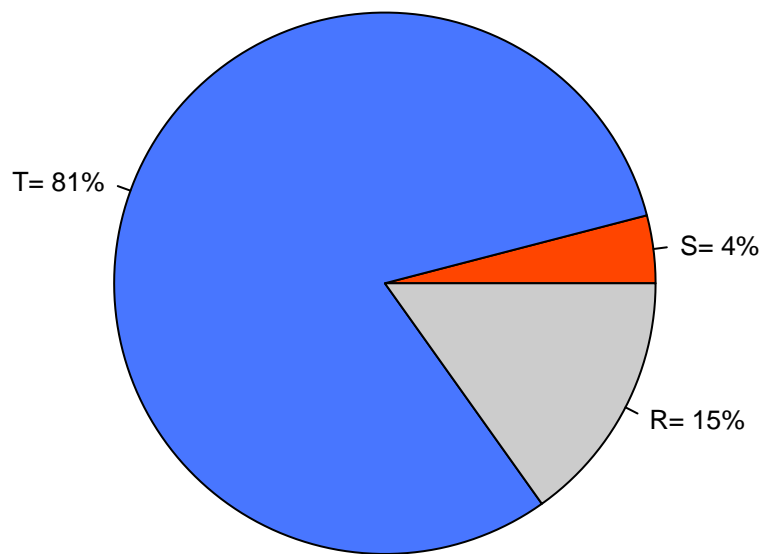


Fig. S78 Computational uncertainty in GRACE-GWS

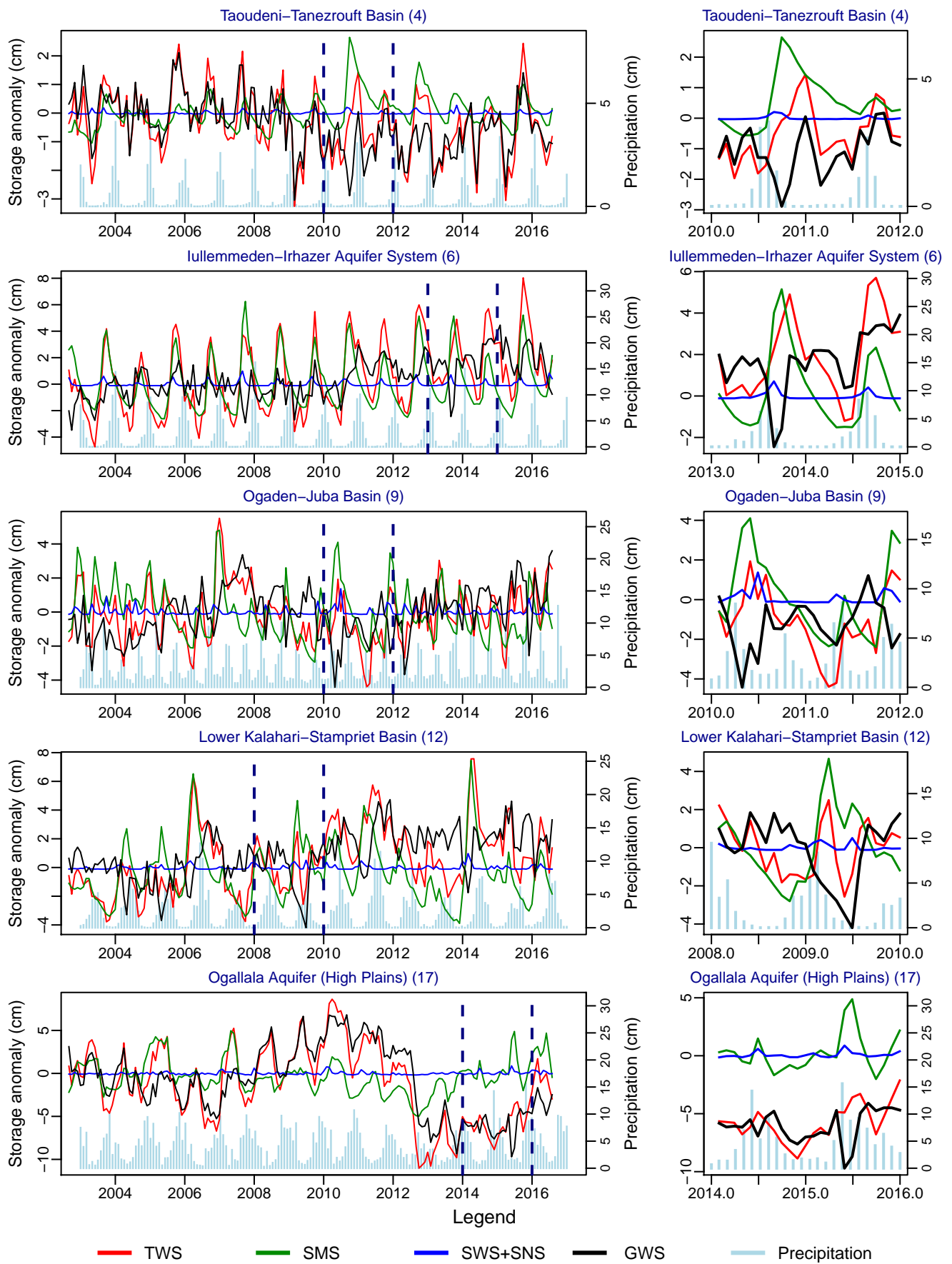


Fig. S79: Uncertainty in the estimates of GRACE-derived GWS from 20 realisations

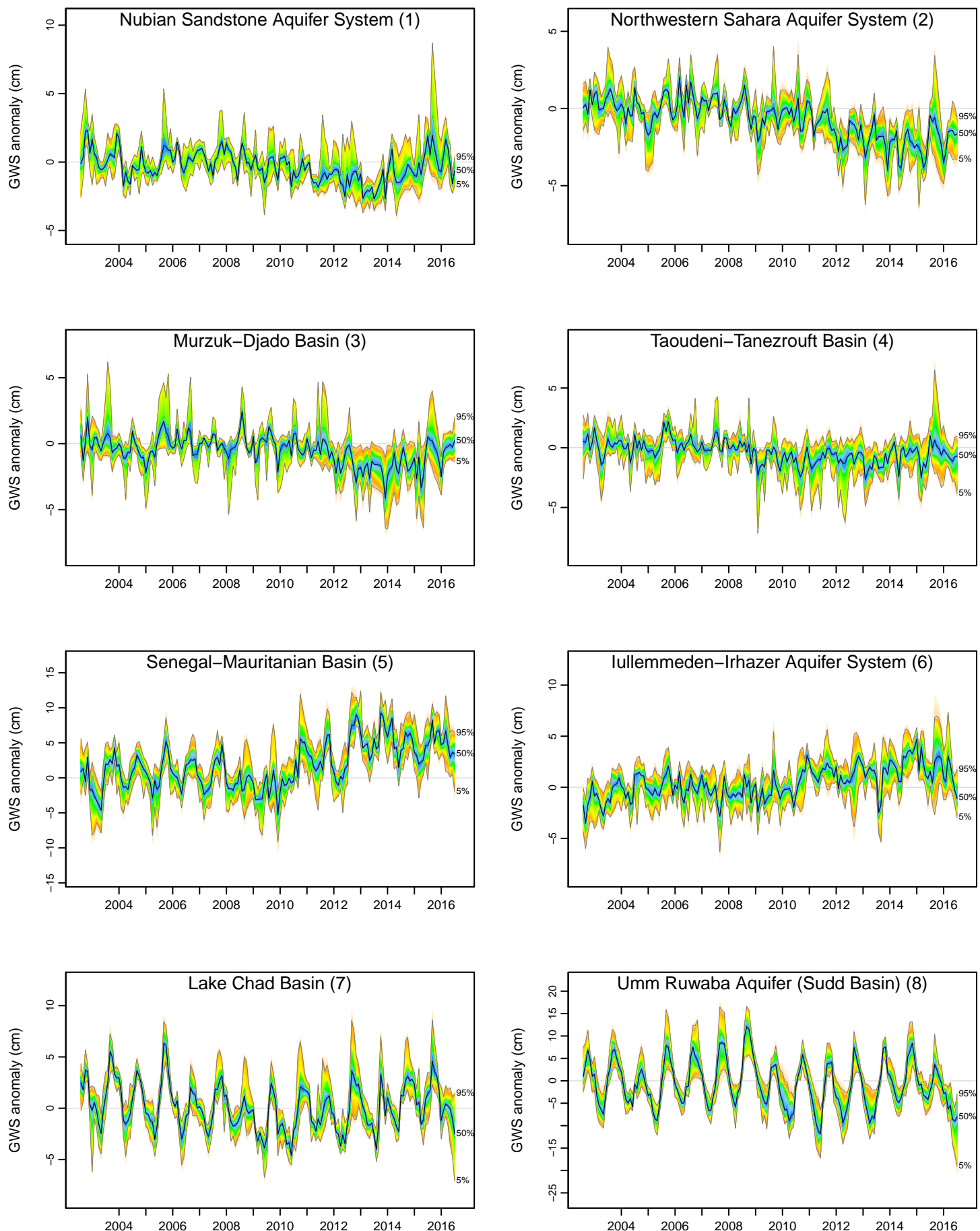


Fig. S79: Uncertainty in the estimates of GRACE-derived GWS from 20 realisations

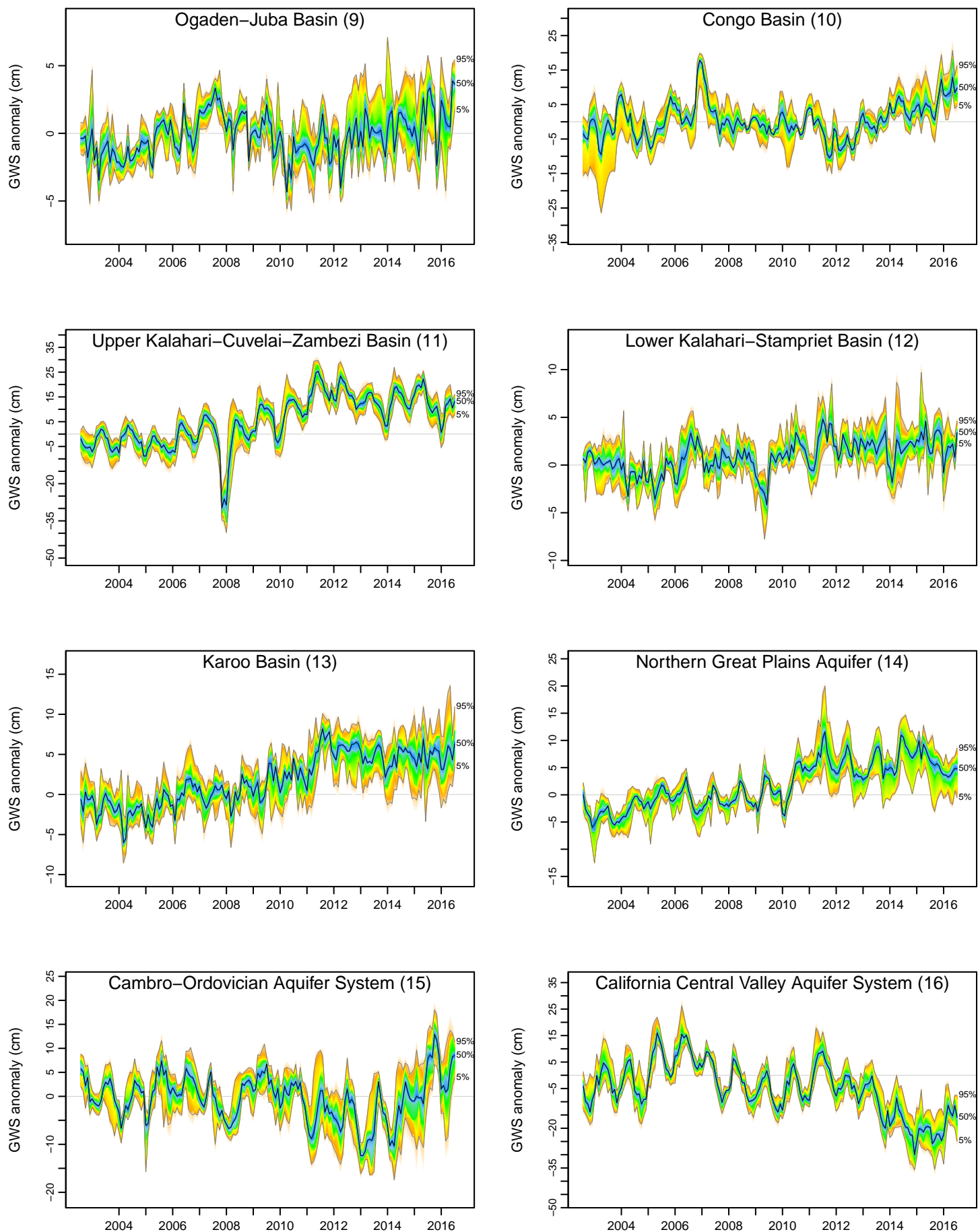


Fig. S79: Uncertainty in the estimates of GRACE-derived GWS from 20 realisations

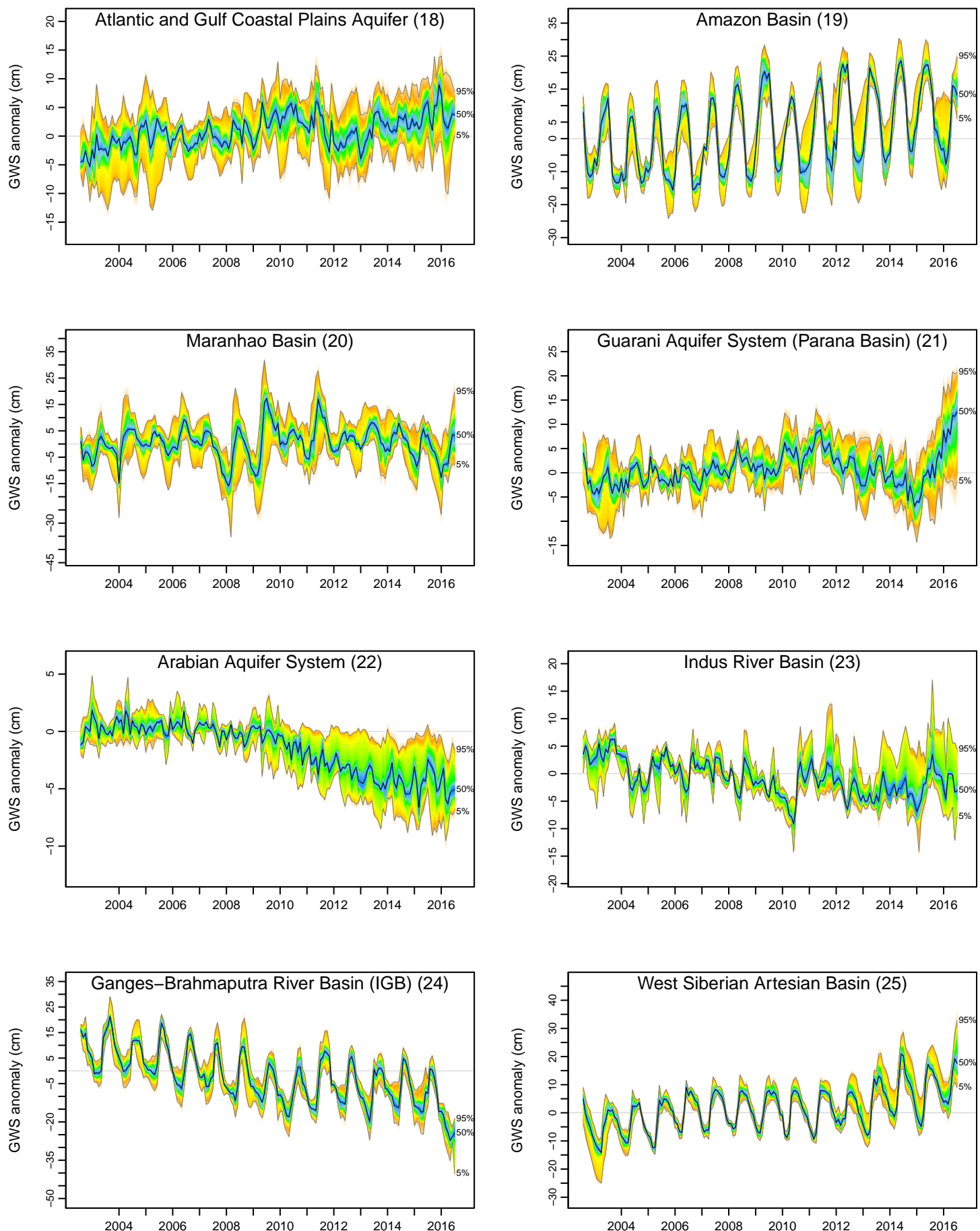


Fig. S79: Uncertainty in the estimates of GRACE-derived GWS from 20 realisations

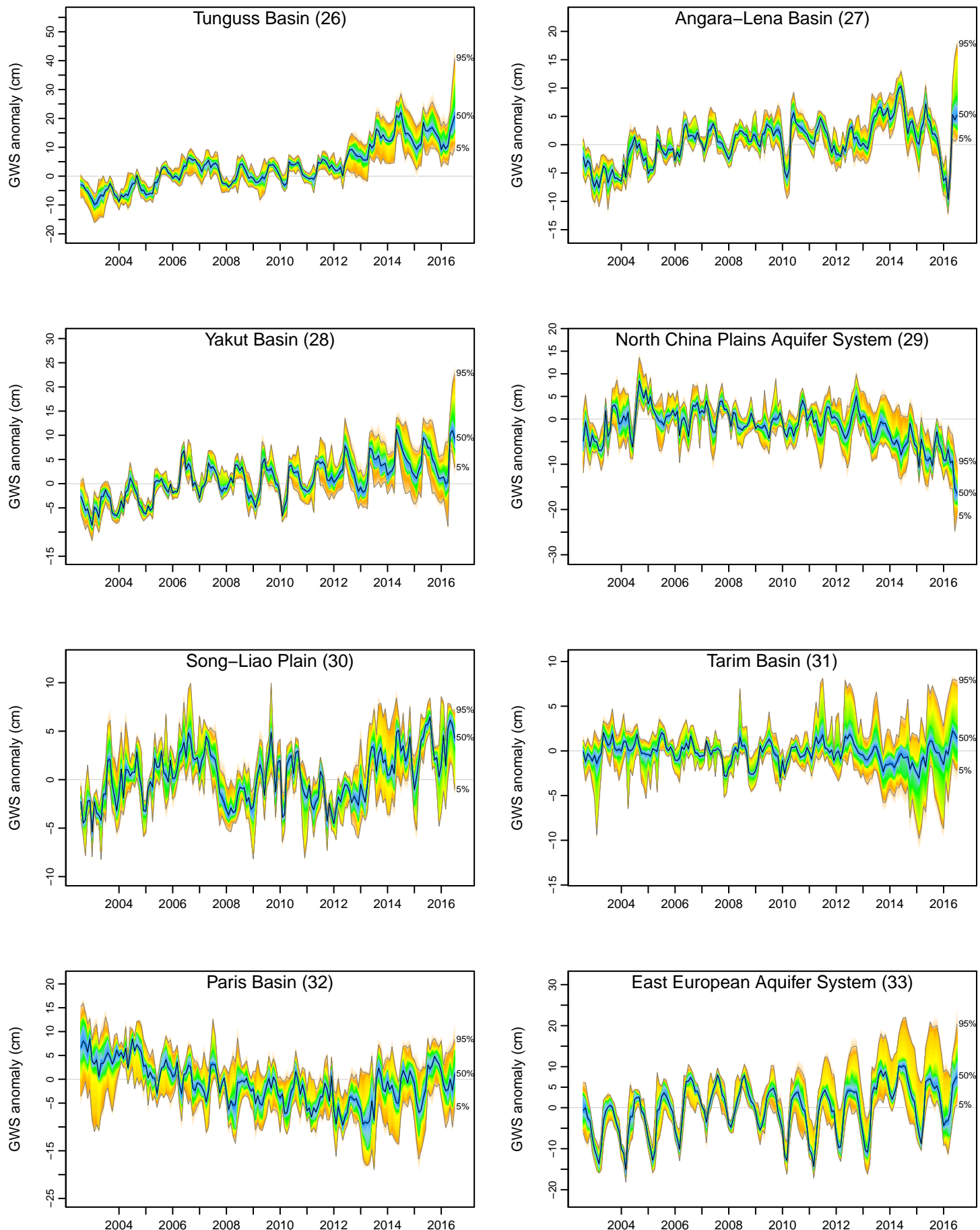


Fig. S79: Uncertainty in the estimates of GRACE-derived GWS from 20 realisations

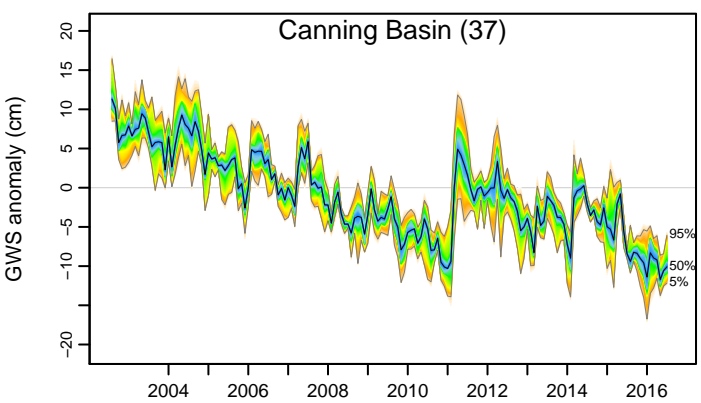
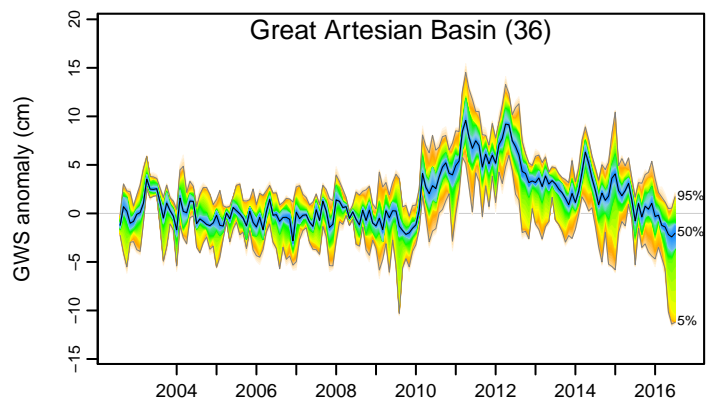
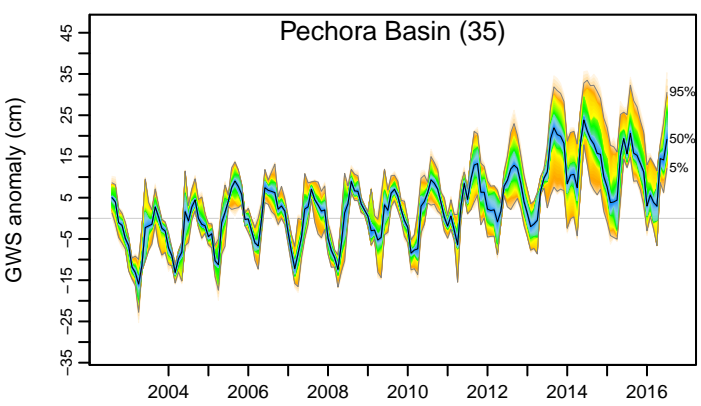
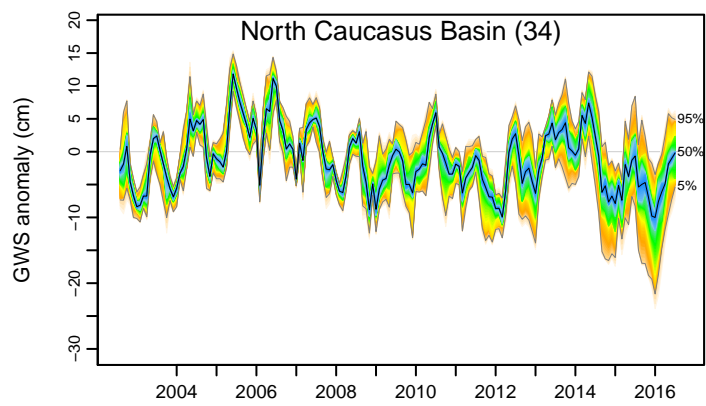


Fig. S80

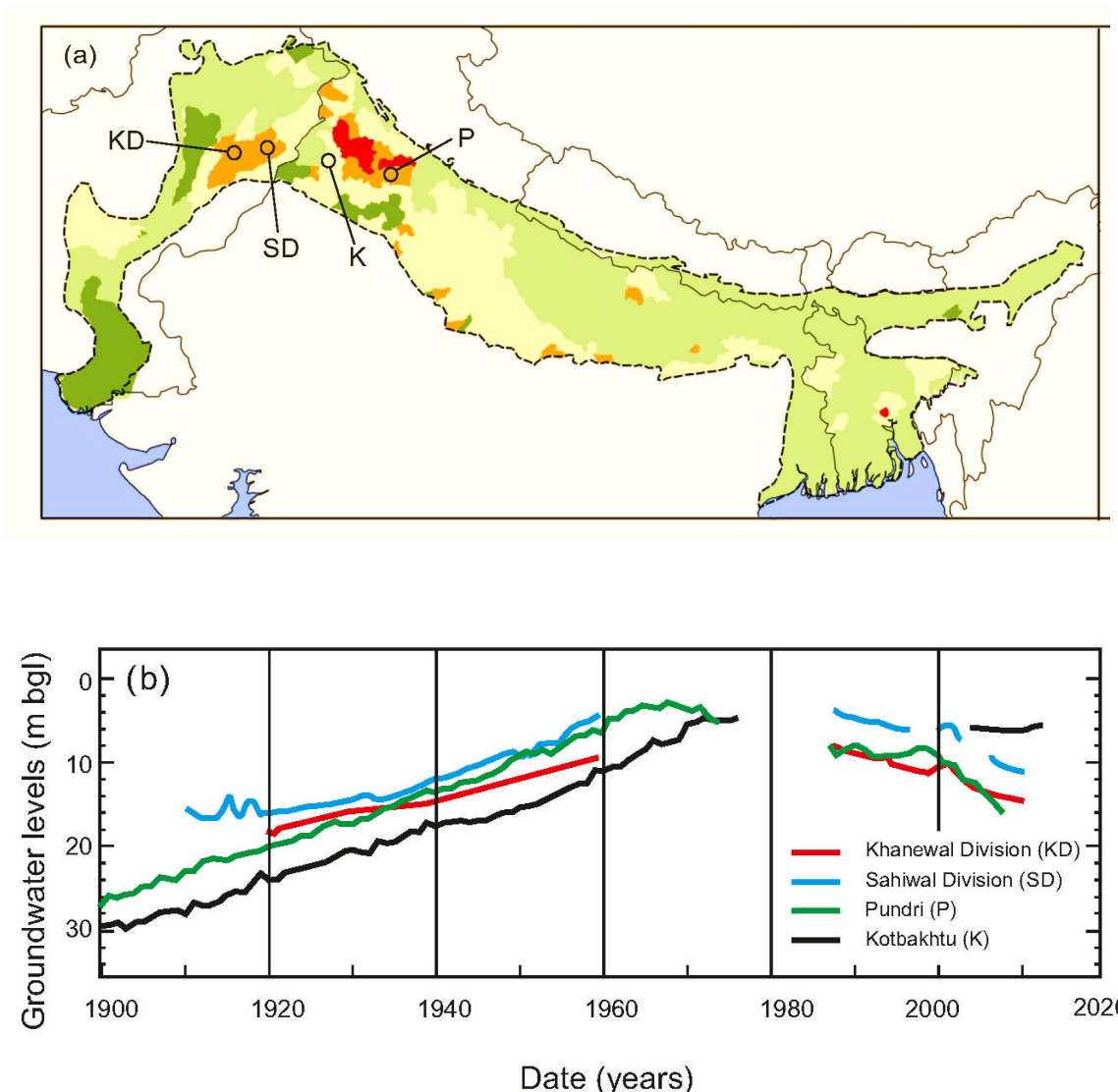
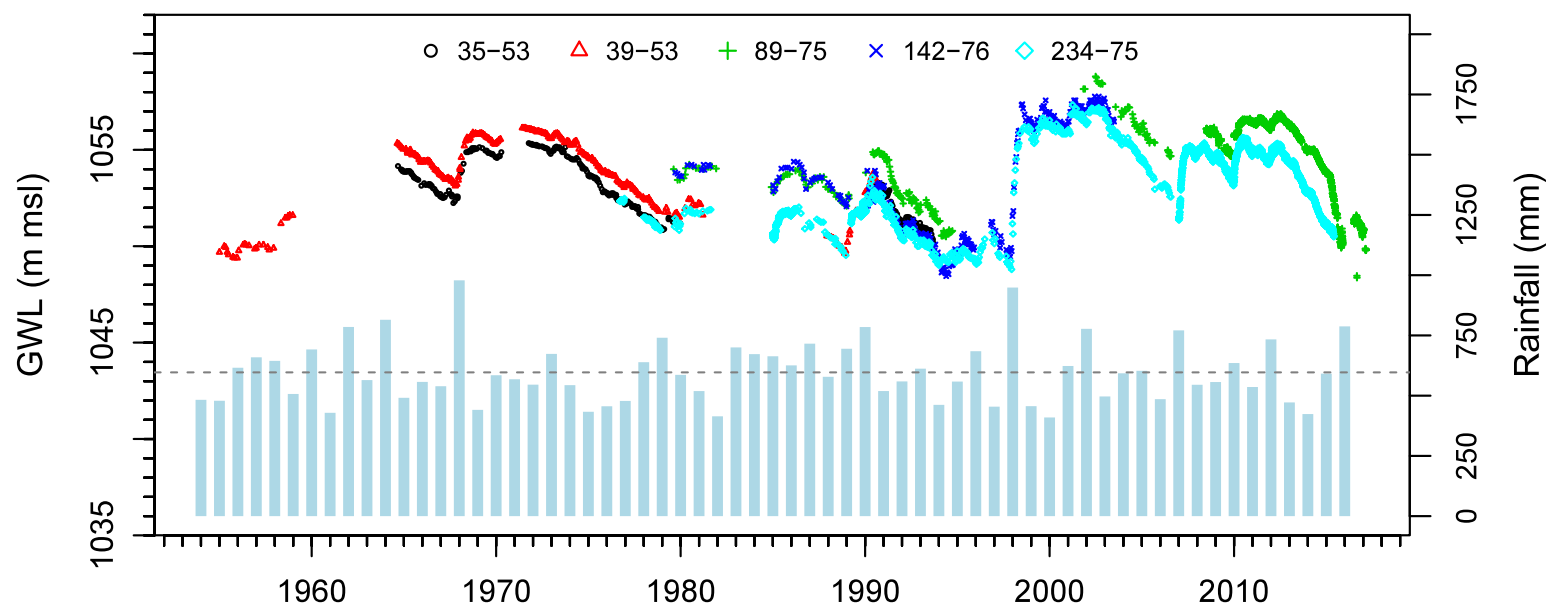


Fig. S81

(a) Makutapora Basin, Tanzania



(b) Limpopo Basin, South Africa

